UNIVERSITA' DEGLI STUDI DI PADOVA

Sede Amministrativa: Università degli Studi di Padova

Dipartimento di Innovazione Meccanica e Gestionale

SCUOLA DI DOTTORATO DI RICERCA IN INGEGNERIA INDUSTRIALE
INDIRIZZO: INGEGNERIA DELLA PRODUZIONE INDUSTRIALE
CICLO XXI

MODELLING OF THE MICRO INJECTION MOLDING PROCESS

Direttore della Scuola : Ch.mo Prof. Paolo F. Bariani
Supervisore : Ch.mo Prof. Paolo F. Bariani

Dottorando : Alberto Gava

SOMMARIO

Con tassi di crescita annui del 20 per cento (dati relativi a Dicembre 2007), si viene a delineare un nuovo ed interessante campo di attività per l'industria nazionale e, in particolare, per quella della trasformazione plastica. I microsistemi conquistano sempre più settori come la meccanica di precisione, telecomunicazione, tecnologia applicata alla medicina e biotecnologia, ma in misura crescente anche l'industria automobilistica. A causa del crescente fabbisogno e volume richiesto, il microstampaggio ad iniezione è destinato ad assumere un ruolo d'eccellenza nei processi di produzione. Così come nel processo di stampaggio convenzionale ci si avvale della simulazione numerica per l'ottimizzazione del prodotto, dei parametri di processo e la riduzione del costo totale. Gli attuali codici di calcolo offrono risultati accurati nel caso del processo convenzionale, ma necessitano di ulteriori sviluppi per quanto riguarda applicazioni più tecnologiche quale il microstampaggio ad iniezione. Ciò è dovuto principalmente al fatto che parametri e modelli del materiale assunti su macroscala non risultano essere altrettanto validi in un processo in cui il polimero è sottoposto ad alte velocità di deformazione e a gradienti termici notevoli. L'obiettivo principale di questo lavoro è fornire un metodo utile a valutare la capacità degli attuali codici di calcolo nel descrivere correttamente l'avanzamento del flusso in componenti microstrutturati. L'approccio proposto consiste nel valutare il riempimento di una cavità opportunamente progettata e lavorata utilizzando le linee di giunzione come indicatori di flusso. Questo metodo si pone come valida alternativa all'approccio più comunemente seguito e basato sul confronto di riempimenti incrementali tra processo sperimentale e simulazione numerica, laddove la posizione e forma del fronte di flusso è fortemente influenzata da contrazioni termiche e rilassamento delle tensioni residue post-stampaggio. Con questo obiettivo sono state condotte simulazioni numeriche in ambiente Moldflow® e si sono confrontati i loro risultati con prove sperimentali. In secondo luogo è stata condotta un'analisi di sensitività al fine di valutare l'influenza di dati reologici e di un coefficiente all'interfaccia polimero/stampo validi su microscala, della pressione sulla viscosità e di un modello unificato che

consideri entrambe la viscosità elongazionale e a taglio sull'accuratezza dei risultati numerici. Una volta appurato che il modello viscoso del materiale implementato nei convenzionali codici di calcolo non risulta essere altrettanto accurato in processi che coinvolgono alte velocità di deformazione, si è deciso di condurre simulazioni numeriche non convenzionali con l'intenzione di considerare anche la componente elastica del polimero. Le simulazioni sono state condotte in ambiente Ansys Polyflow® implementando un modello viscoelastico e confrontando i risultati numerici in termini di evoluzione del flusso durante il riempimento e di caduta di pressione acquisita all'iniezione.

TABLE OF CONTENTS

ABSTRACT

Numerical simulation for injection molding has been developed and accepted by the processing industry to improve productivity, part quality and to shorten start-up times. In the particular case of micro injection molding, numerical simulation is all the more crucial since processors deal with much more basic problems than in the case of classical injection molding. Due to the small part dimensions prevailing in micro molding, it is not uncommon to be faced with the total incapacity to achieve complete filling of the micro cavity or to eject the solid part. This entails solutions such as changing the processing parameters, trying another material, modifying the mold inserts, or even making a new mold insert, when the trial-molding has resulted in irreversible insert damage, needless to say how expensive and time-consuming this trial-and-error process can be. There is, therefore, considerable need for reliable numerical simulation tools dedicated to micro injection molding. Commercial simulation packages are based on a usually legitimate approximation, when dealing with traditional injection molding, which consists in disregarding a dimension in front of the other two. Indeed, they fail to capture important aspects of injection mold filling, such as edge effects through narrow channels, transverse flow in corners, transverse flow at changes in mold thickness unless there are appropriate boundary conditions in these zones. Of course, these effects are more significant for small parts than for conventional ones. This paper aims to investigate the flow behaviour of polymer melt in micro mold cavities and determine the necessary strategies to adapt the traditional injection molding process for the replication of polymeric microstructures. First, the direct application of the injection molding process has been analyzed using the conventional simulation software Moldlfow® Plastic Insight. Different combinations of process parameters have been simulated to investigate the flow behaviour of polymer melt, the relationship between process parameters and the quality of molded microstructures. Using these results, the most significant parameters can be identified and possible processing strategies can be proposed and simulated to test feasibility. Constitutive material models and conservation equations implemented in conventional numerical simulations have been analyzed and different constitutive models or alternative approaches are proposed. For example, the assumption of a generalized Newtonian fluid

has been used in traditional injection molding because the importance of elasticity compared to viscous effects seems negligible. Because of high deformation rates during the injection phase of high speed injection molding, it is expected that elastic effects will occur. The challenge is to translate the complex rheological behaviour of polymeric fluids into suitable equations, and to use these models to predict flow in micro cavities. As a second approach, 3D numerical simulation has been performed on a multi purpose simulation code (Ansys Polyflow®) to evaluate whether the implementation of a viscoelastic material model may improve the accuracy of the micro filling simulation.

The work presented in this thesis was carried out at the Te.Si. laboratory, University of Padua, Italy, from January 2006 until December 2008, under the supervision of Prof. P. F. Bariani and G. Lucchetta.

CHAPTER 1

INTRODUCTION

1.1 THE MICRO MOLDING SCENARIO

Over the last ten years, the fields of micro- and nanotechnology have emerged with the aim of creating tiny, yet functional, devices at a scale difficult to see with the naked eye. Research in laboratories worldwide has realized products with optical, electrical and mechanical properties that enable them to be used in applications many times smaller than previously thought possible. The science is now being translated from research institutions to drive a diverse range of commercial applications (including mechanical actuators and sensors, biomedical implants and optical systems) forming a rapidly growing market that saw a 35% increase in revenue in related products in 2003 [1]. It is a sector that many analysts have forecast to experience exponential growth over the next few years, as these ideas filter down from research and development to the marketplace.

There are a number of (often conflicting) definitions [2] of what order of length or volume the term micro molding refers to. However, a definition based on what is currently possible would suggest that a micro molded product has a maximum dimension of 1 mm and a sub-1mg mass for polymers. Products that have the dimensions of a conventional injection molded product, but which contain fine surface details having length scales of the order of micrometers, also fall the micro molding area. The growing into product demand requires reliable manufacturing capabilities, based on a high level of integration between processing and assembling and supported by precision and micro tooling. Consequently, Microsystem Manufacturing Technology (MMT) should be anchored in a multidisciplinary science approach and should be considered as transversal to the more competitive industrial sectors and materials (namely polymeric systems, metals and ceramics). The main application markets for microsystems are:

- automotive (e.g., micro switches, connectors and airbag sensors)
- computer (e.g., connectors and printer ink heads)
- telecommunications (e.g., fibre optic connectors and mobile phones)
- electronic (e.g., micro switches)
- medical (e.g., cardiovascular implants and hearing aid devices)
- watch industry (e.g., micro gears).

The evolution of micro molding to produce components with ever smaller dimensions imposes technological challenges in a number of areas; one of the most important ones is the mold cavity manufacturing for the production of components with dimensions that meet the required specifications. The need for microscale tolerances, fine details, and desired surface finish surpass those encountered in tool manufacturing for conventional injection molding.

Furthermore, technological challenges are required on the processing equipment. Although it may be possible to mold a product under laboratory conditions, expanding it to a commercially viable process requires acceptable yields. The production of substandard components must be minimized by ensuring acceptable process repeatability, which is dependant on homogenous melting, high precision dosing and a tightly controlled injection dynamic. Micro molding is a thermally dominated process, typically involving high thermal gradients, rapid heat flows and a large product surface area to volume ratios. Therefore, tool temperature has a significant influence on mechanical and morphological properties. Some applications require a variable temperature system, where the temperature is raised just before injection to ensure that fine features are filled adequately and then cooled rapidly when the cavity is completely filled to minimize cycle times. Such systems are useful for ensuring high aspect ratio features (which could not be molded using

conventional tool temperatures) and are filled adequately, but they also incorporate another variable in the process and with it another threat to final product consistency.

Computer modelling of the process is highly desirable for assessing the feasibility of a project without expensive mold fabrication and testing. However, the extreme conditions present in the process can pose problems for computational fluid dynamics solutions. Many micro molded products do not feature the flat, thin-walled structures typically found in conventional injection molding and cannot be accurately modelled using the 2.5D Hele-Shaw approximation, which is usually adopted for mold-filling solvers. Consequently, a fully three dimensional numerical method is required for accurate modelling, which must also employ constitutive equations able to account for the effects which are not considered in conventional analyses, such as material compressibility and thermal transfer at the cavity wall. Pressure and temperature gradients far exceed those found in conventional injection molding and require the use of very small time steps between iterations to ensure convergence of a solution, which also increases solution times.

1.2 THE AIM OF THE WORK

The main challenges to be addressed by this work are to:

- divulge the application of the Microsystem Manufacturing Technology in different industrial fields. This implies the reliable and cost-efficient production of micro components, the assessment of the microfeature reproduction and the use of functionalized materials; the aspect ratios and remarkable accuracy (in the submicron area) achievable in replicating such features are one of the most important process characteristics and constitute a major manufacturing constraint in applying injection molding to a range of applications;
- improve the accuracy of micro molding process monitoring and control. Many of the machines emerging to fulfil market requirement for dedicated micro molding applications incorporate new technologies, including small diameter screws and plunger injection systems, but there is currently little understanding of the influence of these components on parameters such as repeatability and process dynamics;
- gain understanding of the materials properties used in the process.

Available characterization, obtained under standard procedures, can not describe the very hard thermo-mechanical conditions encountered during micro injection (high pressure, enormous cooling rate and velocity gradients). Consequently, the available process modelling codes are unable to describe polymer behaviour in this scale range. Different rheological models and processing strategies can be proposed and simulated to test feasibility of the micro molding process;

- improve the accuracy of computer aided engineering simulation. Dedicated simulation software fail to correctly describe the melt flow in microstructures, mainly because phenomena such as the tendency of polymers to slip in micro channels, viscoelastic polymer behaviour, microscale surface effects, the microscale rheological behaviour and the contact between polymer and mold are not taken into account.

1.3 THE CONTEXT

The work presented in this thesis has been carried out in the framework of the 4M Network of Excellence "Multi Material Micro Manufacture: Technology and Applications" (European Community founding FP6-50027, www.4m-net.org) and in connection with the activities of the Processing of Polymer Technology Division (4M Work Package 4). The main aim of 4M is to develop Micro- and Nano- Technology (MNT) for the batch-manufacture of micro-components and devices, in a variety of materials, into user-friendly production equipment, processes and manufacturing platforms for incorporation into the factory of the future. To achieve this, the Network has sought to integrate currently fragmented R&D capacity into non-silicon micro technologies in the ERA into a European Centre of Excellence. The establishment of such an expert resource and infrastructure at a European level has been designed to help European companies engaged in satisfying the growing demand for portable, wireless communication products and many lifestyle, health and transport related systems incorporating MNT.
Part of this research work has been performed within a collaborative research activity program carried out between the Micro/Nano and Precision Manufacturing (MPP) Research Group at MEK-DTU (Denmark), the Laboratory for Process Technology at IMTEK (Germany) and the Department of Innovation in Mechanics and Management (Italy).

CHAPTER 2

BACKGROUND STUDY AND LITERATURE REVIEW

2.1 THE M-CHAIN OF PRECISION MOLDING

The attainment of tight dimensional and functional tolerances requires the thorough examination of the injection molding operation following the so-called M-chain of precision molding:

- man/operator
- machine
- mold
- method
- material.

While most processes today are fully automated and robotics is widely utilized, the presence of a skilled operator ("man") is essential for high precision applications, when operating at the edge of the capabilities of injection molding technology. These operations are characterized by a very

tight process window, where continuous monitoring and frequent intervention may be required to meet the demanding specifications of the corresponding products. High precision operations require close attention to detail and involve such diverse functions as material specification and handling, mold design, machine design, system operation and maintenance, clean rooms operations, product handling and certification.

The machine is another key element in the chain. It is responsible for melting and plasticising the material and precisely and reproducibly metering the molten resin in the mold. This requires tight control on the temperature, displacement volume and injection speed. Conventional injection molding machines are generally distinguished by precision machining and sophisticated closed-loop control systems used to deliver the necessary injection accuracy and reproducibility [3]. Micro-molding machines, designed to handle small injection volumes and precise displacement, are typically used for very small parts [4]. These machines utilize somewhat different process control algorithms compared to more standard injection molding machines because of the very small displacement volumes and the thermal loads associated with these operations.

The mold is another crucial element in the M-chain. All parts and inserts of the mold must meet precise machining and assembling tolerances. Additionally, it is important to ensure that the temperature is uniform and stable throughout the molding cycle, through careful design and maintenance of the mold cooling/heating system, as well as the close monitoring and control of the mold temperature.

Different types of molding operations (methods) are often considered for molding precision parts. The first type is the conventional molding process wherein a hot melt is injected into a relatively cold mold in which the final part is formed. In this process, the mold is essentially "passive", in the sense that it does not contribute independently to the pressure within the mold cavity. A common variant of the conventional process is the so-called injection-compression molding process in which pressure can be applied directly in the mold cavity and independently of the molding machine. This process is considered more effective in replicating very fine surface features, such as in the case of a compact disc. Other variations of the conventional process (gas or water-assisted injection molding) are also used to minimize shrinkage, sink marks and other surface defects. In these processes, carbon dioxide or water are typically co-injected into the mold to equalize and better control the pressure inside the mold cavity during the packing phase.

Finally, a key element of the M-chain is the material. Polymer properties control both the processibiliy and manufacturability of the molded

article as well as its final attributes and functional performance.

2.2 INJECTION MOLDING FOR MICROSYSTEM APPLICATIONS

Miniaturization methods and technologies are well developed in the integrated circuit industry. They have been used to produce a variety of commercial micro devices, such as camera and watch components, printer heads, automotive sensors, micro heat exchanges, micro pumps and micro reactors over the last 15 years [5]. This new field is known as microelectromechanical systems (MEMS), with a combined international market size of over $15 billion in 1998. In recent years, MEMS applications have also been extended to optical communication and biomedical fields. The former is called micro-optic-electromechanical systems (MOEMS), while the latter is known as bio-microelectromechanical systems (BioMEMS). Potential MOEMS structures include optical switches, connectors, grids, diffraction gratings, miniature lenses and mirrors. Potential and existing BioMEMS products are biochips/sensors, drug delivery systems, advanced tissue scaffolds and miniature bioreactors.

Current micro devices are largely based on silicon (Si), owing to the extensive development of micro fabrication methods (lithography, thin film deposition and wet/dry etching) by the microelectronics industry. Unfortunately, the physical and chemical properties of Si-based materials (poor impact strength/toughness, lack of optical clarity and poor biocompatibility) are not appropriate for many applications. For example, the conductivity of silicon is problematic in many BioMEMS applications that require high voltage for electro kinetic flows. Nonconductive glass or quartz micro devices can be made using the same lithography/etching fabrication techniques. These materials, although less costly than silicon, are still much more expensive than most polymeric materials. In contrast, many polymers exhibit high toughness, optical clarity and recyclability. Some also possess excellent biocompatibility and can provide various biofunctionalities. Future markets for biomedical micro devices for the human genome, drug discovery and delivery in the pharmaceutical industry, clinical diagnostics and analytical chemistry are enormous (tens of billion of US dollars [6]).

Microscale fabrication methods of polymeric materials have been explored in recent years both in industry and academia. Although large-volume production is still rare, many manufacturing processes and commercial

machines are available on the market. The major challenge now is to modify these processes and to optimize the processing conditions, so that low-cost, high-speed and high quality mass production can be realized, such as in the macroscale production. Of the techniques available in plastic molding, injection molding is the most commonly used. It has the advantages of good dimensional control, a short cycle time and high productivity.

2.2.1 Microfluidics

Microfluidics deals with the behaviour, precise control and manipulation of fluids that are geometrically constrained to a small, typically sub-millimetre scale. If the channel dimensions are less than 100 nanometers, the fluid flow is referred to as nanofluidics. This is a core technology in a number of miniaturized systems developed for mechanical, chemical, biological and medical applications. Although both gases and liquids are used in micro- and nanofluidics applications, the low Reynolds number hydrodynamics covers most microfluidic applications. Typical Reynolds numbers for fluids flowing in micro channels with linear velocities in the range up to 10 cm/s are less than 30 [7]. Therefore, viscous forces dominate the response and the flow remains in a laminar condition.

In micro channels, the shear rate can be very high (10^7 1/s), even though the Reynolds number is low. The rheological characterization of polymeric fluids and bio fluids in such a flow field has recently been studied [8]. For solutions containing high molecular weight polymer (or DNA) molecules, polymer degradation is substantial when the shear stress and shear rate are high. Vortex enhancement has been observed in extension thickening solutions flowing in microscale contractions and expansions [8]. At low flow rates, the flow is a perfect laminar flow (figure 2.1 a) and d)). Small vortices emerge at increased flow rate (figure 2.1 b) and e)). Furthermore, figures 2.1 c) and f) show the growth of vortices with flow rate (vortex enhancement). Clearly, this trend is contrary to the observation of Newtonian fluids, where vortices decrease in size with the increasing flow rate or Reynolds number. Vortex enhancement is strongly affected by fluid elasticity. At the moment, the rheology of polymer melts and solutions, flowing in micro channels and micro molds, requires further study because many polymers exhibit strong non-Newtonian and viscoelastic behaviour in these extremely thin and confined flows.

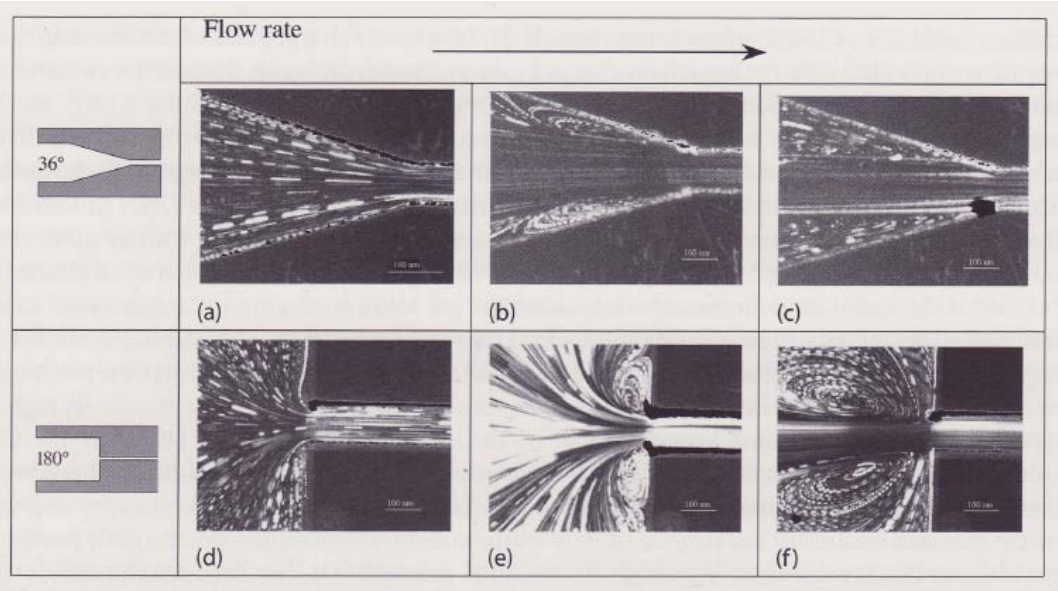

Figure 2.1 - Streak photograph of the entrance flows - vortex enhancement (a) triangular ends: shear rate=$5.9\times10^{2}s^{-1}$, shear stress=1.0×10^{2}Pa, Re=6.3×10^{-3}, Wi=20.1, average extensional rate=$0.57s^{-1}$; (b) triangular ends: shear rate=$1.8\times10^{3}s^{-1}$, shear stress=1.7×10^{2}Pa, Re=6.1×10^{-2}, Wi=42.5, average extensional rate=$2.9s^{-1}$; (c) triangular ends: shear rate=$4.5\times10^{3}s^{-1}$, shear stress=2.5×10^{2}Pa, Re=3.0×10^{-1}, Wi=78.9, average extensional rate=$8.6s^{-1}$; (d) flat ends: shear rate=$4.5\times10^{2}s^{-1}$, shear stress=8.0×10^{1}Pa, Re=3.2×10^{-3}, Wi=16.7; (e) flat ends: shear rate=$1.5\times10^{3}s^{-1}$, shear stress=1.4×10^{2}Pa, Re=2.9×10^{-2}, Wi=37.6; (f) flat ends: shear rate=$2.6\times10^{3}s^{-1}$, shear stress=1.9×10^{2}Pa, Re=7.8×10^{-2}, Wi=54.5.

2.2.2 Microfeatures injection molding

Molding microfeatures with a high aspect ratio (depth vs. width of channel/feature) is not an easy task, in particular when the feature width is small, causing a faster temperature decrease than in regular-sized cavities. Polymer is frozen when its temperature drops to below the no-flow or solidification temperature. For amorphous thermoplastics (PMMA, PC, PS), this no-flow temperature is the glass transition temperature. On the other hand, for semicrystalline thermoplastics (PP, POM), it is the crystallite melting point. While the polymer is filling a micro channel, the thin, frozen layers grow rapidly from the channel walls due to the very fast heat loss. The polymer ceases flowing when the frozen layer covers the whole cross section of the

micro channel. To overcome this difficulty, high injection speed and mold temperature would reduce heat loss from the polymer melt. However, the practical processing conditions are limited by the physical capabilities of the molding tools.

In order to determine the importance of processing conditions on microfeatures filling, several research groups have conducted microfeature injection molding experiments with well-defined simple geometries. Table 2.1 compares the cavities geometries, processing conditions and materials used from four different research groups. The micro channel thickness ranges from 240 to 0.2 microns. In particular, Despa et al. at Louisiana State University conducted the molding of microstructures with an aspect ratio of 8 and lateral dimensions of 90 μm [9]. For the molding material (high density polyethylene), they found that a mold temperature of 135°C allowed the complete filling of the microvoids. Figure 2.2 shows the filled percentages at eight flow rates and six mold temperatures.

Research group	OSU [114]	LSU [44]	UM [95, 96]	Philips	
				[82]	[115]
Microchannel depth (μm)	500	750	400	0.8	27000
Microchannel width (μm)	100	90	40	0.2	237
Microchannel aspect ratio	5	8.33	10	4	113
Main flow region thickness (mm)	2	–	2	2	1.015
Main flow velocity or flow rate	6–1600 mm/s	10–80 cm^3/s	Full machine speed	–	Screw speed 50, 100, 150 mm/s
Mold insert temperature (°C)	25, 80	60–140	25–240	145–152	Highest applicable
Material	PP	HDPE	HDPE	PC	PC, PES, PPS etc.
Material T_g or T_m (°C)	167	132.5	125	~ 150	–

Table 2.1 - Injection molding with microfeatures; results from four research groups.

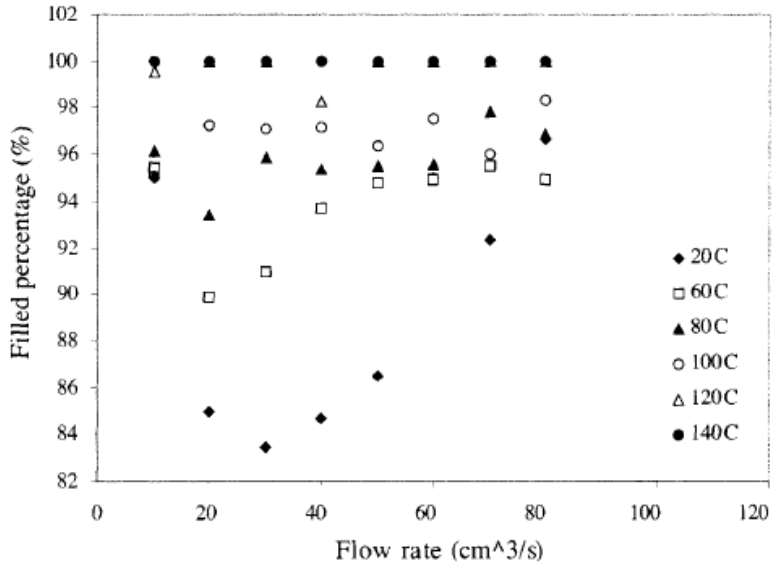

Figure 2.2 – The filled percentage of the replicated HDPE structures vs. flow rate at six mold temperatures

Kim's group, at the University of Massachusetts, conducted a series of microfeature injection molding experiments [10, 11]. Complete replication of 40 μm wide micro channels with an aspect ratio of 10 was achieved at an insert temperature of 140°C. For a temperature lower than 90°C, the replication was close to zero (figure 2.3).

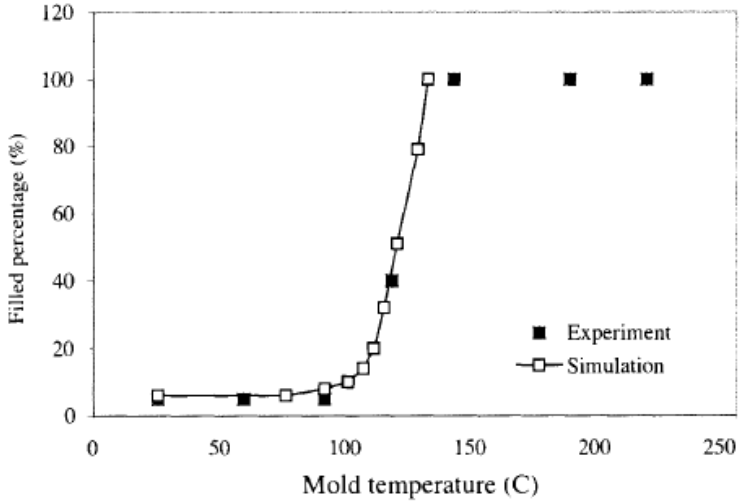

Figure 2.3 – The filled percentage of the replicated HDPE structures vs. mold heating temperature at full machine speed

Winberger-Friedl studied the effect of the mold temperature on the filling depth of PC microstructures, 0.2 μm wide and 0.8 μm deep, on grating optical elements. The filling results, at different mold temperatures, have been plotted in figure 2.4. The transition region is very narrow. The filled percentage varied from 30 to 100% within a temperature range of 7°C. Only at a mold temperature of 152°C, which is above the glass transition of PC, the structures were completely filled.

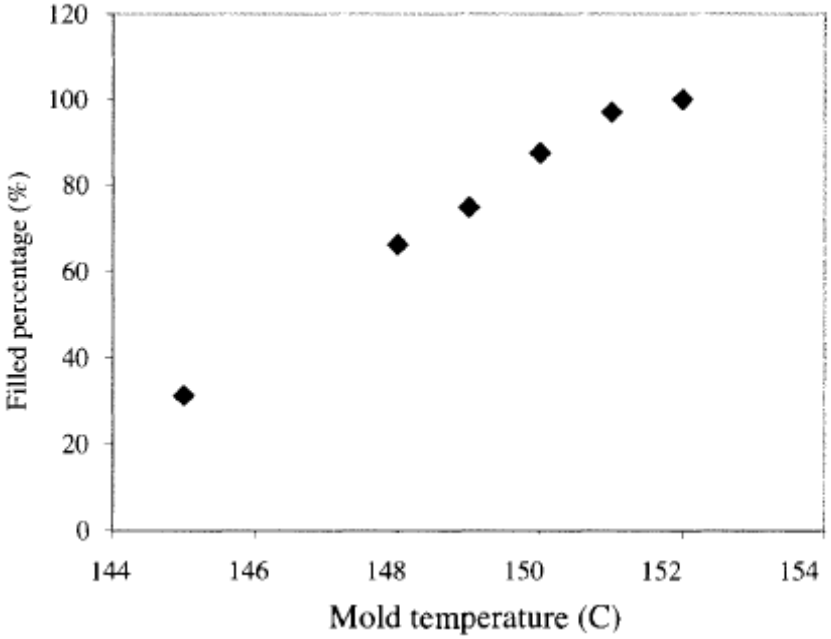

Figure 2.4 – The filled percentage of the replicated PC structures vs. mold temperature.

Yu et al., at the Ohio State University, conducted microfeature injection molding experiments in a rectangular cavity with unidirectional flow [12]. Two mold temperatures, 25°C and 80°C, and two holding pressures, 0 and 3.45 MPa were used. For the case with a 100 μm wide micro channel, on a 2 mm thick base plate, the filled percentage of the 500 μm channel depth has been plotted against the main flow velocity in figure 2.5. In Yu's work, the base plate is 20 times as thick as the micro channel. The filling process consists of two stages. In the first stage, the filling process is essentially the competition between the main flow in the base plate and the branch flow in the micro channel. The pressure required to drive the main flow in the base plate is much lower than in the micro channel. During the base plate filling, the cavity

pressure may not build up to a level high enough to fill the micro channel. The 40 μm channel in Kim's work requires much higher pressure than Yu's 100 μm channel or Despa's 90 μm features. Once the base plate is filled, the second stage starts, during which the cavity pressure increases rapidly. The micro channel filling would be much faster because of the higher pressure. However, if the material at the micro channel entrance has already frozen, then this high pressure can contribute little to the complete filling. The smaller the channel size, the more likely this will happen. This trend is further confirmed by Wimberger-Friedl's result, in which the microchannel size is in the submicron range. The flow in a 0.2 μm channel seems to depend solely on the mold temperature. A mold temperature above the polymer no-flow temperature is essential in this case.

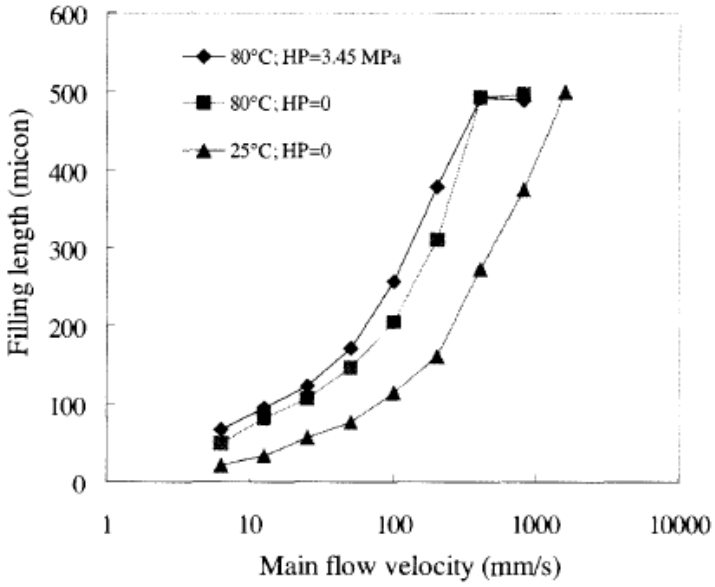

Figure 2.5 – The measured filling length in 100 μm micro channels for PP in the long mold.

2.3 MICRO TOOLING

Micro mold cavity manufacturing is an area of great interest in the micro molding community and is currently one of the main limiting factors on achieving the high precision of product dimensions and surface properties. Recent years have seen tool manufacturing refining conventional machining

techniques (micromachining and micro-electro-discharge machining (μEDM)) and the introduction of other fabrication technologies (LIGA process, laser ablation and micro stereolithography) in an attempt to satisfy the requirements for small but highly detailed cavities with very precise tolerances and the required surface finish. For large features (> 50 μm), with tolerances and repeatability in the range of about 10 μm, traditional computer numerically controlled (CNC)-machining and wire electro-discharge machining (EDM) of materials like tool steel and stainless steel are often accurate enough. The advantage of these techniques is that the tool materials used are the same as those in conventional polymer molding, so their design, strength and service life are well established. Complicated three dimensional structures can also be machined easily. The main drawbacks are that it is difficult to make sharp corners or right angles and the surface quality is usually poor (surface roughness around several μm) [13]. Diamond-based micromilling-microdrilling [14], micro-EDM, and excimer or femtosecond laser-based [15] direct removal processes can reduce the surface roughness to 1 μm or less [16]. While diamond-based methods can also make features smaller than 10 μm, they are only applicable to "soft" metals such as nickel, aluminum and copper. For prototyping, most of these methods can be directly used on polymeric materials to fabricate microfuidic devices. For smaller feature sizes (down to one micron or less), photolithographic methods, e-beam lithography (EBL), or scanning probe lithography (SPL, such as AFM dip pen lithography [17]) have to be employed. Here, a liquid photoresist or self-assembled monolayer (SAM) is placed on a galvanic starting layer by either spin-coating, thin film deposition or self-assembly. The microfeatures are formed after either radiation exposure through a photomask and development or direct e-beam or scanning probe writing. For prototyping, this photoresist structure can serve as a microdevice, itself, or be used as a mold (called a photoresist mold) in low temperature and low-pressure molding processes. More generally, this structure is either used directly for electroplating or for wet/dry etching of silicon, which is subsequently electroplated. Both technologies yield a metal tool, usually nickel or nickel-cobalt. For features with a low aspect ratio or for rapid prototyping, where the lifetime of mold inserts is not crucial, a glass or silicon wafer etched by wet or reactive-ion etching (RIE) can be utilized directly as a mold insert.

For small features (< 1 μm), with high aspect ratios (up to 100 or higher), technologies like LIGA (18) in thick resists (like EPON SU-8) or Deep RIE (DRIE) are required to obtain the mold insert. The LIGA acronym stands for Lithographie (lithography), Galvanoformung (electroplating), Abformung (molding). Originally, the process required X-rays from a

synchrotron to pass through the transparent part of a lithography mask and penetrate several hundred microns into a layer of polymer resist. The mask is removed using a developing chemical to leave a template filled with nickel (or a nickel alloy) by electrodeposition. Once the remaining resist material has been removed, the deposited metal structure is used as a mold for injection molding. Because this process has been hindered by the high cost and scarcity of the synchrotrons required to produce the x-radiation, it was refined to use parallel UV photons with a photosensitive resist to produce the template. The use of photons to form the structures ensures that minimum feature dimensions can be below 1 μm, which are smaller than those formed with conventional machining techniques, where the finite size of the electrode or mill can impose limitations. The LIGA technique is also able to provide an excellent surface finish with less roughness than that produced using conventional fabrication techniques. On the other hand, the main disadvantage of this fabrication method is the fact that it uses a lithography technique to form the structures, which means complex three dimensional forms cannot be produced. Common applications in the micro molding field include mold inserts for the production of channels in microfluidic devices and fine surface details for forming optical gratings or micro filters [19].

Another method that employs light to form structures is laser ablation [20]. In this process a high-power pulsed laser is focused through a lens at a single point on the surface of a target material, raising the temperature of the material in excess of 2000°C and causing it to vaporize. Surface material is selectively removed either by moving the laser in a raster fashion across the target using an optical system, or by moving the material itself on an x-y-z stage. The quality of the resulting geometry depends on a number of key factors, including the beam diameter and the pulse duration and frequency. Laser ablation technology currently offers tolerances of ±1 μm with minimum feature sizes in the order of 10 μm. One of the main advantages of this process over LIGA is that very hard materials can be ablated. On the other hand, the main disadvantage is the cost of the laser, significantly higher than other types of micro machining equipment.

Laser scanning stereo lithography (STL) is a process that allows the creation of three dimensional structures from a digital file format. Typical applications include the rapid prototyping of products for marketing/testing purposes and forming of conventional injection mold cavities. In this process, an ultraviolet laser beam is focused onto the surface of a bath of liquid photopolymer resin and scanned in parallel lines. Resin exposed to the laser is cured and hardened, almost instantaneously, and a thin (virtually two dimensional) layer is built according to the pattern of illumination. Just below

the surface of the liquid photopolymer, a horizontal elevator tray supports the layer of cured resin. As soon as a layer is finished, the elevator tray is lowered one step (one layer thickness) to submerge the previous layer and fresh (liquid) resin immerses the surface in preparation for the forming of the next layer. A three dimensional structure is then created in a step-by-step process until the part is complete and can be removed from the bath. The technology has been refined so that microscale features and high-quality surface finishes are now possible, which makes it a potential route for micro molding cavity manufacture. However, doubt remains as to whether resin-based mold cavities are suitable for the process or if a secondary electroplating process is required for added durability. Resin-based molds/inserts do not possess the same mechanical attributes as steel or even nickel-based moldings, but they possess low thermal conductivities and remove heat from the product at a slower rate than tool steels, which may assist the processing of high aspect ratio features in a micro molding process. In conclusion, a comparison between different mold manufacturing techniques has been proposed in table 2.2, sorted as a function of the achievable structures sizes [21].

Technology/feature geometry	Typical structure size	Feature tolerance	Aspect ratio	Wall roughness	Materials
Ion beam LIGA/2D	0.1 to 0.5 μm	0.02 to 0.5 μm	1	n/a	
Focused ion beam/2D & 3D	0.2 μm	0.02 μm	n/a	n/a	Any
X-Ray LIGA/2D	0.5 μm to 1 mm	0.02 to 0.5 μm	10–100	<20 nm	Electroformable Materials: copper, nickel and nickel alloy
Electron beam LIGA	0.1–0.5 μm		1–2	n/a	"
UV-LIGA/2D	2–500 μm		1–10	n/a	"
Femto-second laser 2D/3D	1 μm	<1 μm	1–10		Any
Excimer laser 2D/3D	6 μm	<1 μm	1–10	1 μm–100 nm	Polymer, ceramics and metal to a lesser degree
Ultra short pulses ECM 2D/3D	Few micrometers	<1 μm	8		
μEDM 2D/3D	10–25 μm	3 μm	10–100	0.3–1 μm	Conductive materials
Micromilling/2D or 3D	25 μm	2 μm	10–50	Few microns	PMMA, aluminum, Brass, steel
Deep UV resists	n/a	2–3 μm	22	≈1 μm	n/a
Deep reactive ion etching	n/a	<1 μm	10–25	2 μm	Silicon

Table 2.2 - Comparison between different processes for mold inserts manufacturing.

2.4 MICRO MOLDING TECHNOLOGY

The micro molding process, while fundamentally similar to that of traditional injection molding, faces several technological challenges in a number of key areas, such as melting, metering, injection, component handling and cleanliness. Improvements in respect of conventional molding technologies will be briefly explained in the following section.

2.4.1 Micro injection molding machines

The injection machine must be able to deliver a homogenous melt to the cavity to ensure process repeatability, which requires the complete, even melting of the polymer feedstock. In traditional polymer processing, this is achieved by using an extrusion screw and the majority of tailor-made micro molding machines incorporate an adaptation of this technology. In practice, the screw geometry is generally designed in order to have sufficient depth of flight to convey commercial feedstock (typically pellets or granules) and yet it contains a minimum volume to ensure that thermal degradation effects are minimized within temperature sensitive materials. Typical screw diameters, in current micro molding machines, range from 12 to 16 mm and can contain up to 6g of material that cause significant material residence times when considering total shot sizes in the order of 10 mg.

Accurate and repeatable dosing of the material is of paramount importance, especially when considering that the total volume of the product can be a fraction of a cubic millimetre. Micro molding hardware must have accurate control of the volume and static pressure dynamics of the melt during the metering process. Therefore, high precision linear servo drives, positional feedback systems and advanced software applications are usually employed to meet these requirements. Shot size repeatability must be strictly controlled because micro molded products typically contain volumes of material many times smaller than those of the injection system used to transport the polymer to the cavity. Consequently, small variations in the total volume of the metered material will result in proportionally larger variations in cavity filling behaviour.

The injection system has to fulfil a number of objectives. Firstly, the high surface area to volume ratio of the product ensures that freezing of the material occurs over a very short time scale, therefore, the shot must be introduced into the cavity as rapidly as possible to ensure complete filling of

high aspect ratio features. Secondly, the injection unit must be able to achieve the high injection pressures required for accurate feature replication. Finally, injection must be performed in a highly repeatable manner. The morphology of the product is highly dependent on the flow dynamics and thermal conductivity of the melt in the mold cavity. So a consistent injection dynamic must be employed to minimize variability in the properties of the end product. Micro molding machine manufacturers have attempted to address the considerable demands upon them using a variety of methods. In table 2.3 a list of micro molding machines commercially available and their main characteristics have been set forth [21].

Manufacturer	Model	Clamp force (kN)	Injection capacity (cm^3)	Injection pressure (Bars)	Plasticization (screw or plunger)	Injection speed ($mm\ s^{-1}$)
Lawton	Sesame Nanomolder	13.6	0.082	3500	10 mm plunger	1200
APM	SM-5EJ	50	1	2450	14 mm screw	800
Battenfeld	Microsystem 50	56	1.1	2500	14 mm screw	760
Nissei	AU3	30	3.1	–	14 mm screw	–
Babyplast	Babyplast 6/10	62.5	4	2650	10 mm plunger	–
Sodick	TR05EH	49	4.5	1970	14 mm screw	300
Rondol	High Force 5	50	4.5	1600	20 mm screw	–
Boy	12/AM 129-11	129	4.5	2450	12 mm screw	–
Toshiba	EC5-01.A	50	6	2000	14 mm screw	150
Fanuc	Roboshot S2000-I 5A	50	6	2000	14 mm screw	300
Sumimoto	SE7M	69	6.2	1960	14 mm screw	300
Milacron	Si-B17 A	147	6.2	2452	14 mm screw	–
MCP	12/90 HSE	90	7	1728	16 mm screw	100
Nissei	EP5 Real Mini	49	8	1960	16 mm screw	250
Toshiba	NP7	69	10	2270	16 mm screw	180

Table 2.3 – A list of micro molding machines commercially available and their main characteristics.

One of the most commercially successful dedicated micro molding machines is the Battenfeld Microsystem 50 [27]. The Microsystem incorporates servo-electric-driven components designed specifically to obtain accurate and repeatable process control, enclosed within a clean room environment. The machine incorporates a 14 mm diameter extrusion screw, mounted at an angle of 45° to the injection axis (figure 2.6), ensuring that a homogenous melt is achieved. Material is extruded into a metering chamber containing a servo-driven piston to accurately prepare a dose of material having a maximum volume of 1100 mm^3 in 0.01 mm^3 increments with user-definable back pressure up to 250 bar. A second servo-driven injection piston

is then used to inject the shot with a velocity up to 1000 mm/s. The injection nozzle passes through the fixed half of the mold to the split-plane to limit the amount of material required to fill the feeding channels and to ensure that the melt is still at the desired temperature as it reaches the cavity. The rapid injection and cooling rates allow for mold opening within a second or two, and total cycle times are determined predominantly by the time taken for ejection and handling. Therefore, to ensure maximum productivity, two separate molds can be mounted to a rotating moving plate, which allows a part to be manufactured, as the previously molded part is removed from the cavity.

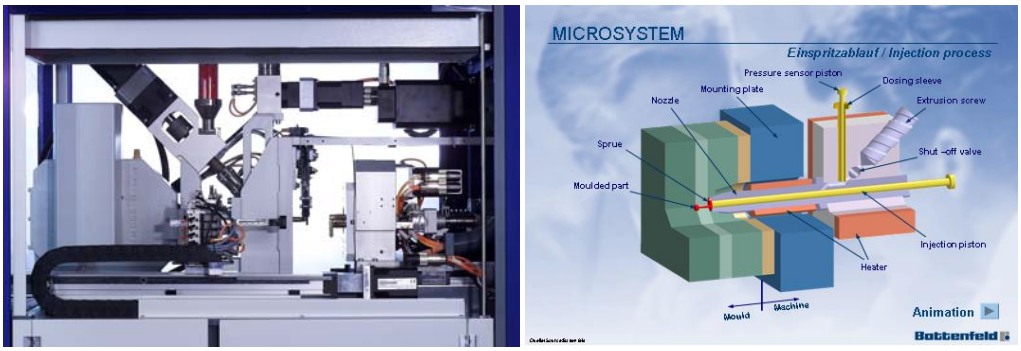

Figure 2.6 - Plastication and injection system of Battenfeld Microsystem 50

2.4.2 Microfeature injection molding machines

Conventional injection molding machines used for microfeatures are expanded with special features for the molding of parts with high aspect ratio. The injection molding machine periphery includes a vacuum unit for the evacuation of the mold cavity and a temperature control unit for the molding tool. It is desirable to use one temperature control cycle on each tool surface. The flow temperatures are adapted to the respective half base plate of the tool or to the molding and demolding process to achieve a relatively short cycle time and a homogeneous tool temperature. To keep the cycle time as short as possible, the thermal mass of the tool sections to be heated is minimized and thermally insulated from the adjacent assemblies. The guiding mechanisms of the tool halves and the ejector system must have tight tolerances, as small transverse movements would damage the microstructures during demolding. The machines and tools to be evacuated have to comply with tolerances in the

micrometer range. Demolding of the microstructures is accomplished by means of ejector pins, which are located at the substrate plate. Under laboratory conditions, the microstructures can be removed manually.

2.5 PROCESS MONITORING AND ASSESSMENT

Dedicated micro injection machines incorporate new technologies, including small diameter screws and plunger injection systems, but there is still little understanding of the influence of these components on parameters such as repeatability and process dynamics.

At the University of Bradford [28], a suite of sensors were installed on a standard Battenfeld Microsystem to allow evaluation of injection and cavity pressures, displacement and velocity of the injection piston and accurate thermal monitoring of the mold platen. Piezoelectric force transducers were placed behind the injection piston and cavity ejector pin to provide indirect measurements. Data generated from a single cycle of a process molding of a 25 mg component have been illustrated in figure 2.7.

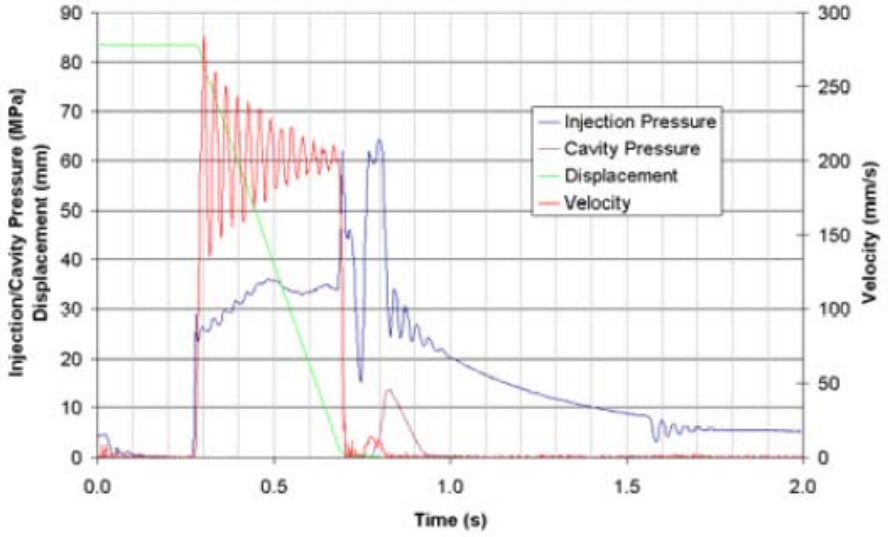

Figure 2.7 - Typical process data

Interesting features to note are the rapid acceleration of the injection piston to the desired velocity and the corresponding increase in the injection pressure trace caused by friction between the injection piston and barrel. The pressure

trace, as the cavity fills, shows a twin peak feature, the first occurring at the end of fill and the second one at the end of the hold phase, where the piston traverses, at much lower velocity, with a total displacement of one millimetre. This "twin peak" profile differs from what has seen in conventional injection molding, where a pressure feedback system allows a switchover from injection velocity to pressure control as the mold becomes full, ensuring that pressure spikes do not result and pressure is constant as cavity filling is completed. Cavity pressure measurement suggests that the product freezes less than 200 ms after it enters the cavity.

The data acquisition system provides detailed information about the process dynamics, but in a monitoring situation, it is useful to condense the data to a few values sensitive enough to indicate process variation. Previous works in this area, within conventional injection molding, have shown that integration of select regions of the injection pressure curve during mold filling can provide a useful parameter for evaluation of the repeatability of a process [29]. This method would not be seen to be directly applicable to the micro molding process because of the short injection times, but integration of the entire injection pressure curve, up to the point when the mold opens, may provide useful information about the process. Experiments have been performed at the University of Bradford to assess the sensitivity of injection and cavity pressure measurements to changes in the process conditions [30]. Four values were calculated from the process data – peak injection pressure, peak cavity pressure, integral of the entire injection pressure curve and integral of the cavity pressure curve – and the correlations of these values with mold temperature variations were calculated. The experiments highlighted the need for cavity pressure measurement in micro molding but the dimensions, fine features and complexity of micro molds make sensor installation problematic. The smallest, commercially available sensor for direct pressure measurement has a tip diameter of 1 mm, but the total volume of the device can pose challenges when considering installation in a mold where complex heating/cooling and ejection systems are commonplace. Some cavity pressure measurement systems perform an indirect measurement using ejector pin/piezoelectric force sensor techniques, but these are susceptible to sources of error such as pin friction and bending. A solution to these problems may be found by using alternative technologies. Ultrasound techniques have found use over a wide range of polymer processing applications, and recent developments in sensor technology by the Industrial Materials Institute [31] have realized the production of bismuth titanate/lead zirconate titanate (BIT/PZT) film-based transducers, which offer good thermal resistance and high sensitivity in a very small form factor. The piezoelectric films are applied

to the target surface using a Sol-Gel spray technique and poled using a corona discharge method. Sensors are then created by painting/printing a conductive electrode onto the upper side of the film and attaching the cabling to the electrode and grounded surface. The sensor uses the mold material to propagate the ultrasound signal and no machining of the cavity is required, eliminating the problem of witness marks on the product. The technology is still in its infancy, but already sensors of 2 to 3 mm diameter have been used successfully to monitor cavity filling during the micro molding process, and future refinements and signal processing techniques will ensure that the electrode size can be scaled down further for smaller cavities.

2.6 MATERIAL PROPERTIES AND REQUIREMENTS

The majority of micro molded products today are purely functional with tightly defined mechanical or optical criteria and little importance given to aesthetic or tactile properties. Therefore, typical adopted resins are engineering thermoplastics, such as liquid crystal polymers (LCP), polyoxymethylene (POM), cycle-olefin polymers (COP) and polyetherether-ketones (PEEK), which exhibit desirable mechanical and optical properties and good processibility. The use of filler materials can improve the mechanical performance of the resins, but the small feature dimensions present in micro mold cavities deny the use of conventional fillers, such as glass or carbon fibres. Nano fillers such as exfoliated clay platelets, polyhedral oligosilesquioxanes (POSS) and carbon nano tubes show potential for use in the micro molding environment. The addition of montmorillonite nano clays [32, 33, 34] to polymer systems has recently emerged as a viable method to improve mechanical, barrier and flame-retarding properties. The maximum benefits of clays, however, are only realized if care is taken to disperse the platelets evenly throughout the material (exfoliation). Exfoliation is best achieved through pre-polymerization dispersion of the clay in the monomer, but can also be achieved by shear-driven melt processing (usually extrusion). Since their discovery in 1991, carbon nano tubes [35] have caused excitement in the scientific community because of their extraordinary mechanical, electrical and thermo conductive properties. Dispersion of the nano tubes, within a polymer matrix, is possible using conventional polymer processing technology. Some microscale product applications demand material properties that cannot be satisfied using polymer resins, promoting an increasing interest in microscale powder injection molding (PIM). This technology incorporates

the blending of fine ceramic (CIM) or metal (MIM) powders with a polymer binder to form a feedstock of suitable rheology for injection molding. Once the part is molded, the polymer binder is removed in either a solvent or thermal de-binding process, and the part is subsequently sintered to form the final product. The technique offers a rapid, low-cost route for the net-shape production of complex three dimensional geometries in hitherto difficult to machine ceramics and metals.

The microscale dimensions of features and rapid filling rates, typically found occurring within micro molding cavities, ensure that the shear rates experienced by the polymer during the micro molding process are orders of magnitude higher than those experienced in conventional injection molding. By taking some typical gate dimensions and performing some simplistic calculations [38], it can be observed from figure 2.8 how shear rates in excess of 10^8 s^{-1} are feasible.

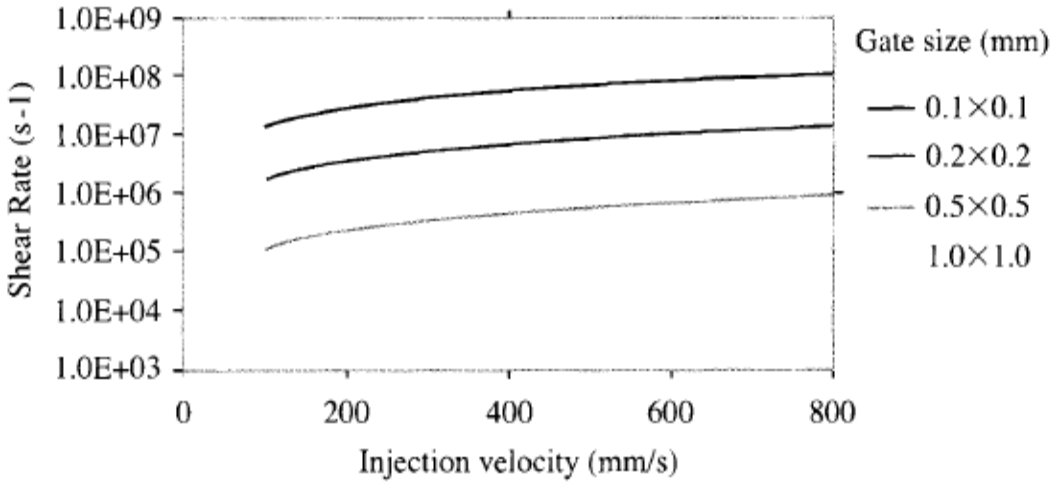

Figure 2.8 - Calculated wall shear rates for a range of gate sizes on a Battenfeld Microsystem

Rheological characterization of materials rarely extends to such rates, and the investigation of the upper end of the shear rate curve is out of the range of a conventional capillary rheometer. To evaluate the flow characteristics of polymer melt in this region, experiments have been performed using both the Battenfeld Microsystem and a Cincinnati Milacron 30 t conventional injection molding machine with a specially designed nozzle that could accept standard capillary dies. The experimental technique consisted of preparing a shot of material and then ejecting it into free space while recording the pressure within

the melt reservoir. The apparent viscosity of the melt could then be calculated from the pressure measurements combined with the known die geometry. (figure 2.9 [36]). It is interesting to note that the conventional injection molding machine is able to provide higher shear rate information than the Microsystem because, although the Battenfeld machine has a higher injection velocity, it displaces a lower volume of material and a correspondingly lower rate of melt flow through the capillary-die flow rate. The data suggest that the shear viscosity curve is smooth and continuous even in the high shear region, indicating that this polymer still behaves predictably even when subject to shear rate in excess of 10^6 s^{-1}. However, the extensional data underline that the POM material, considered in the experiments, has a tendency to strain harden at high strain rates.

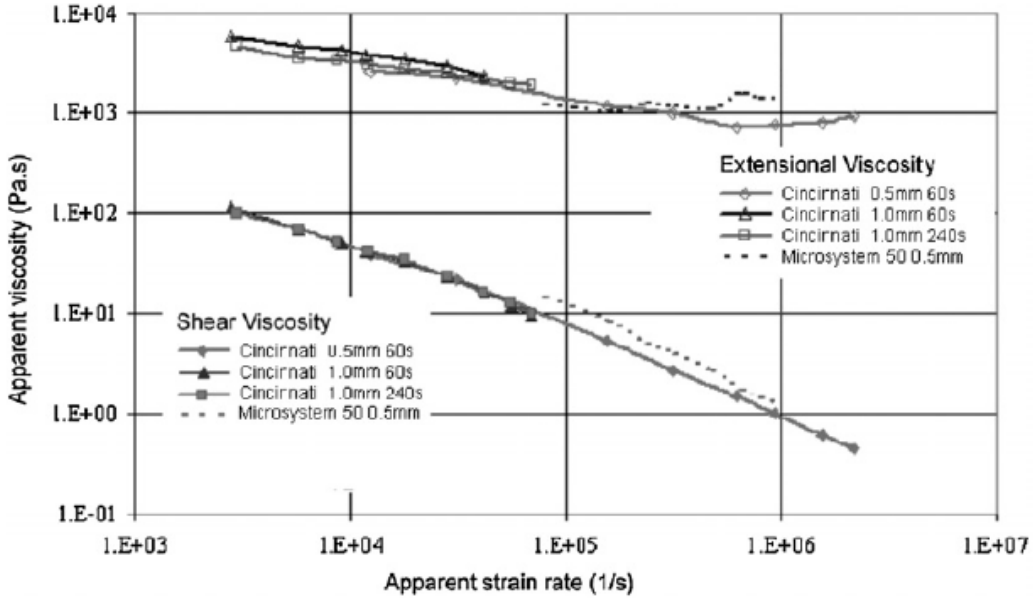

Figure 2.9 - Variations of shear viscosity vs apparent shear rate on a micro molding machine and on a classical injection molding machine as a function of strain rate

2.7 NUMERICAL SIMULATION

Given the irregular geometry of many precision components and the complex thermo-mechanical history during the injection molding cycle, it is

generally necessary to resort to numerical simulation methods to properly simulate the molding process and develop the capability of predicting the final configuration of the molded part, which is particularly important in precision injection molding operations. The first attempts to simulate the filling phase in injection molding were made in the 1980s, taking into account the spatially inhomogeneous cooling and vitrification process during filling [37], using combined finite element (2D) and finite difference (2½D) methods [38]. The focus of simulation codes has been the analysis of filling phase for precision injection molding operations [39]. To improve the predictive capabilities of the simulation codes and allow for the prediction of residual density distributions among other features, it is necessary to include a rate-dependent glass transition model in the analysis and realistic viscoelastic constitutive equations. The simulation of dimensional changes in molded parts produced from semicrystalline polymers is much less advanced because of the very complex nature of polymer crystallization in the presence of rapidly changing temperature, pressure and deviatoric stresses.

2.7.1 Filling and packing analysis

Filling is the most thoroughly studied stage of the injection molding process. Many of the early efforts were directed towards the prediction of pressure and temperature distributions and the advancement of the melt front. Barrie [40] gave an analysis of the pressure drop in both delivery systems and a disk cavity by assuming the frozen layer has a uniform thickness and that it is proportional to the cube root of the filling time. William and Lord modelled the runner system using the finite difference method and extended their analysis considering the flow front evolution during the cavity filling phase [41, 42]. A major advance was the work of Hieber and Shen [43]. Their paper introduced a hybrid analysis technique for the filling phase in which temperature and pressure equations were solved using finite differences and finite elements, respectively. Frequently referred to as 2.5D, this analysis technique remained the cornerstone of commercial simulation until the mid 1990s, when full three dimensional analyses appeared. Numerical simulations were performed according to the mass, momentum and energy conservations laws, briefly described here.

For a compressible melt, the conservation of mass equation takes the form:

$$\frac{\partial \rho}{\partial t} + (\nabla \cdot \rho \bar{v}) = 0 \tag{1}$$

where $\rho = \rho(\bar{x}, t)$ is the density of the fluid and $\bar{v} = v(\bar{x}, t)$ is the fluid velocity. The conservation of momentum equation may be written:

$$\frac{\partial}{\partial t}(\rho \bar{v}) + \nabla \cdot \rho \bar{v} \bar{v} = \nabla \cdot \bar{\sigma} + \rho \bar{g} \tag{2}$$

where $\bar{\sigma}$ is the stress tensor and $\bar{g} = \bar{g}(\bar{x}, t)$ is the acceleration due to gravity. The above equation deals with the conservation of linear momentum only. It is also necessary to consider the conservation of angular momentum. Indeed, it turns out that the necessary and sufficient condition for the conservation of angular momentum is that the stress tensor $\bar{\sigma}$ be symmetric [44]. Finally, the conservation of energy takes the form:

$$\rho c_p \left(\frac{\partial T}{\partial t} + \bar{v} \cdot \nabla T \right) = \beta T \left(\frac{\partial p}{\partial t} + \bar{v} \cdot \nabla p \right) + p \nabla \cdot \bar{v} + \bar{\sigma} : \nabla \bar{v} + \nabla \cdot (k \nabla T) \tag{3}$$

where c_p is the specific heat, measured at constant pressure, T is the local temperature, β is the coefficient of volume expansion, p is the local pressure and k is the thermal conductivity of the fluid. The above equations are quite general. For simulating injection molding process, some simplifications have to be taken considering:

- material properties;
- geometric considerations;
- mathematical manipulation.

2.7.2 Material properties

For fluids, the stress tensor can be decomposed in a pressure part and an extra-stress tensor as follows:

$$\bar{\sigma} = -p\bar{I} + \bar{\tau} \tag{4}$$

where $\bar{I}$ is the identity tensor, p the pressure, and $\bar{\tau}$ is known as the deviatoric or extra-stress tensor. To make some progress in modelling using a continuum approach, a relationship between the stress and the kinematics of the fluid motion is required. A particularly simple relationship is the Newtonian fluid assumption defined by setting:

$$\bar{\sigma} = -p\bar{I} - \frac{2}{3}\eta(tr\bar{D})\bar{I} + 2\eta\bar{D} \tag{5}$$

where η is the fluid viscosity and $\bar{D}$ is the strain rate tensor. Hence, the extra stress tensor has the form:

$$\bar{\tau} = -\frac{2}{3}\eta(tr\bar{D})\bar{I} + 2\eta\bar{D} = \eta\dot{\gamma} \tag{6}$$

where $\dot{\gamma}$ is the deviatoric strain tensor rate. In order to better capture the behaviour of polymer melts, we allow the viscosity to depend on the strain rate. This defines a class of fluids, called generalized Newtonian fluids, which are of use in describing flows dominated by shear forces [45].

There are several possible choices for the viscosity function. The Cross model is commonly used and has the form:

$$\eta = \frac{\eta_0}{1 + \left(\frac{\eta_0\dot{\gamma}}{\tau^*}\right)^{1-n}} \tag{7}$$

where η_0 is the viscosity at zero shear and τ* is the shear stress at the transition between Newtonian and power law behaviour. It is usual to include the effect of temperature on the viscosity by means of an Arrhenius or WLF (William Landel ferry) correction. In the case of WLF, it is set:

$$\eta_0 = D_1 \exp\left[\frac{-A_1(T - T^*)}{A_2 + (T - T^*)}\right] \tag{8}$$

where D_1, A_1, A_2 and T* are constants to be determined.

2.7.3 Geometric considerations

The afore-mentioned equations are quite general and impose no constraint on the flow geometry. However, most injection molded components are thin walled (typical thickness 2H is much smaller than a typical length). Adopting a Cartesian coordinate system in which the x-y plane is defined as the plane of the part and considering the density dependent on pressure and temperature, the continuity, momentum and energy equations for a generalized Newtonian fluid take the form:

$$0 = k\frac{Dp}{DT} - \beta\frac{DT}{Dt} + \frac{\partial v_x}{\partial x} + \frac{\partial v_y}{\partial y} + \frac{\partial v_z}{\partial z} \tag{9}$$

$$\frac{\partial p}{\partial x} = \frac{\partial}{\partial z}\left(\eta\frac{\partial v_x}{\partial z}\right) \tag{10}$$

$$\frac{\partial p}{\partial y} = \frac{\partial}{\partial z}\left(\eta\frac{\partial v_y}{\partial z}\right) \tag{11}$$

$$\frac{\partial p}{\partial z} = 0 \tag{12}$$

$$\rho c_p\frac{DT}{Dt} = \beta T\frac{Dp}{Dt} + \eta\dot{\gamma}^2 + \frac{\partial}{\partial z}\left(k\frac{\partial T}{\partial z}\right) \tag{13}$$

where

$$v = \frac{1}{\rho} \tag{14}$$

$$k = -\frac{1}{v}\left(\frac{\partial v}{\partial p}\right)_T \tag{15}$$

$$\beta = \frac{1}{v}\left(\frac{\partial v}{\partial T}\right)_p \tag{16}$$

are the specific volume, the isothermal coefficient of expansion and the expansivity of the material, respectively. That the pressure has no dependence on the z coordinate is of particular importance; the pressure is assumed constant through the thickness of the part.

2.7.4 Simplification by mathematical analysis

The momentum equation (equations 10 and 11) may be integrated twice with respect to z across the cavity thickness. Carrying out the integration and assuming the fluid velocity is zero at the mold wall (no slip condition), the following relationships are obtained:

$$v_x(x,y,z) = \frac{\partial p}{\partial x}\left[\int_{-H}^{z}\frac{z'}{\eta}dz' - C(x,y)\int_{-H}^{z}\frac{dz'}{\eta}\right] \tag{17}$$

$$v_y(x,y,z) = \frac{\partial p}{\partial y}\left[\int_{-H}^{z}\frac{z'}{\eta}dz' - C(x,y)\int_{-H}^{z}\frac{dz'}{\eta}\right] \tag{18}$$

where

$$C(x,y) = \frac{\int_{-H}^{H}\frac{z}{\eta}}{\int_{-H}^{H}\frac{dz}{\eta}} \tag{19}$$

To establish an equation for the pressure involving only the x and y coordinates, equation 13 is substituted into equation 9 and integrated across the cavity thickness to obtain:

$$0 = \int_{-H}^{H}\left\{k\frac{Dp}{Dt} - \frac{\beta}{\rho c_p}\left[\beta T\frac{Dp}{Dt} + \eta\cdot\gamma^2 + \frac{\partial}{\partial z}\left(k\frac{\partial T}{\partial z}\right)\right] + \frac{\partial v_x}{\partial x} + \frac{\partial v_y}{\partial y} + \frac{\partial v_z}{\partial z}\right\}dz =$$

$$= \int_{-H}^{H}\left\{k\frac{Dp}{Dt} - \frac{\beta}{\rho c_p}\left[\beta T\frac{Dp}{Dt} + \eta\cdot\gamma^2 + \frac{\partial}{\partial z}\left(k\frac{\partial T}{\partial z}\right)\right]\right\}dz + \int_{-H}^{H}\left(\frac{\partial v_x}{\partial x} + \frac{\partial v_y}{\partial y}\right)dz + \left[v_z\right]_{z=-H}^{z=H}$$

$$= \int_{-H}^{H}\left\{k\frac{Dp}{Dt} - \frac{\beta}{\rho c_p}\left[\beta T\frac{Dp}{Dt} + \eta\cdot\gamma^2 + \frac{\partial}{\partial z}\left(k\frac{\partial T}{\partial z}\right)\right]\right\}dz + \frac{\partial}{\partial x}\int_{-H}^{H}v_x dz + \frac{\partial}{\partial y}\int_{-H}^{H}v_y dz$$

where, in the last step, the no-slip condition has been assumed. Defining the melt fluidity as:

$$S = \frac{1}{2}\left\{\int_{-H}^{H}\frac{z^2}{\eta}dz - \frac{\left(\int_{-H}^{H}\frac{z}{\eta}dz\right)^2}{\int_{-H}^{H}\left(\frac{dz}{\eta}\right)}\right\} \tag{20}$$

the final equation for pressure can be written as:

$$\frac{\partial}{\partial x}\left(S\frac{\partial p}{\partial x}\right) + \frac{\partial}{\partial y}\left(S\frac{\partial p}{\partial y}\right) = \frac{1}{2}\int_{-H}^{H}\left\{k\frac{Dp}{Dt} - \frac{\beta}{\rho c_p}\left[\beta T\frac{Dp}{Dt} + \eta\dot{\gamma}^2 + \frac{\partial}{\partial z}\left(k\frac{\partial T}{\partial z}\right)\right]\right\}dz \tag{21}$$

The left-hand side of the final equation is immediately recognizable as a two-

dimensional Hele-Shaw flow. Mathematical studies of such flows have been considered by Richardson [46] as a model for the injection of a fluid into a thin-walled cavity well before any commercial program was available.

2.7.5 Solution of the governing equations

The equations used for simulation of the injection molding process are a single equation for pressure as a function of the x and y coordinates (equation 21) and an equation for temperature (equation 13). With appropriate boundary conditions, these equations may be readily solved a hybrid scheme introduced by Hieber and Shen [47] in which finite element and finite difference methods are used for the solution of the pressure and temperature fields, respectively. Kennedy has provided details on the solution algorithms and methods [48].

As the pressure field varies only in x and y, the mesh required for the finite element scheme is a two dimensional network of triangles or quadrilaterals embedded in three dimensional space. The nodes forming the mesh are located at the part midplane. The grid for the temperature field, however, fills the domain occupied by the melt and so is fully three dimensional. The fact that calculated pressure and temperature fields are respectively 2D and 3D has led to the use of the term 2.5D analysis for this kind of injection molding simulation.

2.7.6 Thermal boundary conditions

In microscale injection molding, various experimental results have revealed that surface heat transfer plays an important role. For numerical simulations, this means that thermal boundary conditions need to be chosen carefully. Several researches [52, 53, 54] have investigated the interface heat transfer coefficient in microscale injection molding. It has been found that the coefficient changed with time during an injection cycle. During the filling stage, the typical value could vary from 2000 to 5000 W/m^2K [55]. A smaller value of 1200 W/m^2K has been proposed in Ainoya's work [56]. During the cooling stage, the cavity pressure can drop to zero locally after the gate has frozen, resulting in the formation of an air gap between the polymer and the mold wall due to shrinkage. The heat transfer coefficient could drop down to around 100 W/m^2K. In micro injection molding, the detachment of the

polymer from the mold wall could occur earlier in the filling stage because solidification in microstructures may have already begun during the filling phase. This may give rise to a significant change in the thermal properties at the interface. Yu et al. have compared two types of boundary conditions for the calculation of heat transfer at the melt-wall interface:

$$q = h(T_{z=b} - T_w) \tag{22}$$

$$q = h_x(T_m - T_w) \tag{23}$$

where q is the heat flux, $T_{z=b}$ is the melt temperature at wall, T_m is the gapwise average temperature and T_w is the wall temperature. In equation 22, the melt/wall interface heat transfer coefficient is assumed constant. A default value of 25000 W/m²K has been employed in the Moldflow® simulations for most conventional injection molding applications. In equation 23, the local heat transfer coefficient h_x has been introduced to include the varying heat transfer rate. The value of h_x is dependent on the flow field as:

$$h_x = \frac{Nu_x k}{D_h} \tag{24}$$

where Nu_x and D_h are the local Nusselt number and the hydraulic diameter, respectively. According to Shah and London [59], a correlation proposed for forced convection in laminar flow between two parallel plates is:

$$Nu_x^0 = \left\{1.233(x^*)^{-1/3} + 0.4\right\} \qquad \text{for } x^* \le 0.001 \tag{25}$$

$$Nu_x^0 = \left\{7.541 + 6.874(1000x^*)^{-0.488} e^{-245x^*}\right\} \qquad \text{for } x^* > 0.001 \tag{26}$$

Here x^* is the dimensionless axial distance from the channel entrance, defined as:

$$x^* = \frac{x}{D_h \,\mathrm{Re}\,\mathrm{Pr}} \tag{27}$$

where Re is the Reynolds number and Pr is the Prandtl number. In order to take into account the effect of viscosity variation when the fluid is being cooled, the Nusselt number has to be corrected as:

$$Nu_x = Nu_x^0 \left(\frac{u_b}{u_w}\right)^{0.25} \tag{28}$$

where u_b and u_w are the bulk viscosity and the viscosity at wall.

2.7.7 Inverse analysis for the heat transfer coefficient estimation

Filling simulations have been performed using the x-z plane hybrid numerical approach with different heat transfer coefficients on a macroscale component with opportunely designed micro features and their results have been compared to the experimental ones [60]. To quantify the effect of the heat transfer coefficient variation, the relative differences of pressure for each h with respect to the one obtained with h_x is calculated as:

$$\text{Relative difference} = \frac{p_h - p_{hx}}{p_{hx}} \tag{29}$$

where p_h and p_{hx} are the predicted pressure drops assuming a constant h (equation 22) and variable h_x (equation 23), respectively. Simulation results are obtained using the default value h=25000 W/m²K in the main flow. Three different values (500, 2000 and 25000 W/m²K) are used for the heat transfer coefficient in the micro channel. For a default value of the transfer coefficient and most of the main flow velocities, the filling lengths in the micro channel are underpredicted. This is because the melt near the wall of the main flow freezes too quickly when its temperature drops below the melting point before it can enter the micro channel. When the main flow heat transfer coefficient is reduced, the filling is overpredicted or underpredicted depending on the value of the heat transfer coefficient (figure 2.11). Using a constant heat transfer coefficient does not appear to be a good choice.

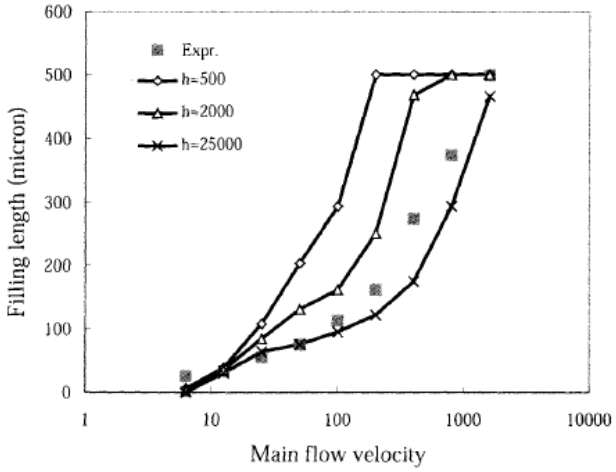

Figure 2.11 – Comparison between filling length prediction and experimental results.

2.7.8 Other microfluidic related issues

In the microscale the polymer flow may behave differently from the macroscale. Size-dependent rheological models may be required for flow in micro channels. Furthermore, polymers have a tendency to slip in micro channels at high wall shear stresses. Elastic effects and flow instabilities can also be significant. A number of publications indicate that the viscosity of liquids like water, silicon oil, alcohol and polymer solutions close to the micro channel wall can be 50 to 80% higher than their bulk viscosity [61, 62]. This increase may be due to the collective molecular motion or the immobility of the layer at the interface. Eringen et al. [63] introduced a nonlocal continuum theory of viscous liquids. The following equation is used to calculate the viscosity while taking into consideration the microscale effects:

$$\eta = \eta_b[1 + \xi(g/D)^2] \tag{30}$$

where η_b is the bulk viscosity, ξ is a non-dimensional constant, g is the gyration radius of fluid molecules and D is the external characteristic length. The variable η is referred to as "microscale viscosity". Yao et al. [64] used this equation in calculating the gapwise velocity profiles of the steady state power-law viscous flow in a slit. The calculated data show that the flow rate with the microscale viscosity is lower than that with the bulk viscosity by 2, 5, 36 and 94% for 200, 20, 2, 0.2 μm gaps.

Rosenbaum et al. have introduced a power-law slip model for slip velocity [65]:

$$u_s = \frac{a}{1 + (\sigma_c / \sigma_w)^K} \sigma_w^i \tag{31}$$

where σ_w is the wall shear stress, σ_c is the critical wall stress for slip, i is a power-law index, and a is a scalar coefficient. When the wall stress exceeds the critical value, wall slip will occur. This critical stress was estimated as 0.1 MPa for many polymer melts [65]. Yao et al. [66] conducted isothermal filling simulations between two parallel plates with the gap varying from 0.2 to 2000 μm and the filling time kept the same. Considering the wall slip effect, the velocity at the wall increases when the wall stress exceeds the critical value. The wall slip effect results in a plug flow-like velocity profile as the gap decreases to 0.2 μm. However, the microscale viscosity effect tends to compensate for the wall slip effect in their calculations.

2.8 PRODUCT PROPERTY MEASUREMENT

The scale of micro molded products causes problems when considering assessment of dimensional and mechanical properties. Conventional geometry assessment and standard mechanical testing techniques are difficult to apply and alternatives must be sought. Many commercial micro molding processes adopt machine vision systems to allow evaluation of dimensional properties for quality assessment during the fabrication process. A typical system photographs each product after ejection from the mold using an array of up to four cameras and is able to assess the quality of the molding using a number of predefined dimensional tolerances. This system is very useful for identifying part-filled (short shots) and over-filled (flashed) components.

Scanning electron microscopy (SEM) is a popular tool for looking at three dimensional details and evaluation of dimensions and features of microscale components and systems. However, evaluation of surface properties (R values) and information about the depth of features is not possible using this technique. A further drawback of the technique is that polymer products usually requires a layer of gold plating to make them conductive so as to produce an acceptable image and also to avoid erosion caused by the high-power electron beam.

White light interferometry is a surface characterization technique for measuring the height profile of objects. It is a non-contact technique that uses the interference pattern of light reflected from a surface with a reference beam from the same source to calculate surface height. The equipment uses high magnification lenses to ensure good lateral resolution and large area scan can be performed by traversing the stage upon which the sample is mounted in a raster fashion and stitching together the resulting images. The equipment can also be calibrated to provide accurate three dimensional assessment of a feature and can perform a variety of roughness calculations for surface property measurement. The equipment is well suited for evaluation of polymer and cavity surfaces, but problems can occur when attempting to image a sample that reflects light poorly or one containing large inclines or highly curved surfaces that scatter light away from the lens, causing data loss.

Atomic force microscopy (AFM) is a technique that has been developed to characterize sample surface properties which employs a probe consisting of a microscale silicon device containing a protruding and flexible cantilever with a fine tip at the unconstrained end. The tip is traversed across a sample material using a piezoelectric tube and the deflection of the tip is monitored optically using a laser and position sensitive detector. This

technique allows for measurements of the topography of a sample to nanometre precision in three dimensions but over a limited area of approximately 100 μm x 100 μm. The friction present at the tip as it is translated across the sample can be problematic during the study of soft materials because damage to the sample surface can occur. To overcome this problem, the AFM can operate in a "tapping mode", where the silicon component is piezoelectrically oscillated causing the cantilever to tap the surface approximately 104 times per second as it travels across the sample. This mode offers a number of benefits over the standard mode. As first, the frictional force at the tip is reduced so no surface damage or lateral bending of the cantilever occurs and good contrast can be seen between the component materials in multiphase systems such as polymer blends or filled suspensions such as nano composites. The AFM can also be used to measure the mechanical properties of surfaces by forcing the tip into the sample and measuring the resulting deflection over a sample area. The main limitations of the AFM are the maximum scanning range of 100 μm x 100 μm and the head geometry, which restricts analysis of cavity depths greater than 100 μm.

X-ray diffraction is a useful tool for characterizing crystal structure formation within a crystalline material. X-rays are generated in a synchrotron and focused to form a beam that is incident upon the target material and may be scattered. Small angle X-ray diffraction (SAXS) and wide angle X-ray diffraction (WAXS) can be used to determine crystal structure and molecular orientation. This is of great interest when considering micro molded products that contain high strain rate flows and high temperature gradients.

CHAPTER 3

VALIDATION OF FILLING SIMULATIONS IN MICRO INJECTION MOLDING

3.1 THE IMPORTANCE OF A QUANTITATIVE METHOD IN EVALUATING MICRO FILLING PERFORMANCE

The rapid growth in the use of advanced materials in a large number of highly demanding automotive, electronic and consumer applications has promoted the development of new and more complex material forming processes. A good understanding of the interaction between material and processing conditions is important in order to comply with stricter tolerances and demanding service conditions. This is particularly important in the case of forming processes involving the filling of a mold where the coupled phenomena of fluid flow and heat transfer determine, to a large extent, the

final properties of the molded part. Because of their cost effectiveness and rapid response, numerical simulations have become an increasingly important tool for the design and evaluation of processing parameters. Numerical investigations are able to estimate aspects of the physical model which would be difficult to quantify otherwise. They allow quick responses on what will be the effects of process parameters changes on the final part. Although Computer Aided Engineering (CAE) has been used with increasing success in the design and manufacture of polymer products and processes, the injection molding process involving microstructures (μIM) presents many challenges. The flow behaviours of polymer melts in micro mold cavities have not been fully understood. It is believed that, due to the large surface-to-volume ratio, surface effects will dominate the flow behaviour at the microscale [67]. Material data and constitutive equations are, together with software processors and validation procedures, the three elements that equally contribute to the effective use of process simulation technology. Over the last decade, before the availability of efficient, easy-to-use and economical simulation software and computer systems, not so much attention and resources were paid to investigate constitutive models and materials data relevant to micro process conditions. The first aim of this work is to develop a systematic and quantitative method to evaluate whether the present numerical commercial codes are suitable to characterize melt flow patterns in micro cavity filling. The outcome will be the identification of the limits of present numerical codes in order to:

- investigate physical effects and parameters with different behaviours on micro/macro scale, which could have more influence on micro cavity filling;
- perform the correct interpretation of the numerical simulation results in industrial applications;
- implement new constitutive equations or material models in order to improve numerical simulation results.

3.2 CONVENTIONAL METHODS TO VALIDATE FILLING SIMULATIONS

In conventional injection molding (macro dimensional range), a common approach to study the melt flow development inside the cavity is the "short shots" analysis, which consists in the comparison between simulation and partial filling steps (figure 3.1). One of the main condition that has to be

respected, in order to apply this method, is that the machine resolution (the smallest shot that can be injected in a controlled manner) has to be smaller than a fraction of the part which is significant to give information about intermediate filling stages. This condition can be fulfilled by injection molding machines having an injection-plunger unit. On the other hand, small injection molding machines, with the conventional plastication unit with reciprocating screw, cannot provide controlled short shots in the order of fraction of 1 mm^3 (typical volume of polymer micro parts). Furthermore, in conventional machines the screw acceleration may not be high enough to provide the required injection speed in the short time needed to produce micro short shots.

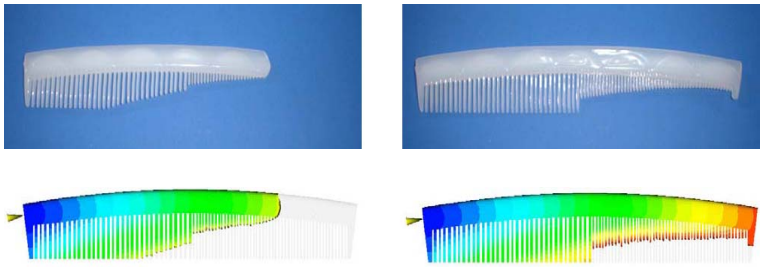

Figure 3.1 - Short shots of a conventional product compared to software prediction.

Flow visualization can also be used to describe the flow front advancement during the filling stage. It consists in the use of a high speed camera capable of actually recording, at high frame rates (in the order of 103-104 frames per second), the flow advancement inside the micro cavity. In order to achieve such results, the mold has to be provided with a lateral opening (camera access to the mold) and one side of the cavity made of glass. By subsequent image processing of the recorded film of the cavity filling, it is possible to perform a time-dependent analysis of the flow front displacement (figure 3.2). The flow visualization method offers a better resolution than the short shots method. On the other hand, the construction of the mold itself is quite complicated due to the presence of a perfectly aligned optical glass and an optical mirror conveying the image from the cavity, through the glass and on to the external camera. As a consequence, the method seems of difficult implementation in an industrial environment.

Another method, commonly used in conventional injection molding to validate software simulations, is the pressure evolution comparison during cavity filling. The pressure history (in-cavity pressure) is imposed on the material during the molding cycle and is closely associated with several process

parameters (injection pressure, holding/packing pressure, shot size, clamping force and injection rate), but its evolution, over time, depends on the cavity geometry and the temperature history/compressibility of the polymer material.

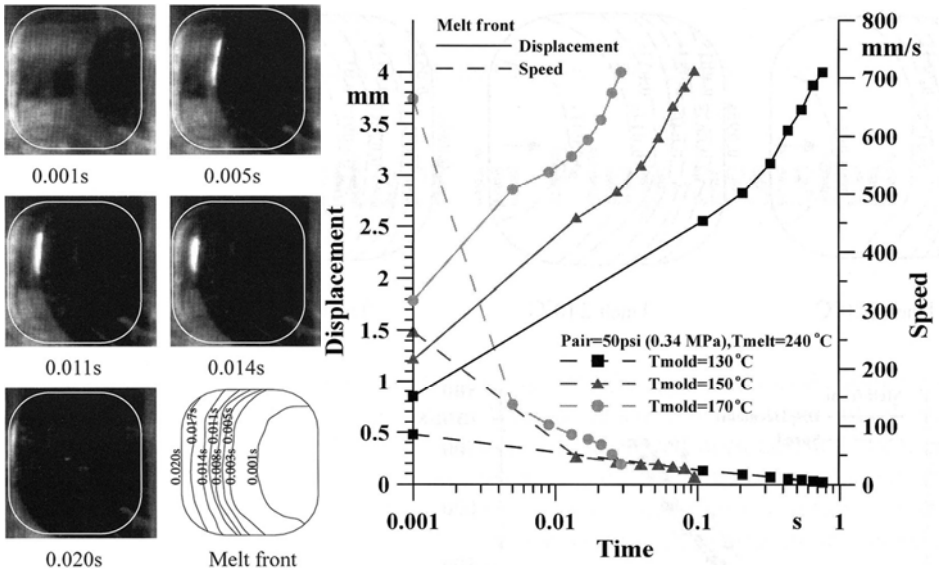

Figure 3.2 - Flow visualization of the melt front using high frame rate speed camera and subsequent flow tracing (left). Displacement and speed of the flow front as a function of the mold temperature (right) [68].

The experiments, conducted at the University of Bradford [4], have also underlined the need for cavity pressure measurement during the micro molding process, but the dimensions, fine features and complexity of micro molds make sensor installation problematic. The smallest, commercially available sensor for direct pressure measurement has a tip diameter of 1 mm, but the total volume of the device can pose challenges when considering installation in a mold where complex heating/cooling and ejection systems are commonplace. Some cavity pressure measurement systems perform an indirect measurement using ejector pin/piezoelectric force sensor techniques, but these are susceptible to sources of error such as pin friction and bending. Ultrasound techniques have found use in a wide range of polymer processing applications, and recent developments in sensor technology, by the Industrial Materials Institute [69], have realized the production of bismuth titanate/lead zirconate titanate (BIT/PZT) film-based transducers, which offer good thermal resistance and high sensitivity in a very small form factor. The

technology is still in its infancy, but already sensors of 2 to 3 mm diameter have been used successfully in monitoring cavity filling during the micro molding process, and future refinements and signal processing techniques will ensure that the electrode size can be scaled down further for smaller cavities.

3.3 A NEW APPROACH FOR THE VALIDATION OF FILLING SIMULATIONS

The scaling-related question to be answered in injection molding is how the standard molding know-how for part and tool design, process setup, material characterization, modelling and simulation can be properly scaled and used for miniaturized parts. The standard injection molding process is characterized by a filling time of several tenths of a second to several seconds, an injection molding pressure of several megapascals to about 200 megapascals, and a cycle time of several seconds to several 10s of seconds. Such process conditions comply with the physical limit of the standard tools with which the thermoplastics can flow well in the mold cavity in forming regular products as demanded. By physically understanding the scaling limitations of the existing molding technology, improvements, alternatives, and solutions could be developed to overcome the current difficulty in molding high aspect ratio microstructures and ultrathin-wall sections with high L/T ratios. In this work, dimensionless analysis has been performed first to study the size effect on the flow and heat transfer process, succeeded by moldability analysis using molding simulations. A new approach has been introduced in order to evaluate whether the present numerical commercial codes are suitable to characterize melt flow patterns and compare micro filling results to numerical simulations. It consists in the determination of the flow pattern by using the weld lines as flow markers. The proposed approach is an alternative technique to the "short shots" method, which predicts the shape of the free surfaces with a large approximation due to the stress relaxation and thermal contraction. The prediction from three dimensional models and standard Hele-Shaw flow are compared to molding results (figure 3.3). Furthermore, this approach has been used to determine which factors or parameters models, with different behaviour on micro/macro scale, could have a significant effect on micro cavity filling. By implementing constitutive equations and parameters models valid on microscale, improvements in molding simulation accuracy are expected.

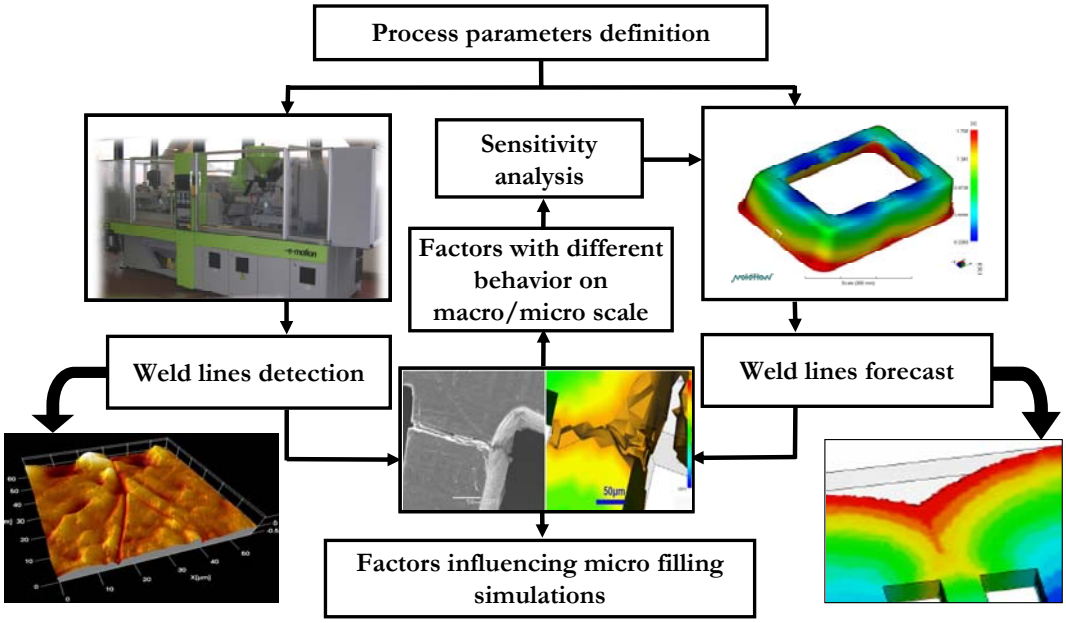

Figure 3.3 - A new approach for filling validation

.

CHAPTER 4

DEDICATED MICRO CAVITY DESIGN AND MANUFACTURING

4.1 CAVITY DESIGN AND DIMENSIONS DEFINITION

The main objective of micro cavity design has been to create an effective response variable to compare the results of numerical simulations and experiments. Obstacles as high as the total depth of the cavity were created. In this way, the melt flow was not allowed to climb over the features and when the separated melt fronts rejoined, at some downstream location, weld lines were formed. Geometries and dimensions (figure 4.1) were selected according to existing industrial devices (blood separators and micro pumps) and in order to exalt such factors that change their relevance when shifting from conventional to micro injection molding, such as:

- elongational flow;
- heat transfer in different thickness;

- wall slip;
- elastic behaviour of polymers.

In the first part of the cavity, a convergent geometry was created in order to pull out the extensional flow and elastic behaviour of the melt in convergent/divergent geometries. A step was created in the middle part of the cavity in order to originate a three dimensional flow and to align the flow front before the micro channels entrance; furthermore, the direction of the expected weld line, after the two holes, could give information regarding the shape of the flow front in the second part of the cavity. Channels as wide as 150µm, 200µm, 300µm, 450µm and 600µm were created in the second part. Heat transfer in variable thickness and different rheological models were considered. The gate (400 µm wide and 250 µm thick) was realised, as small as possible, in order to approximate it as an injection point. The filling by film layer, indeed, would have permitted consideration of the flow in the two dimensional range and this was considered irrelevant to the project.

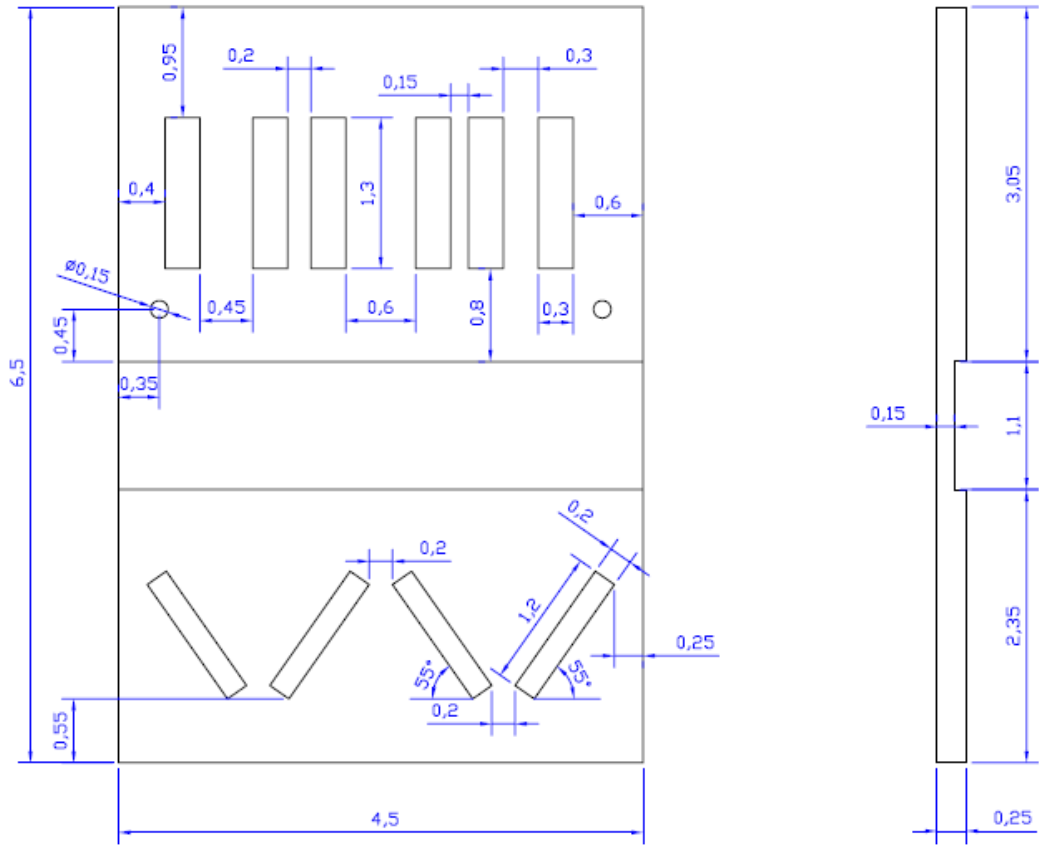

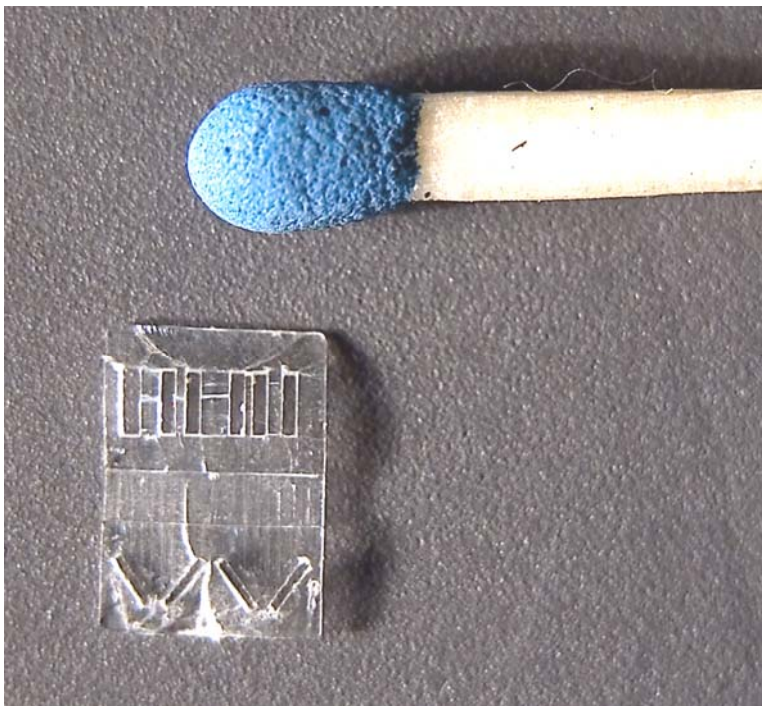

Figure 4.1 - micro cavity design (dimensions in mm) and manufactured part compared to a match.

The alternative that has been proposed in this thesis is to use the weld lines as a comparison term between software simulation and experimental filling results. The exact prediction of the weld line position will demonstrate a good degree of accuracy of the filling simulation software.

4.2 CAVITY MANUFACTURING AND MOLD CONFIGURATION

Due to the dimensions and high tolerances required for the features of the final micro part, a scaled down version of the conventional electro-discharge machining (EDM) process has been employed. Electro-discharge machining is a technique that can be used to form shaped cavities in any material that reasonably conducts electricity. A voltage is applied through a dielectric medium between the tool electrode and the workpiece, using electro-discharge generated when the electrode and workpiece are positioned close to each other (figure 4.2).

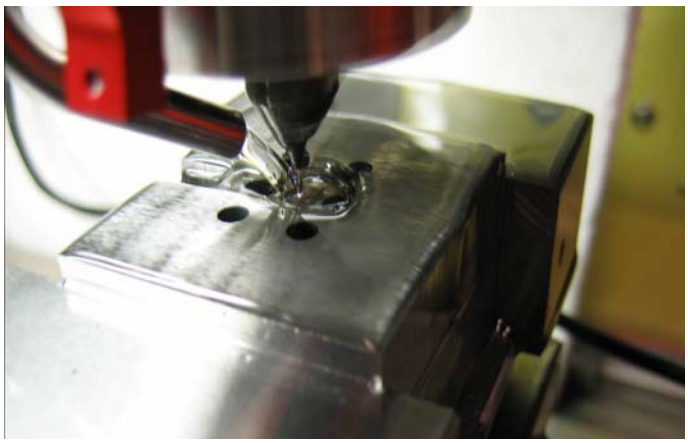

Figure 4.2 – Micro electro-discharge machining

The required shape is eroded into a workpiece electrode with an electrical discharge from a shaped tool electrode in a dielectric bath. The bath cools the electrodes and removes debris from the workpiece; the voltage across the electrode can be altered to determine the amount of material removed by each spark. Using this method, a cavity can be formed initially using a high voltage, which is then reduced slowly as the product approaches the desired dimension to give an acceptable surface quality. The process is well suited to machining hard materials to single figure micron tolerances. The characteristics of the hard steel material used in the process have been set forth in table 4.1. Good surface finishes were achieved by using a minimal discharge and reducing the gap between the electrode and component to sub-micron tolerances. Average surface roughness (Ra) was measured and resulted in a value of 0.15 μm. Details on the micro cavity manufacturing, including optimization of machining parameters and surface topographical analysis, have been set forth in [70].

Mold material: IMPAX® SUPREME	
Density	7.8 g/cm^3
Specific heat coefficient	460 J/Kg-C
Thermal conductivity	29 W/m-C
Elastic modulus	200000 Mpa
Poisson ratio	0.33
Linear expansion coefficient	1.27 ·10 1/C

Table 4.1 - Mold characteristics of IMPAX® SUPREME.

As it is typical in the micro injection molding process, the mold is characterized by modular parts. The employed mold was made up of the sprue system, the runner system and the micro cavity insert to be filled (figure 4.3 [71]). The sprue and the runner system were obtained from a unique steel block, while the micro cavity was machined in an insert that was then connected to the runner system.

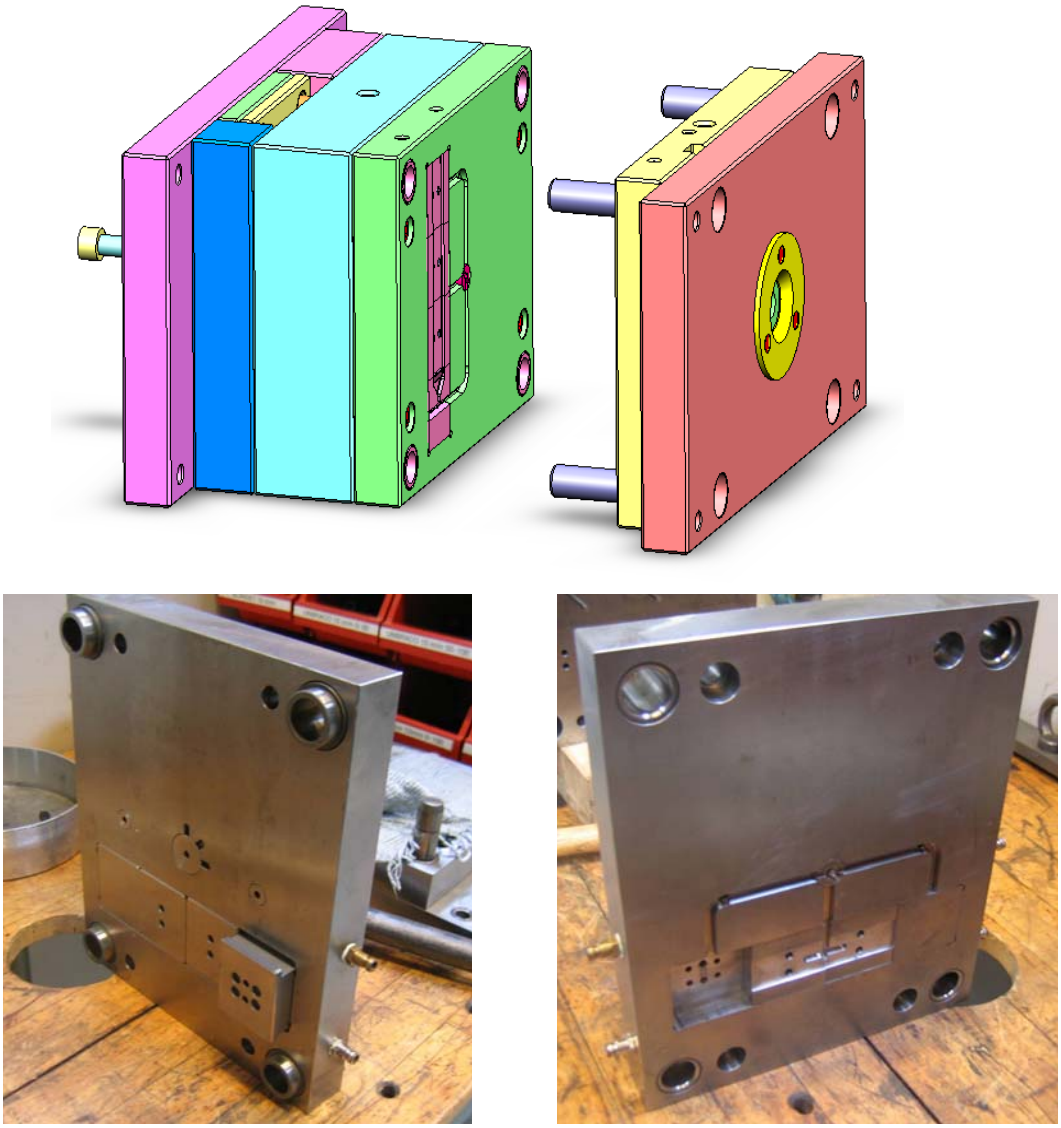

Figure 4.3 - CAD model of experimental mold (no specific scale); employed mold and particular of the micro cavity insert.

CHAPTER 5

PROCESS SETUP AND DATA ACQUISITION

5.1 EXPERIMENTAL PLAN DESIGN

This chapter will focus on the analysis of pressure and thermal conditions development in the micro cavity and claims to determine the impact of that development on the cavity properties. Comprehensive accounts of process analysis from a practical engineering perspective have been given by Sarholz [71, 72] and Stitz [73]. The machine settings can directly affect process conditions in the cavity. However, the relationship between machine settings and process conditions in the cavity depends on other factors, such as actual machine performance, machine control system, plastic material, part geometry, location in the cavity, feed system, mold cooling system, mold material and

mold elasticity. In addition, the relationships between machine-settings and cavity process parameters typically involve substantial parameter interaction and non-linearity. As an example of non-linearity, the relationship between the injection flow rate and injection pressure can be mentioned [74]. At low injection flow rates (the thermally dominated domain), the development of the frozen layer and the cooling of the bulk plastic material give rise to increasing injection pressure at decreasing injection flow rate. At higher flow rates (the shear dominated domain), the move towards more isothermal conditions is overshadowed by increased shear, causing injection pressure to increase with increasing injection flow rate. In order to determine a correlation between different machine settings and process conditions in the micro cavity (weld lines position), an experimental plan has been designed. The same process parameter settings will then be implemented in software simulations and experimental results will be compared to the numerical ones in order to assess the software sensitivity to the same process changes.

5.1.1 Control factors definition

To investigate the influence of process parameters on the weld lines formation in the micro cavity, a statistically designed experiment was carried out. Four different process parameters were varied in order to determine their influence on the micro injection molding process: the melt temperature, the mold temperature, the injection velocity and the packing pressure. A full factorial design was carried out performing $2^4=16$ molding experiments (each parameter being varied between two levels) with 5 replications. In this way, the influence of the main effects as well as the interactions was evaluated. The sequence of experimental runs was organized around the mold temperature change and secondary the melt temperature change. This was done because the mold temperature, followed by the melt temperature, took the longest time to achieve stability after change. The experimental sequence has been summarized in table 5.1.

Factor levels were established with the aim of keeping a realistic industry relevant perspective. To cover the limits of an actual process window (figure 5.1), the minimum and maximum values for each process factor were determined. The melt temperature (implemented as barrel temperature) and the mold temperature (implemented as coolant temperature and controlled using temperature sensors placed in the mold) levels were selected according to recommended values and limits published by the material suppliers. No

rigid guidelines exist for the specific values of the injection speed.

Run order	T melt	T mold	Pack P	Inj vel
1	-1	-1	-1	1
2	-1	-1	1	-1
3	-1	-1	1	1
4	-1	-1	-1	-1
5	1	-1	-1	-1
6	1	-1	-1	1
7	1	-1	1	1
8	1	-1	1	-1
9	-1	1	-1	-1
10	-1	1	-1	1
11	-1	1	1	-1
12	-1	1	1	1
13	1	1	1	1
14	1	1	-1	-1
15	1	1	-1	1
16	1	1	1	-1

Table 5.1 - Experimental plan design

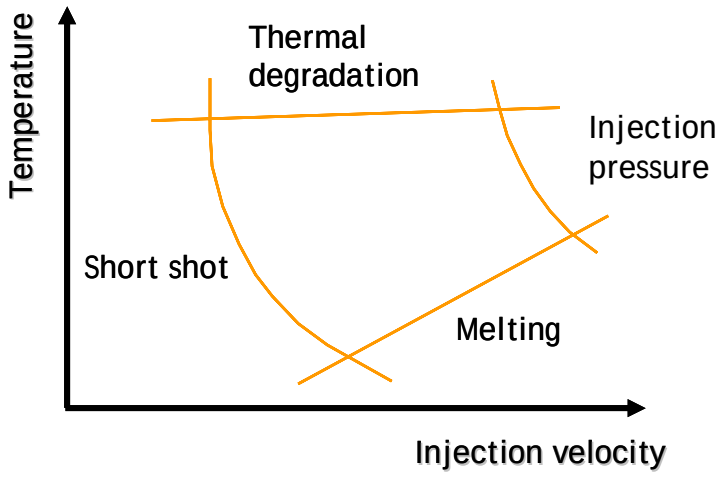

Figure 5.1 - Process window

Qualitative recommendations for injection velocity can be found in various published guidelines for generic material types [71]. Such recommendations

are typically given in the high, medium or low form. One possible way of quantifying these levels of injection speed is to interpret the qualitative injection speed statements relative to the machine capabilities. It was, therefore, decided to interpret low/medium injection speed as 40% of the machine maximum injection speed, 70% as medium/high and 100% as high (table 5.2).

Level	Relative [%]	Absolute [mm/s]
1	40	200
2	55	275
3	70	350
4	85	425
5	100	500

Table 5.2 - Injection speed statements relative to the machine capabilities.

The low level of the injection speed was selected in order to assure the complete filling of the cavity in conditions of minimum mold and melt temperatures (200 mm/s corresponding to 40% of the maximum injection speed). On the other hand, the high limit was selected in order to reach the maximum injection pressure of the machine under conditions of minimum mold and melt temperatures (350 mm/s corresponding to 70% of the maximum injection speed and to maximum pressure at injection location of 180 MPa). Regarding the injection speed, a somewhat arbitrary rule of thumb could be used to establish a typical or recommended level as some percentage of the maximum hydraulic pressure under the injection stage. Packing pressure was selected as 8.5% and 85% of the maximum hydraulic injection pressure (120 bar, corresponding to 180 MPa at injection location). The process parameters levels settings have been summarized in table 5.3.

Molding Parameter	Units	PS 143 E	
		Low	High
T_{mold}	°C	230	270
T_{melt}	°C	45	70
P_{pack}	bar	10	100
v_{inj}	mm/s	200	350

Table 5.3 - Summary of process parameters levels settings

5.1.2 Noise factors

The process variability in injection molding further complicates process control. The variability sources were attributed to the thermoplastic resin, injection molding machine and environmental factors. Product inconsistencies, among a batch of molded parts, were frequently blamed on lot-to-lot variations in material properties. Small changes in viscosity, density or composition could occur when regrind was mixed with virgin material, a material was used after it has been stored over an extended period of time, or a switch was made between different batches of the same material grade. Small changes in material properties could lead to inconsistencies in part weight, part dimensions, aesthetics and strength. The process machinery was considered as the second source of variability. The quality variation of the molded parts were probably due to internal controller variation relating to the shot size, injection velocity, switchover point and pack pressure. The third source of variability was considered as being human and environmental interaction with the process. For instance, the outdoor temperature could affect the effectiveness of evaporative coolers that determine the temperature of the plant water. The indoor temperature could, likewise, have a significant effect on the mold wall temperature as well as the post-molding behaviour of the molded parts. Humidity could affect the dryness of the polymeric material entering the barrel, thus, introducing further quality inconsistencies.

5.2 MICRO INJECTION MOLDING PROCESS

A high-speed and high-pressure injection molding machine (Ferromatik Milacron K 60) with a reciprocating screw of 32 mm diameter was used in the experiments (machine photos and capabilities have been set forth in figure 5.2 and table 5.4). The polymer material selected for the experiments was a high fluidity class polystyrene resin (PS 143 E) from the BASF® polymer products company. Polystyrene is relevant in micro injection molding due to its very high flowability, good biocompatibility, high optical clarity, high transparency and high impact strength, if compared with silicon or glass. The polymer was injected into the mold cavity implementing a rectangular speed profile of 200 and 350 mm/s. The melt temperature in the feeding zone was maintained at 230 and 270°C respectively. The mold temperature was maintained at a temperature of 40 and 70°C. In order to obtain closer control of the boundary

conditions and a good comparison between simulations and experiments, four temperature transducers were positioned near the cavity surface. The temperature transducers (model Kistler 6992A0.4) were mounted in the fixed mold part to avoid any disturbance when changing the insert in the moveable mold part. Water with the selected temperature was forced to circulate through the cavity plate channels; the temperature of the water was controlled by retroaction, comparing the signal obtained from the thermocouples with the temperature that was set in the heater system.

Machine characteristics	Unit	Value
Clamping force	[KN]	500
Injection screw diameter	[mm]	32
Maximum injection velocity	[mm/s]	500
Maximum pressure	[MPa]	180
Ejector force	[KN]	33.1
Cylinder capacity	[cm^3]	2.694
Number of heating zones	[-]	4

Table 5.4 – The main characteristics of the Ferromatik Milacron K 60 injection molding machine

Figure 5.2 – The Ferromatik Milacron K 60 injection molding machine at the IPL/DTU Polymer Centre. Mold and clamping system.

The data acquisition was controlled with a program written in Visual Basic. All signals were converted to Volt signals in the range 0-5 V. The example of a mold temperature acquisition (trial 9 of the experimental plan) during the entire cycle has been set forth in the following figure.

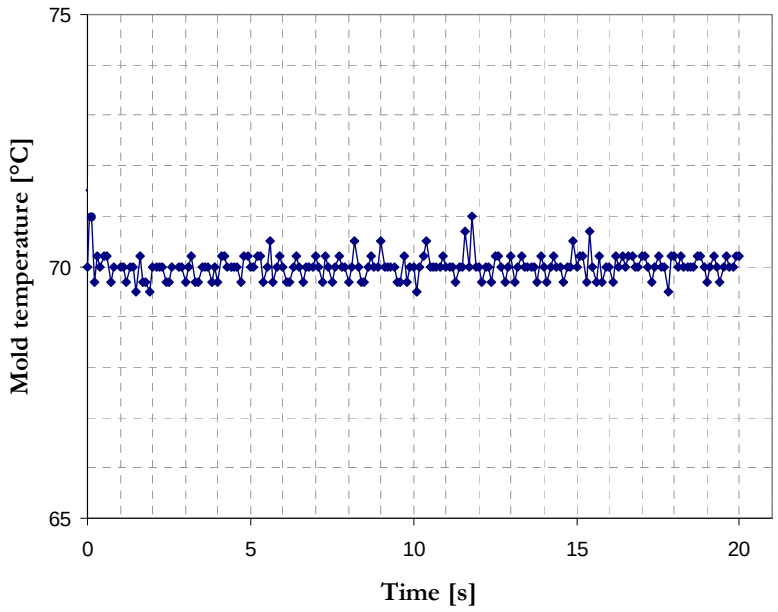

Average mold temperature	69.98 °C
Standard deviation	0.16 °C

Figure 5.3 - Mold temperature data acquisition (above). Average mold temperature and standard deviation estimation (below).

The packing pressure was controlled by implementing the desired percentage (8.5% and 85%) of the maximum injection pressure and the time that elapsed between the beginning and end of the packing phase. The packing time should be long enough so the gate has a chance to freeze off. This time was estimated only after a series of experimental trials. Constant packing pressure profiles, with an increasing amount of time, were implemented until the piece weight variation was negligible. A packing time of 3 s was selected.

CHAPTER 6

CHARACTERIZATION AND ANALYSIS OF WELD LINES POSITION ON THE MICRO MOLDED CAVITY

6.1 MEASURING STRATEGY DEFINITION

Experiments have been performed at the IPL/DTU Centre to assess the sensitivity of the cavity filling to changes in the process conditions (mold and melt temperatures, injection velocity and packing pressure). The alternative, proposed in this thesis, is to use the weld lines as flow markers and a comparison term between software simulation and experimental filling results. The exact prediction of the weld lines position will demonstrate the

good level of accuracy of the filling software simulation. In order to analyze the filling of the micro cavity, two dimensional analysis was performed. The position of the weld lines was determined and the correlations with process parameters variation were established. The investigation strategy was to detect the X and Y coordinates of some points on the weld lines with an optical coordinate measurement machine (optical CMM DeMeet220). This work was one of the most ticklish parts of the whole project. The reason was that one half of the factorial plan was measured by one group of operators, while the other half was measured by a different operator who, at the beginning, had no experience in working with CMM. Therefore, the uncertainty of measurements was assessed and implemented in the statistical analysis. The contributors considered and the related standard uncertainties in the measurements of the micro molded part have been presented and discussed in [75, 76, 77]. Before starting the detection of the weld lines points, the definition of a reference system was required. It was decided to orientate the Y direction parallel to the main flow direction and the X direction parallel to the edge of the feature from which the weld line starts. The zero point was located in the corner of the feature. The experimental weld lines were, therefore, measured considering a relative dedicated reference system for each of the four weld lines which were detected on the micro part (figure 6.1).

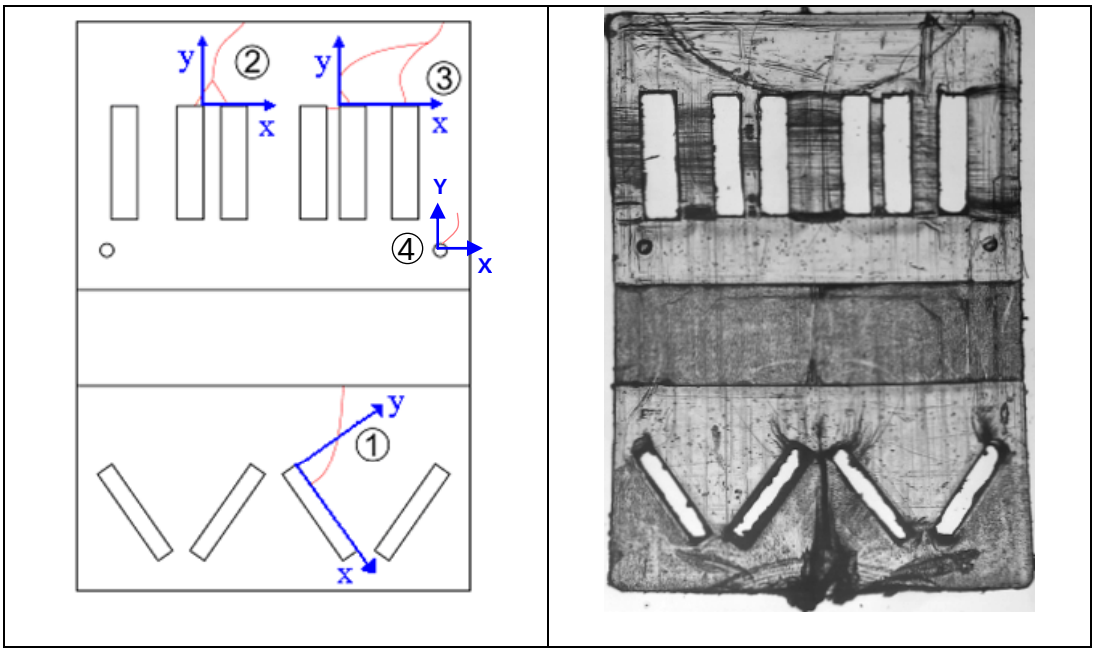

Figure 6.1 - Workpiece (drawn and photo) and the four weld lines investigated.

6.2 CMM WORKING PRINCIPLES

CMMs refer to those machines that measure single points on the workpiece surface with a probe and give the position of the probe itself relative to a single coordinate system. All probed points are expressed in terms of their measured coordinates and are combined in ideal geometric elements, the so-called substitute geometric elements, by applying a best fit algorithm. In this way it is possible to evaluate parameters, such as the diameter, distance and angle of the workpiece from the coordinates of the measured points [78].
Modern manufacturing processes for discrete parts require fast and accurate measuring devices to check critical dimensions against their specified values. Conventional CMMs are equipped with mechanical probes and the measuring principle is based on the physical contact between the probe and the workpiece. Over the last few years, the use of CMMs, equipped with optical sensors and probes, has become very common in the industrial environment. Their integration into production is mainly due to advantages, such as:

- the measuring force, equal to zero, allows for measurements on soft materials, glass specimens and flexible objects which would deflect if contacting probes were used;
- the measuring speed is higher than tactile sensors;
- small-sized features can be measured using different magnification lenses.

6.2.1 Optical CMM DeMeet 220

In order to investigate the weld lines position, a CCD (charge coupled device) optical CMM was used. Due to the transparent property of the polymeric material (polystyrene), the weld lines were easily detected using a machine model DeMeet 220. It is a versatile CMM that can work as video as well as contact machine. The DeMeet machine is designed with a fixed bridge construction. Both sensors (optical and tactile) can move only in the Z-X plane, while the table can only move in the Y direction (figure 6.2). The investigation strategy was to detect the X and Y coordinates of some points on the weld lines. The X-coordinate comes from the position of the camera on the bridge respect to the reference position, while the Y-coordinate comes from the position of the working table. The Z coordinate is provided by vertical movements of the camera which are necessary to focus the workpiece.

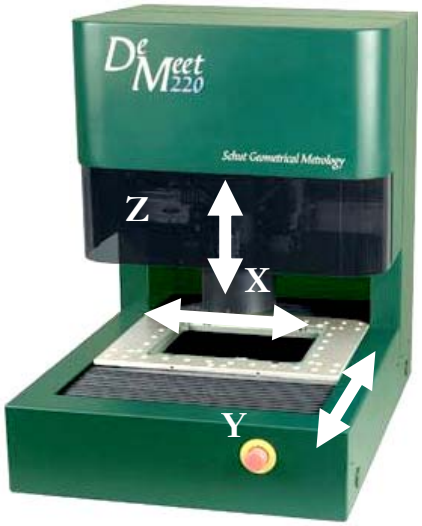

Figure 6.2 – DeMeet 220 camera and table movements

The DeMeet 220 can mount different lenses. Due to the dimension of the workpiece under investigation, the 20 magnification one was used. The machine characteristics have been set forth in the following table.

Demeet 220	
Measurement functions:	2½D
Resolution:	x-axis: 0.5 μm y-axis: 0.5 μm z-axis: 0.5 μm
Measurement range:	x-axis: 220 mm y-axis: 150 mm z-axis: 100 mm
Max. workpiece dimension:	220 mm x 150 mm x 100 mm
Max. workpiece weight:	200 N

Table 6.1 - DeMeet 220 characteristics

6.3 WELD LINES DETECTION

An accurate measurement of the weld line path on the sample was required to describe the shape of the weld lines. The investigation strategy was to detect the X and Y coordinates of points on the weld lines and to plot them in a determined and repeatable reference system. Measuring uncertainty was estimated taking into account the optical CMM calibration on the measured dimensional range, repeatability of the measurement on 5 repetitions, CMM resolution, definition of the measurand and the influence of the temperature (i.e. expansion of the plastic due to temperature variations). The combined expanded measuring uncertainty, calculated with a coverage factor k =2 (level of confidence 95%), resulted in 4 µm on the X direction and in 3 µm on the Y direction (details on uncertainty analysis have been set forth in [75, 76, 77]). According to the reference system definition, it was decided to orientate the Y direction parallel to the main flow direction and the X direction parallel to the edge of the feature from which the weld line starts. So it was decided to fix the Y coordinate with an increment of 50 µm and then to read the correspondent X coordinate. The procedure was repeated, step by step, in the Y direction (figure 6.3). The alignment was done by steps of 50 µm, starting from the origin of the reference system, up to the end of the weld line. The measuring strategy was repeated for all weld lines (figure 6.4, 6.5 and 6.6).

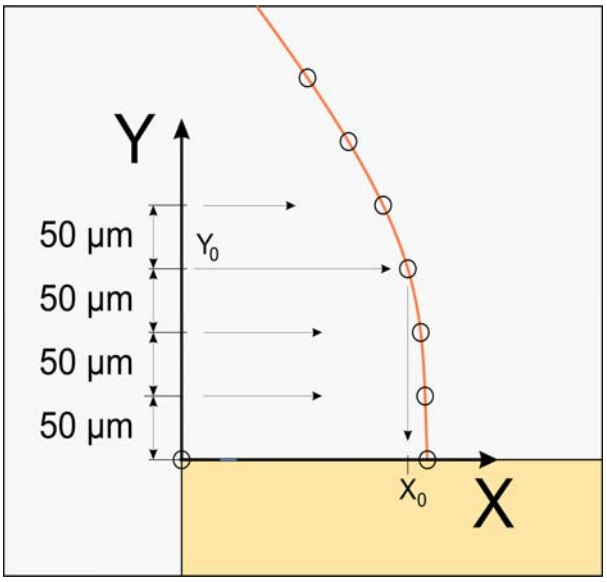

Figure 6.3 – The measuring strategy to detect the points coordinates. The rectangular coloured box represents the cavity feature from which the weld line starts.

Point	X	Y (nominal)	Y (measured)
0	0.0000	0.0000	0.0000
1	0.2001	0.0000	0.0002
2	0.1977	0.0500	0.0500
3	0.1953	0.1000	0.0998
4	0.1933	0.1500	0.1501
5	0.1896	0.2000	0.1999
6	0.1791	0.2500	0.2500
7	0.1658	0.3000	0.2999
8	0.1498	0.3500	0.3501
9	0.1332	0.4000	0.4000
10	0.1126	0.4500	0.4502
11	0.0921	0.5000	0.5000
12	0.0502	0.6000	0.6002
13	0.0055	0.7000	0.6999
14	-0.0384	0.8000	0.8003
15	-0.0904	0.9000	0.9002
16	-0.1314	0.9500	0.9500

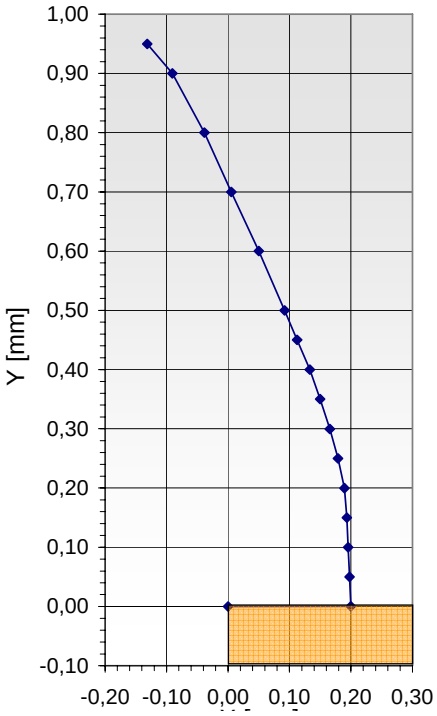

Figure 6.4 - Weld line number 1: example of measuring results

	Line 1			Line 2			Line 3		
Point	**X**	**Y nom**	**Y meas**	**X**	**Y nom**	**Y meas**	**X**	**Y nom**	**Y meas**
1	0.0650	(*)	0.3028	0.0650	(*)	0.3028	0.0650	(*)	0.3028
2	0.0396	0.2500	0.2502	0.0927	0.2500	0.2502	0.0664	0.3500	0.3500
3	0.0150	0.2000	0.1999	0.1229	0.2000	0.2000	0.0656	0.4000	0.3999
4	-0.0079	0.1500	0.1501	0.1532	0.1500	0.1502	0.0644	0.4500	0.4501
5	-0.0320	0.1000	0.0999	0.1819	0.1000	0.0999	0.0636	0.5000	0.4999
6	-0.0517	0.0500	0.0501	0.2093	0.0500	0.0501	0.0648	0.5500	0.55
7	-0.0714	0.0000	-0.0001	0.2366	0.0000	-0.0001	0.0664	0.6000	0.6002
8							0.0709	0.6500	0.65
9							0.0789	0.7000	0.7002
10							0.0922	0.7500	0.7501
11							0.1112	0.8000	0.8
12							0.1382	0.8500	0.8502
13							0.1414	(**)	0.8684

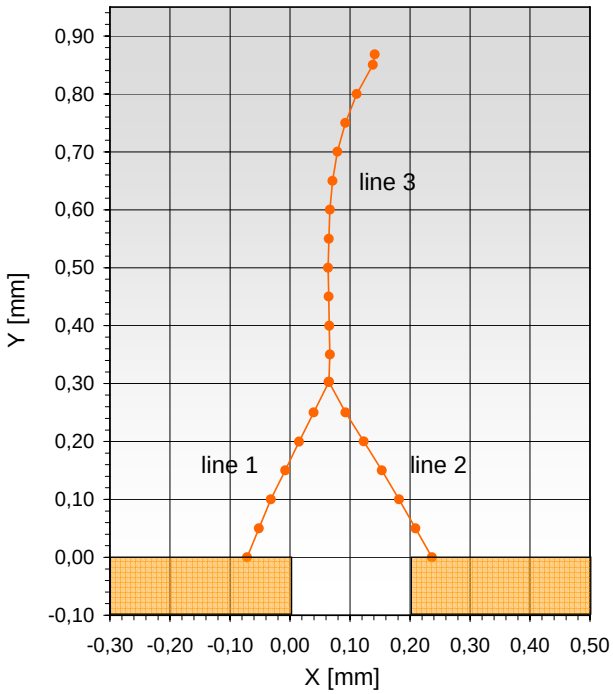

Figure 6.5 - Weld line number 2: example of measuring results

	Line 1			Line 2			Line 3		
Point	**X meas**	**X nom**	**Y meas**	**X**	**Y nom**	**Y meas**	**X**	**Y nom**	**Y meas**
0	0.0000	0.0000	0.0000						
1	0.0001	0.0000	-0.0403	0.1628	0.0000	0.0002	0.7140	0.0000	-0.0001
2	-0.0402	-0.0400	-0.0431	0.1535	0.0500	0.0500	0.7140	0.0500	0.0501
3	-0.0800	-0.0800	-0.0435	0.1492	0.1000	0.1002	0.7188	0.1000	0.1001
4	-0.1199	-0.1200	-0.0399	0.1516	0.1500	0.1500	0.7184	0.1500	0.1499
5	-0.1501	-0.1500	-0.0389	0.1655	0.2000	0.2002	0.7148	0.2000	0.2001
6				0.1821	0.2500	0.2501	0.7099	0.2500	0.2499
7				0.2059	0.3000	0.2999	0.7083	0.3000	0.2999
8				0.2349	0.3500	0.3501	0.7079	0.3500	0.3501
9				0.2699	0.4000	0.3999	0.7115	0.4000	0.3999
10				0.3126	0.4500	0.4499	0.7200	0.4500	0.4501
11				0.3617	0.5000	0.5001	0.7333	0.5000	0.5000
12				0.4209	0.5500	0.5499	0.7494	0.5500	0.5502
13				0.4927	0.6000	0.6002	0.7683	0.6000	0.6000
14				0.5821	0.6500	0.6502	0.7884	0.6500	0.6502
15				0.7006	0.7000	0.7002	0.8086	0.7000	0.6999
16				0.7847		0.7164	0.8189	(*)	0.7095
17				0.8189	(*)	0.7095	0.8677	0.7500	0.7501
18							0.9180	0.8000	0.7999
19							0.9397	(**)	0.8457

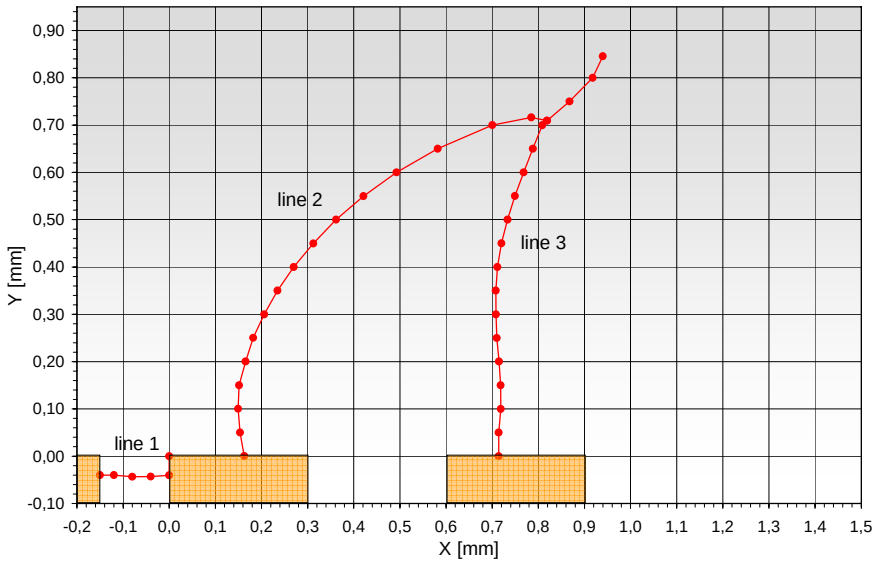

Figure 6.6 - Weld line number 3: example of measuring results.

6.4 INFLUENCE OF PROCESS PARAMETERS ON THE MICRO CAVITY FILLING

The influence of process parameters on the weld lines position was determined according to the full factorial DOE analysis defined on paragraph 5.1.1. A complete description of process parameters, which have more influence on the weld lines position, including the main effects determination and interactions estimation, has been set forth in [76, 77, 79]. In this section, only results related to the main effects have been set forth in order to clearly establish the correlations between process parameters variations and the coupled phenomena of fluid flow/heat transfer in different geometries. The definition of a parameter able to describe the shapes of the weld lines was needed to carry out the statistical analysis. This parameter needs to:

- be sensitive to the parameter settings. It means that its value changes according to the process parameters level;
- be calculated by means of a repeatable method. The output has to be calculated for each parameter setting, so the procedure has to be repeated each time.

Looking at the measured shape of each weld line, it was decided to use as output the:

- position of characteristic points: in all weld lines there are particular points that are easily recognizable and their positions change according to the DOE settings. For example the starting point from the pockets and the meeting point of two or three melt flows were considered;
- slope of the weld line: it is strongly dependent on the process parameters level. It was, therefore, decided to establish correlations between the process parameters and its interpolating line.

The dimensional measurements and the quality of measurements were a fundamental step in order to obtain reliable data results to be analyzed. Therefore, the measuring uncertainty was estimated [75, 76, 77]. In order to evaluate if the change of the weld lines position was completely due to the variation of parameters setting or only to the measurement process, the uncertainty was included in the statistical analysis. Depending on the considered output, the measurements uncertainty could create a spread of the measurements which could partially/totally hide the real effect of the factor variation on the response. It was, therefore, important to assess the measuring equipment and procedure uncertainty [77]. In the statistical analysis a

coefficient of uncertainty (COU) was therefore introduced and defined as:

$$COU = \frac{U}{|effect|} \tag{32}$$

where U is the expanded uncertainty of the output analyzed [77] and |effect| is the absolute value of the effect. Three different results were expected:

- COU>>1: the uncertainty is wider than the output variation. When this result is obtained, there is no sense in continuing the analysis because the effect due to process variation is inside the uncertainty range;
- COU≈1: the effect of the parameter has the same magnitude of the uncertainty. The statistical analysis is unreliable because the output variation, due to the factor level change, can be hidden by the uncertainty;
- COU<1: the uncertainty budget is negligible if compared to the output variation.

The results of statistical analysis have been briefly discussed for each weld line and reported in terms of Pareto and the main effects chart [80].

6.4.1 Weld line number 1

As far as this weld line is concerned, two outputs in the statistical analysis were used to trace it. The position of the starting point and the average slope of the weld line were considered (figure 6.7):

- starting point: the average X coordinate of the first four points (at Y=0 mm, Y=0,05 mm, Y=0,1 mm and Y=0,15 mm) was considered as the first output. It describes the distance from the left edge of the pocket.

  Output 1_1: $\frac{\sum_{i=1}^{4} x_i}{4}$ [mm].

- average slope: it was calculated in the middle part of the line, between Y=0,4 mm and Y=0,6 mm. The interpolating line and its relative pendency were calculated (m_1 represents the slope of the interpolating line between points Y=0,4 mm and Y=0,6 mm).

  Output 1_2: arctan(m_1) [degrees].

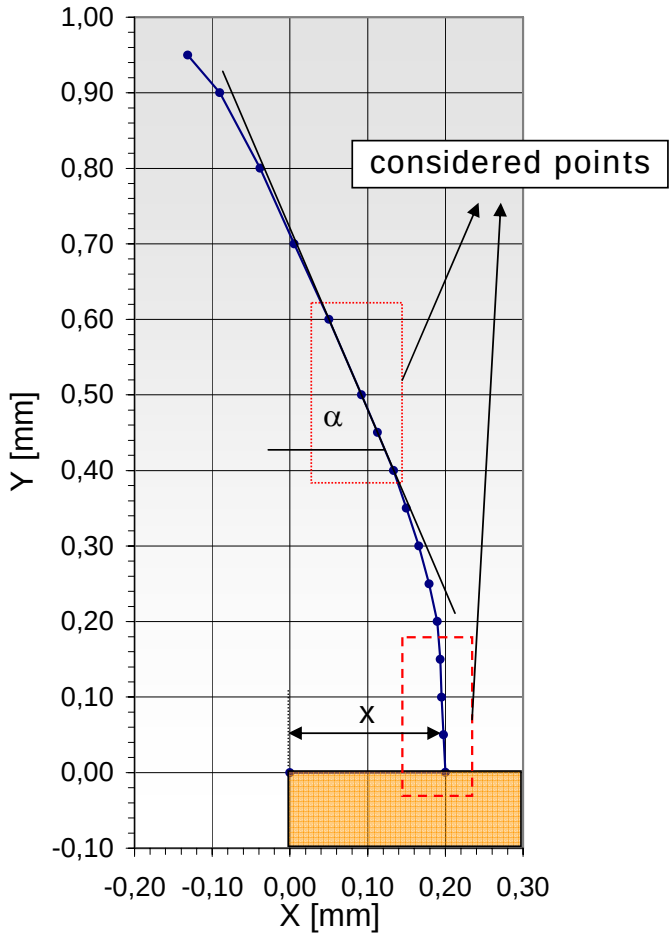

Figure 6.7 - Outputs definition for the weld line number 1: X is 1_1 and α is 1_2

6.4.1.1 Position (Output 1_1)

As a first step, the residuals plot, obtained from the factorial plan with five replications, was studied (figure 6.8). Looking at the normal probability plot and the residuals histogram, it is noticeable that the hypothesis of normal distribution of the residuals is not respected. The normal probability plot has the distinctive shape of a bimodal distribution as highlighted in the histogram too. It is double bell shaped instead of single bell. Two different and symmetrical trends are present, probably due to the measuring procedure: half factorial plan was measured by one operator and the other half by another group of operators. In order to eliminate this noise source, it was decided to

split the factorial plan in two parts. In this way, the noise factor was closed off in each fraction of the whole plan and did not affect the analysis. In this case, the noise source was the operator. It was known that the half part of the measurements was carried out by the operator A and the other half by the operator B. Therefore, the factorial plan was split into two fractions: in the first one, all the measurements were performed by the operator A and in the other one by the operator B. Thus, the operator influence was eliminated analyzing only one half of the factorial plan. As can be observed from the residuals analysis of one fraction of the factorial plan (figure 6.9), all the hypotheses about the model have been verified. In this way, the suspect that the non normal residuals distribution was due to the multiple operators was confirmed. One of the most probable causes of the lack of repeatability between the measurements was due to the alignment of the zero reference in the pocket corner. Once all the hypotheses had been verified, the analysis of the factorial plan was carried on. Only interactions between two factors were considered because higher level interactions were considered irrelevant to the project. Since the full factorial plan was reduced to a half factorial plan, some of the second level interactions were not considered because aliases of other ones [80]. The effects and COU coefficients were calculated for each term.

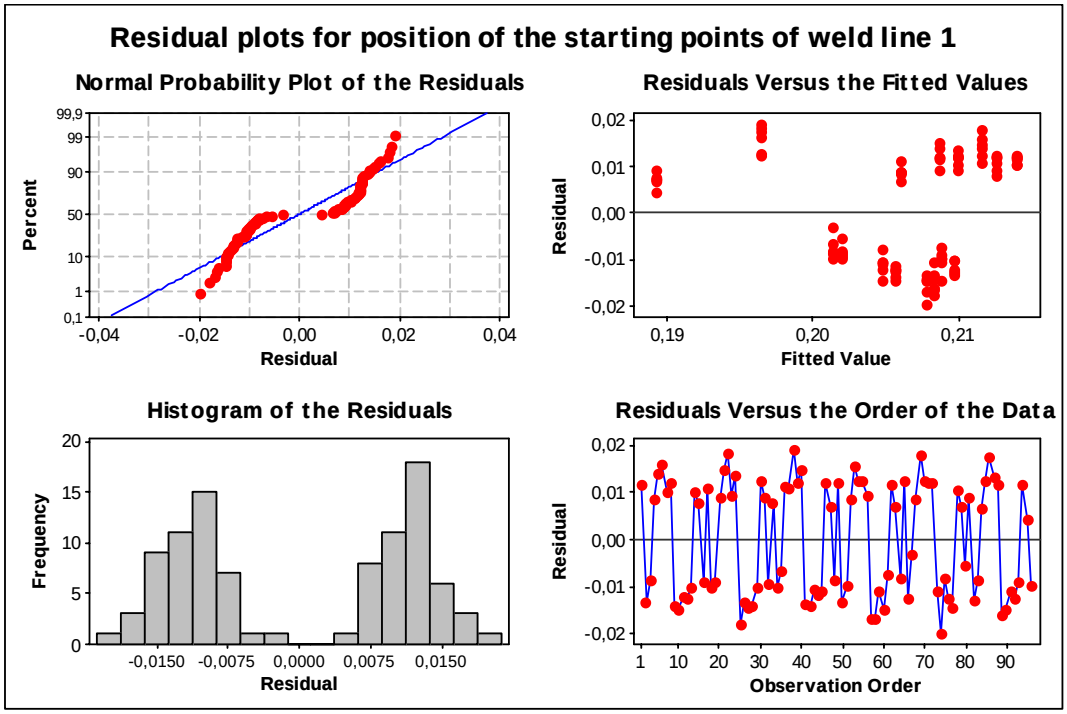

Figure 6.8 - Residuals plots for the starting position of the weld line number 1

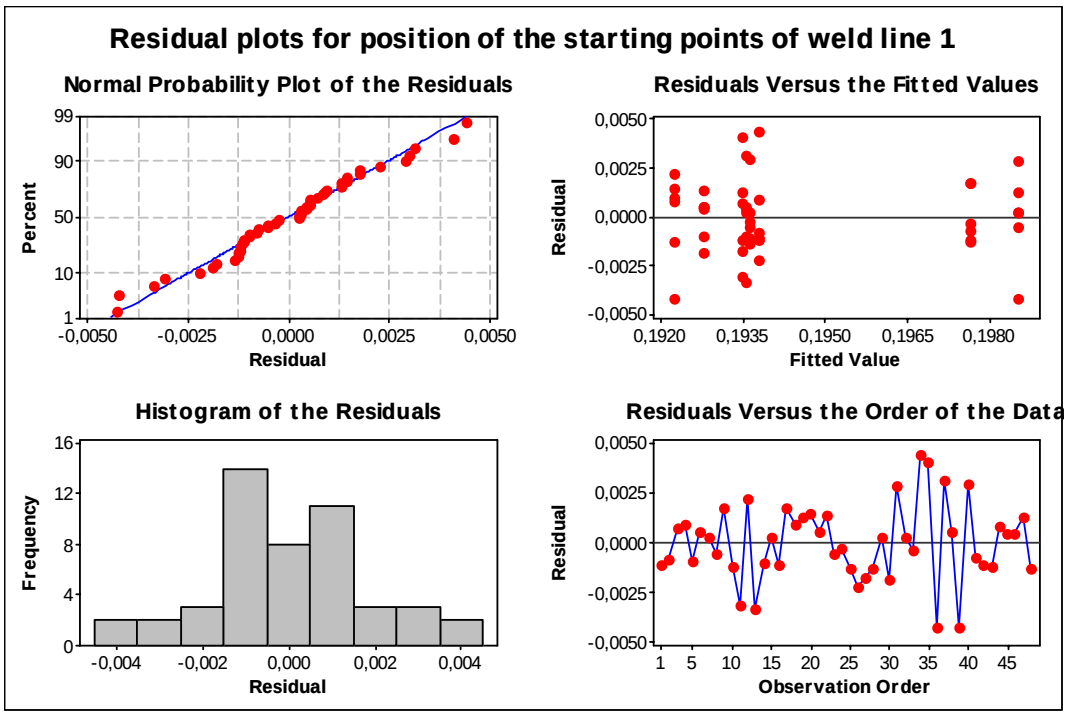

Figure 6.9 - Residuals plots for the starting point position of the weld line number 1 (half fraction of the factorial plan).

Term	Average effect [mm]	COU
T melt	-0.0001	81.1
T mold	0.0029	1.6
P hold	0.0008	6.2
V inj	0.0020	2.3
T melt - T mold	-0.0003	16.2
T melt - P hold	-0.0023	2.0
T melt - V inj	0.0003	18.9
Exp. uncertainty [mm]	0.0047	

Table 6.2 - Average effects and COU for the position of the weld line number 1.

From the previous analysis, it is clear how the uncertainty contribution is too high to evaluate output variation due to the change of the parameters setting.

This finding is further confirmed in the Pareto chart; the effects are lower than the uncertainty contribution (figure 6.10). No definite findings can be drawn on the influence of different process parameters on the weld line position.

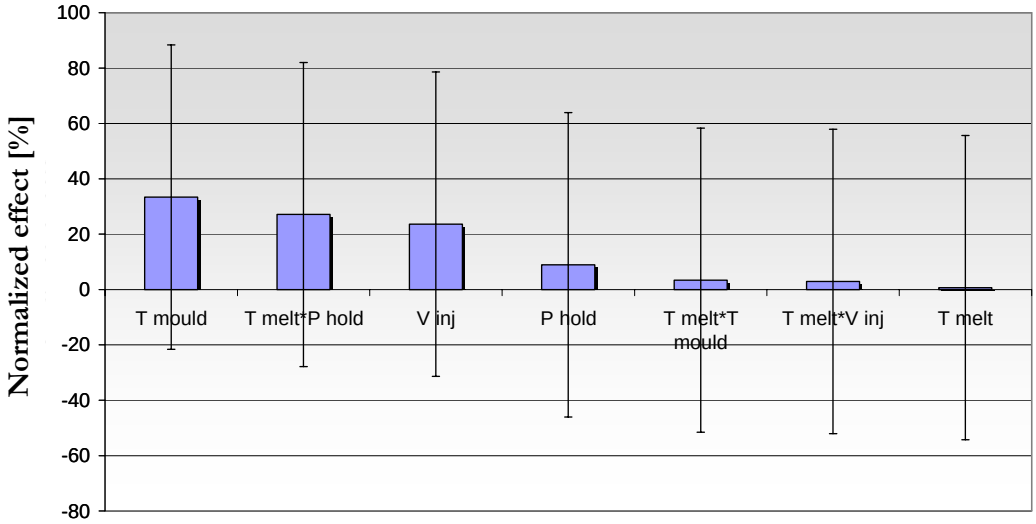

Figure 6.10 - Pareto chart with the uncertainty bars for the weld line position.

6.4.1.2 Slope (Output 1_2)

The analysis of residuals shows that all the hypotheses on the model have been respected (figure 6.11). The weld line slope was not affected by the different groups of operators because it was not dependant on the starting point position. Thus, the full factorial plan was analyzed. The factors effects were calculated, as well as the COU coefficient. Far as the angle is concerned, all the terms have a COU greater than 1 (table 6.3). It means that the uncertainty contribution is too high to assess the influence of the process parameters on the output variation, as it is also clear on the Pareto chart (figure 6.11).

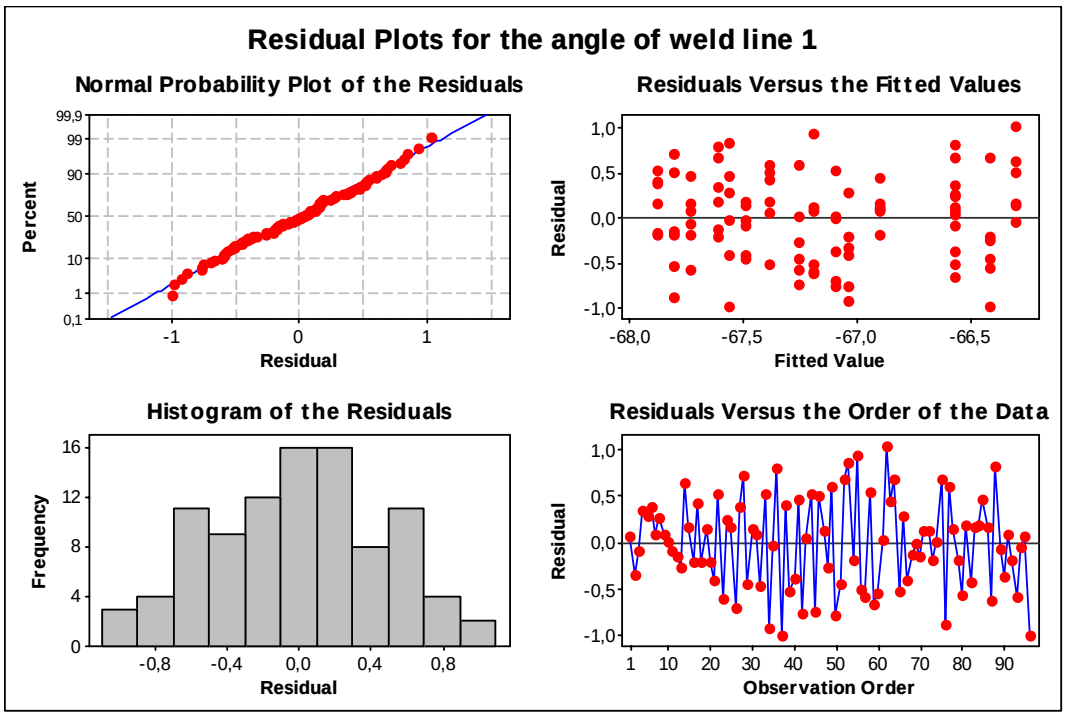

Figure 6.11 - Residuals plots for the angle of the weld line number 1

Term	Average effect [degrees]	COU
T melt	-0.6833	1.7
T mold	0.2517	4.6
P hold	-0.1733	6.7
V inj	-0.2133	5.4
T melt - T mold	0.0183	63.0
T melt - P hold	0.3083	3.7
T melt - V inj	0.2283	5.1
Tmold - P hold	-0.2450	4.7
Tmold - V inj	0.3200	3.6
P hold - V inj	-0.2333	4.9
Exp. uncertainty [degrees]	1.2000	

Table 6.3 - Average effects and COU for the angle of the weld line number 1.

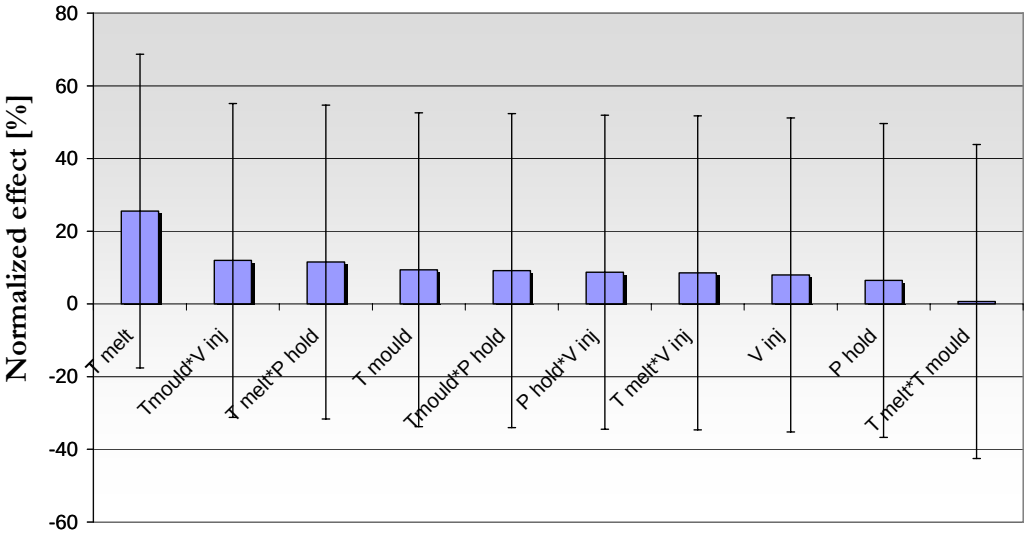

Figure 6.12 - Pareto chart with the uncertainty bars for the weld line angle.

6.4.2 Weld line number 2

This weld line originates from the joining of three flow fronts. They come from channels with different dimensions (figure 6.13): the outer ones are larger than the central one. It means that a central meeting point has been created, which can be used as a comparison term for different process settings.

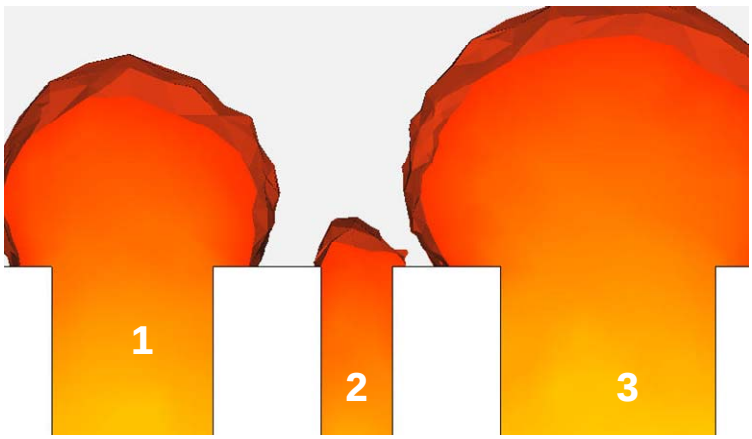

Figure 6.13 - Weld line 2: flow fronts displacement before the weld line formation

Two outputs were considered in the statistical analysis:

- meeting point: the average X coordinate of the first four points of the line 3 (figure 6.14) was calculated. The Y coordinate was not considered because it did not show a meaningful change:

  Output 2_1: $\frac{\sum_{i=1}^{4} x_i}{4}$ [mm].

- slope of the tangent: looking at the weld line shape, it was possible to see that line 3 (figure 6.14) moved if the level of some process parameters was changed. In order to determine the influence of process parameters on its position, it was decided to calculate the slope of the tangent line in Y=0,6 mm (the position in which the line starts to lean to the right).

  Output 2_2: arctan(m_2) [degrees].

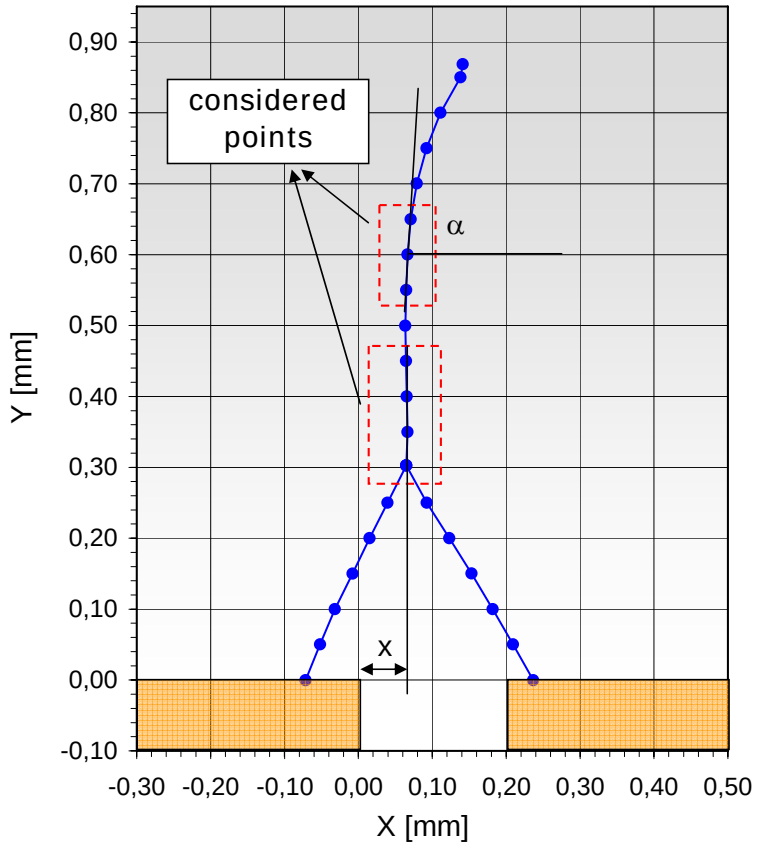

Figure 6.14 - Outputs definition for weld line number 2: X is 2_1 and α is 2_2

6.4.2.1 Position of the meeting point (Output 2_1)

Only the X meeting point coordinate was considered as output, because any influence of process parameters on the Y coordinate was observed. Even for this output, the residuals plots confirm that all the hypotheses on the model are respected (figure 6.15). Although some outliers are present, they do not affect the model. Considering the COU values (table 6.4), it was observed how the variation of both the melt and mold temperatures produced an effect on the meeting point position which is dominant if compared to the uncertainty budget. On the other hand the holding pressure, the injection speed and all the interactions can be neglected (Pareto chart). As a conclusion the main effect plots were considered [77]. An increment of both the melt and mold temperatures produced a movement on the left of the X meeting point coordinate. This can probably due to a higher relative viscosity reduction in the macro channel on the right (number 3 in previous figure 6.13) if compared to the viscosity reduction in the central micro channel (number 2), where the convection heat flux from the melt to the mold has not a negligible contribute (higher area to volume ratio if compared to the outer macro channel).

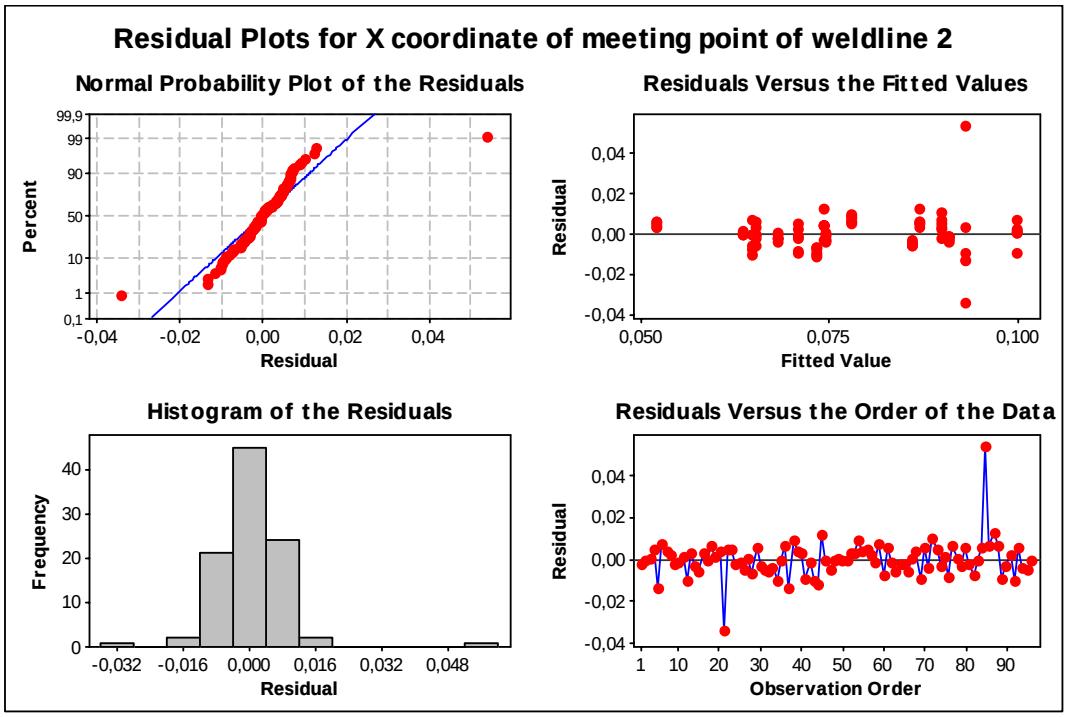

Figure 6.15 - Residuals plots for the X coordinate of the weld line number 2

Term	Average effect [degrees]	COU
T melt	-0.0177	0.6
T mold	-0.0136	0.8
P hold	0.0068	1.6
V inj	0.0029	3.8
T melt - T mold	0.0016	6.6
T melt - P hold	-0.0045	2.4
T melt - V inj	0.0017	6.2
Tmold - P hold	0.0052	2.1
Tmold - V inj	0.0040	2.7
P hold - V inj	-0.0040	2.7
Exp. uncertainty [degrees]	0.0110	

Table 6.4 - Average effects and COU for the X meeting point coordinate of the weld line number 2

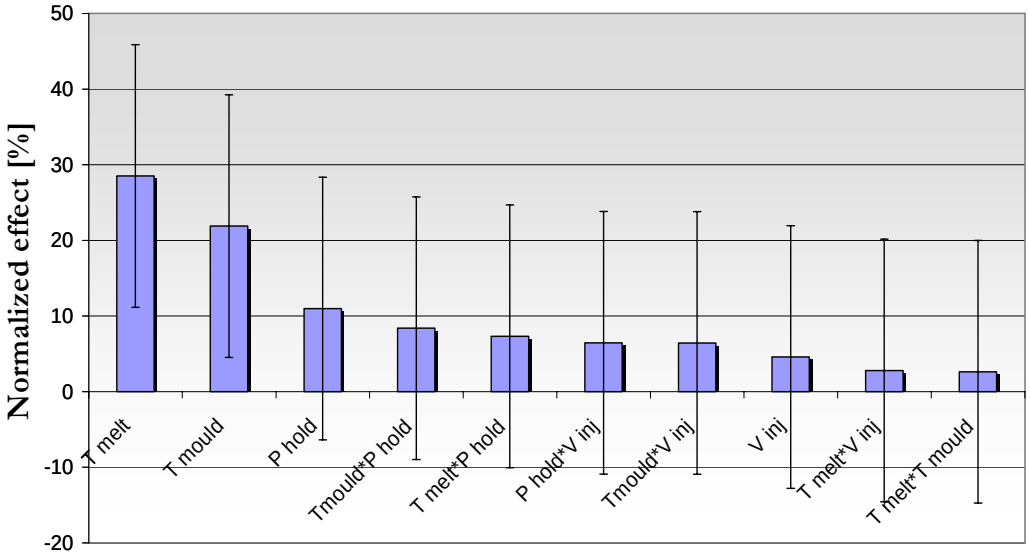

Figure 6.16 - Pareto chart with the uncertainty bars of the X meeting point coordinate of the weld line number 2

6.4.2.2 Slope of the line 3 (Output 2_2)

From the residuals analysis (figure 6.17), it is clear how the hypothesis of normal distribution has not been respected. The shape of the normal probability plot is characteristic of hyper normal distribution. Errors in the micro cavity alignment as well as the critical definition of the output were considered the cause of the non normal residuals distribution. Since one of the basic hypotheses was not respected, the analysis was not continued.

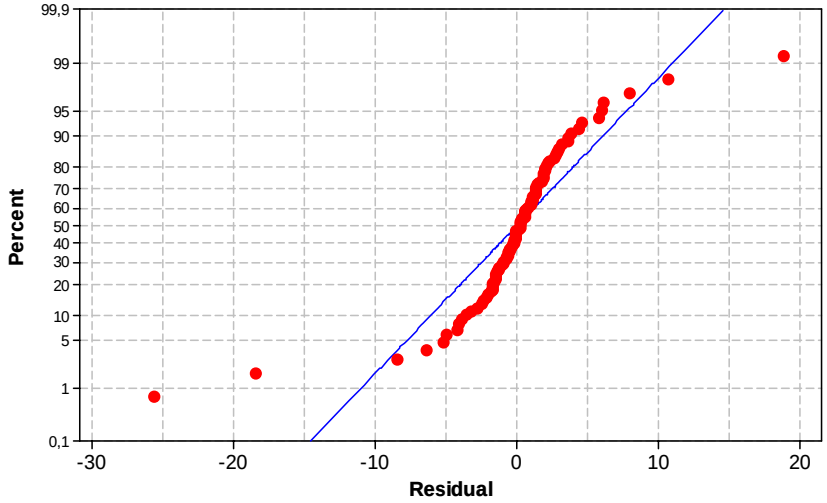

Figure 6.17 - Normal probability residuals plot for the weld line slope.

6.4.3 Weld line number 3

This weld line originates from the joining of four flow fronts. They meet together, creating a straight weld line, where flow fronts numbers 1 and 2 join (inside the 150 μm wide channel) and a meeting point where flow fronts 1, 3 and 4 join together (figure 6.18). Because of the amount of information that it was possible to obtain from the meeting point of flows in channels with different dimensions, three outputs were defined:

- line 1 (figure 6.6): the weld line is almost perfectly horizontal for all different parameters settings. The average points distance from the upper edge of the pockets was therefore considered as output:

  Output 3_1: $\frac{\sum_{i=1}^{4} y_i}{4}$ [mm].

- position of the meeting point: the meeting point is a good flow marker and is easy to detect. But for some parameters settings, the flow fronts numbers 1 and 4 did not join, so that the meeting point was missed (figure 6.19(b)). In this case, the lines interpolating the last three points of the line 2 and 3 were traced (figure 6.20). It was, therefore, possible to obtain a virtual meeting point. In both cases, the X and Y coordinates were considered (figure 6.21):
  Output 3_MP_X: $X_{meeting\ point}$
  Output 3_MP_Y: $Y_{meeting\ point}$

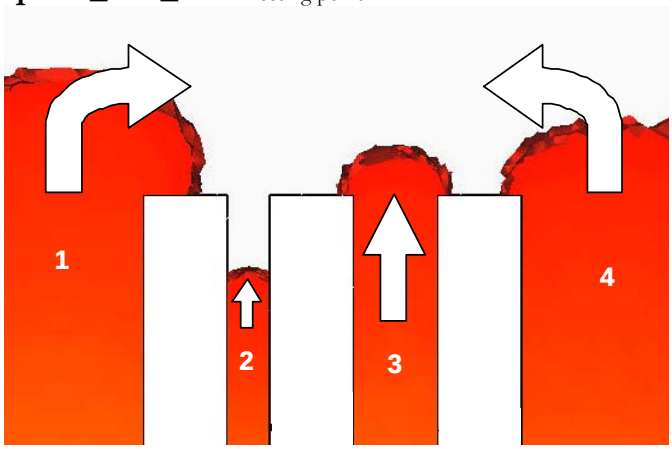

Figure 6.18 - Flow front displacement before the weld line formation

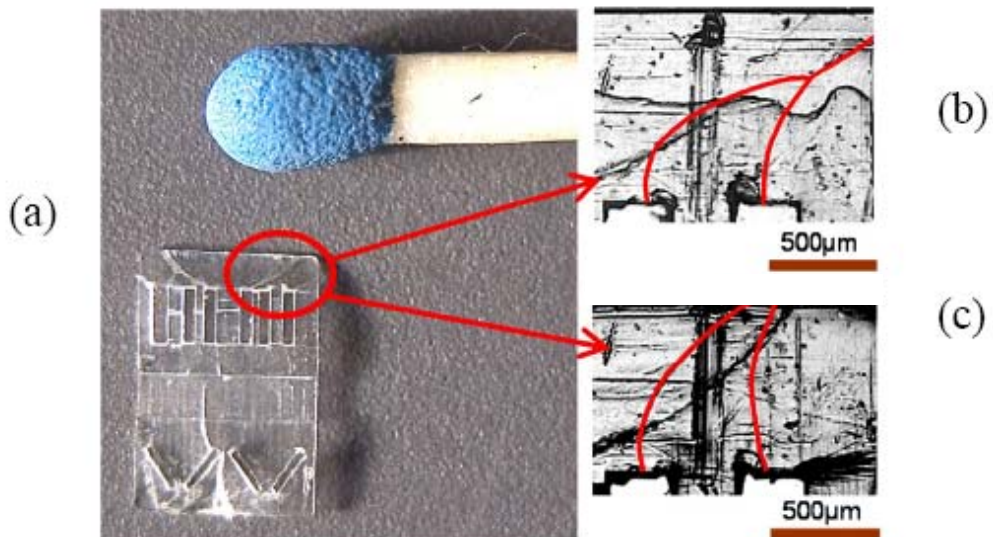

Figure 6.19 - An optical microscope image of a micro part (a); flow patterns observed at two different injection speeds: 200 mm/s (b) and 350 mm/s (c).

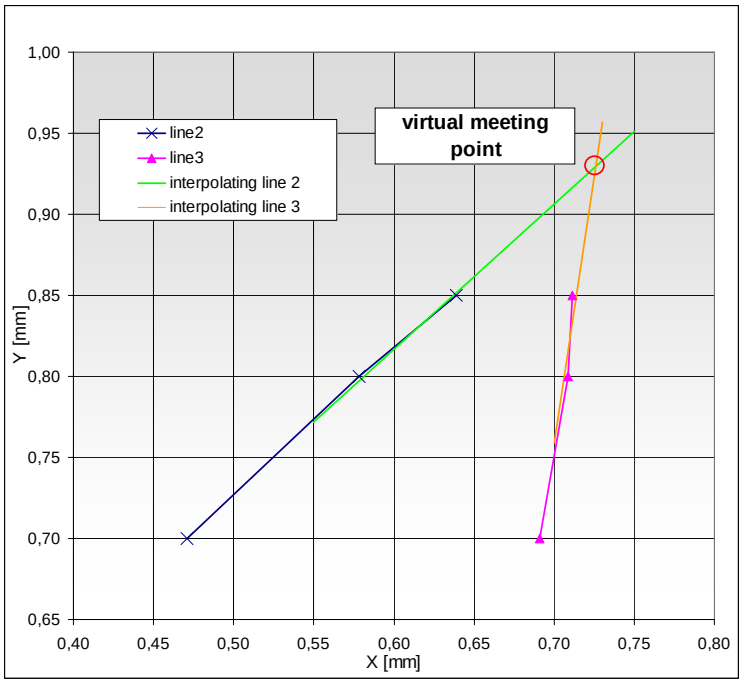

Figure 6.20 - The interpolating lines and virtual meeting point in the upper part of the line 2 and line 3 of the weld line number 3.

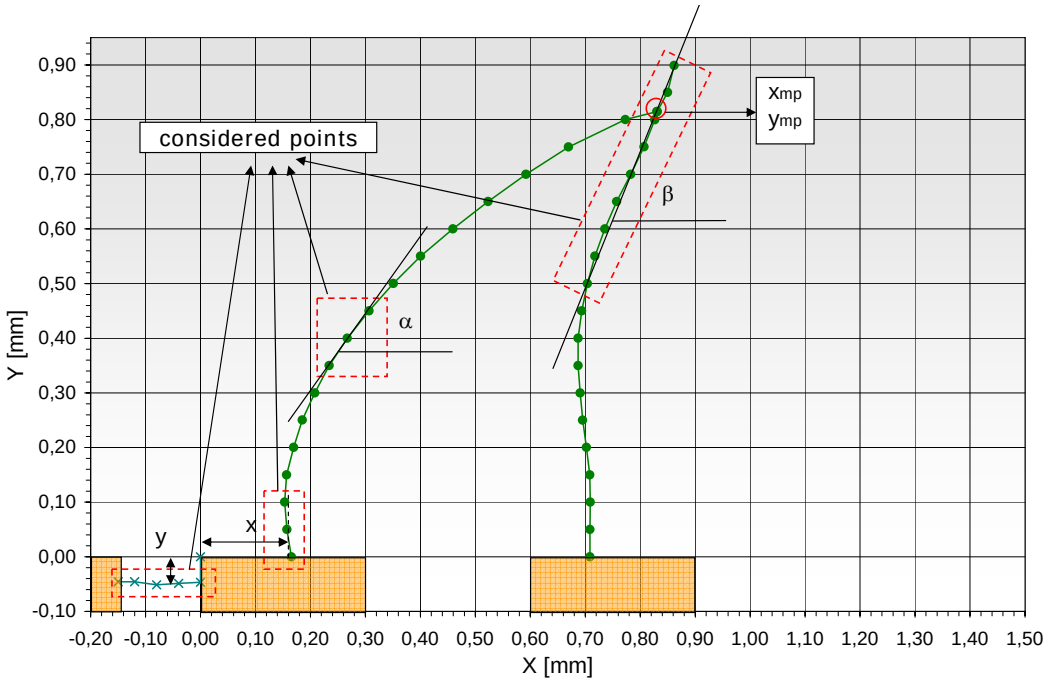

Figure 6.21 - Outputs definition for the weld line number 3.

6.4.3.1 Average Y coordinate of the line 1 (Output 3_1)

The analysis of residuals has established that all the hypotheses on the statistical model were respected [77]. Thus, the statistical analysis was carried on and the COU coefficients were estimated. Regarding the main effects results, only the speed velocity, mold and melt temperatures did not have a negligible influence on the output, if compared to the measurements uncertainty. Furthermore, the Pareto chart shows their effects extend beyond the reference line (significant at the level of 0.05). When the level of one of these three factors is increased, the horizontal weld line moves up (figure 6.23). The effect of the injection speed is obvious. On the other hand, the mold and melt temperatures influence on the viscosity reduction is expected.

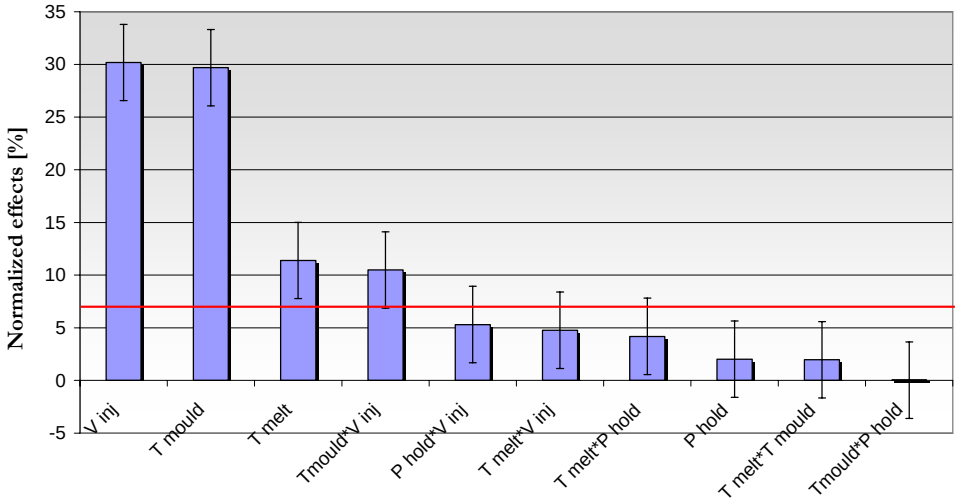

Figure 6.22 - Pareto chart of the average Y coordinate and reference line (α=0.05)

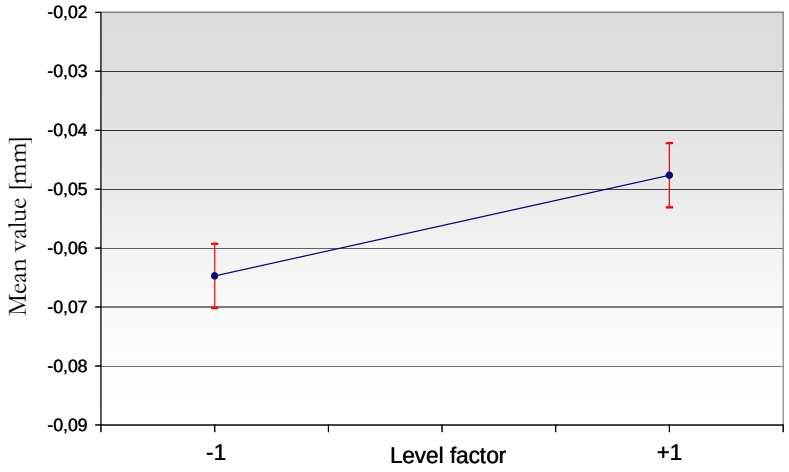

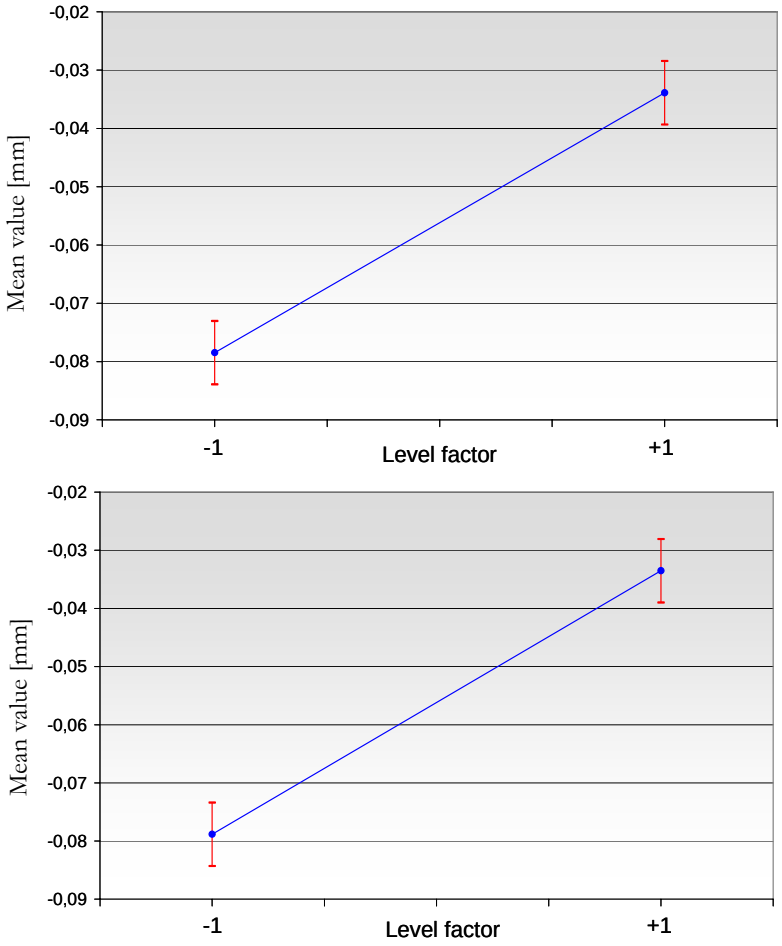

Figure 6.23 - Main effect plots for the average Y coordinate: melt temperature (above), mold temperature (centre) and injection velocity (below).

6.4.3.2 Meeting point coordinates (Output 3_MP_X and 3_MP_Y)

The analysis of residuals has established that all the hypotheses on the statistical model were respected. Thus, the statistical analysis was carried on and the COU coefficients were estimated. Regarding the main effects results, only the injection velocity and the mold temperature did not have a negligible influence on the meeting point position. The Pareto chart shows their effects extend beyond the reference line (significant at the level of 0.05). When the level of one of these two factors is increased, the meeting point moves up and on the left [77]. The effect of the injection velocity is obvious. On the other

hand, the mold temperature influence on the viscosity reduction is expected.

Term	Average effect [mm]	COU
T melt	0.0118	1.2
T mold	-0.1233	0.1
P hold	-0.0106	1.3
V inj	-0.1330	0.1
T melt - T mold	0.0225	0.6
T melt - P hold	-0.0324	0.4
T melt - V inj	0.0328	0.4
Tmold - P hold	0.0108	1.3
Tmold - V inj	0.0083	1.7
P hold - V inj	-0.0134	1.1

Exp.uncertainty [mm]	0.0140

Term	Average effect [mm]	COU
T melt	-0.0043	0.9
T mold	0.1244	0.03
P hold	0.0078	0.5
V inj	0.2018	0.02
T melt - T mold	-0.0066	0.6
T melt - P hold	0.0500	0.08
T melt - V inj	0.0255	0.2
Tmold - P hold	-0.0159	0.2
Tmold - V inj	-0.0518	0.08
P hold - V inj	0.0512	0.08

Exp. uncertainty [mm]	0.0039

Table 6.5 - Average effects and COU coefficient for the X (above) and Y coordinates (below)

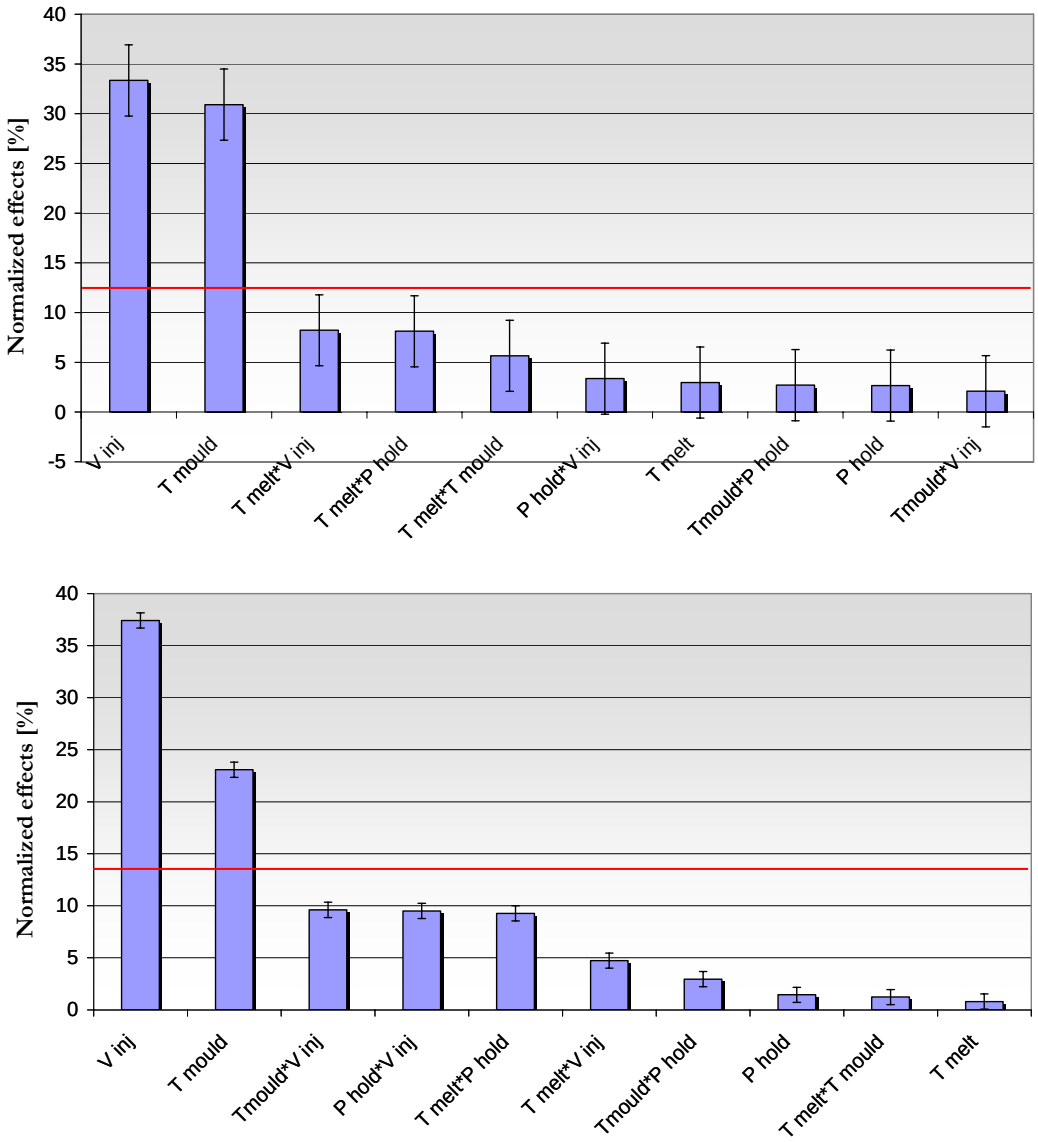

Figure 6.24 - Pareto chart of the X (above) and Y coordinates (below) and the reference line (α=0.05)

CHAPTER 7

DEDICATED SIMULATION OF THE FILLING STAGE IN THE MICRO MOLDING PROCESS

7.1 SCALING ISSUES

The scaling-related question that requires an answer in injection molding is how the standard molding know-how for part and tool design, process setup, material characterization, modelling and simulation can be properly scaled and used for miniaturized parts. The standard injection molding process is characterized by a filling time of several tenths of a second to several seconds, an injection molding pressure of several megapascals to about 200 megapascals, and a cycle time of several seconds to several 10s of seconds. These process conditions comply with the standard tools physical

limit. By physically understanding the scaling limitations of the existing molding technology, improvements, alternatives and solutions could be developed to overcome the current difficulty in the molding of high aspect ratio microstructures [81]. In this section, a dimensionless analysis is performed first to study the size effect on the flow and heat transfer process in the injection molding, succeeded by a comparison analysis with the experimental results.

7.1.1 Modelling

The first question to ask when dealing with the process modelling is which physical phenomena play a significant role. The modelling process can be schematically represented as follows [82]:

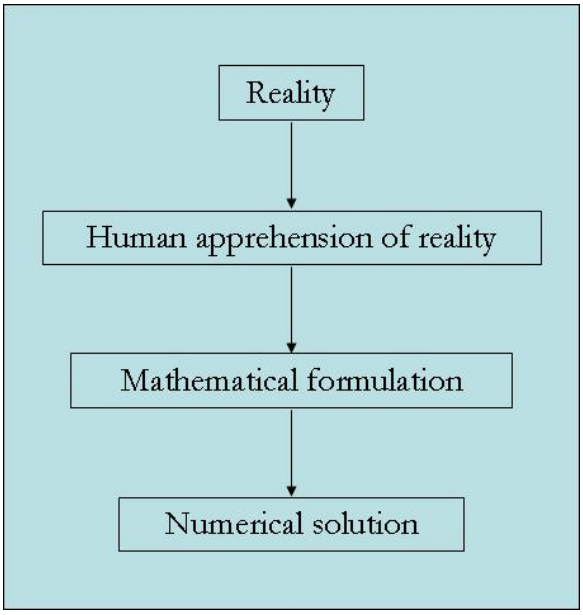

Figure 7.1 - Scheme of the modelling process

If it appears quite obvious that modelling aims at giving a mathematical formulation to physical reality, it might be useful to recall that this formulation is strictly dependent on the perception of reality in terms of comprehension and observation. This mathematical formulation, most of the time, resorts to numerical solutions, because analytical solutions are made vain by the complexity of the equations. This solution is the approximate solution to a

mathematical problem which, itself, is an approximation of physical reality.

7.1.1.1 Physical effects

A mathematical model is, thus, required to accurately represent the physics of micro injection molding. The problem is extremely complex. Indeed, compared with the shear-dominated physics of classical injection molding, the space and time scale reduction that occurs in filling micro parts can enhance unusual physical behaviours, among which the following ones have been picked out:

- viscoelasticity
- elongational viscosity
- capillary effects
- wall slippage.

It is expected that small space and time scales coupled with the velocity of the order of classical injection molding will increase the importance of viscoelastic effects. Moreover, extensional effects should be present in addition to shearing, in view of the three dimensional nature of the flow. Possibly, the role of both the fluid-atmosphere surface tension and the fluid-wall contact angle could be enhanced at the microscale. It also appears that the stress boundary conditions prevailing at the fluid-wall interface could be more complex in the filling of micro parts.

The principal objective of the mathematical modelling is to scale the problem in order to determine which of the above effects can be neglected. But before undertaking any scaling, it would be appropriate to proceed with all preliminary simplifications required. Other modelling effects should be taken into consideration, besides the aforementioned potential phenomena, such as:

- polymer crystallization: with reference to semicrystalline polymers, the degree of crystallization certainly affects the viscosity, the heat transfer (through both the polymer heat capacity and thermal conductivity) and most of the polymer material functions;
- thermodynamics: the role of compression and thermal dilation can be important. In addition, structural relaxation (i.e. delayed thermal dilation) may occur;
- heat transfer: the heat capacity and thermal conductivity of the injected polymers depend on temperature but also on pressure and molecular orientation;
- viscosity law: the viscosity depends on temperature, shear extensional

rate and pressure.

7.1.1.2 Restriction of the study

At the moment all the phenomena that change their relevance when shifting from macro to micro injection molding have been considered. It was decided to focus on a very precise and concise problem, described as follows.

7.1.1.2.1 First assumption: amorphous polymer

After processing and cooling, the polymers can be either semicrystalline or amorphous. In the first case, crystallization is bound to happen during the process due, on one hand, to the flow (flow-induced crystallization) and, on the other hand, to the temperature evolution (thermal crystallization). Of course this, in turn, has some impact on the rheological behaviour of the polymer. Hence, crystallization is a quite complex process. Therefore, it made sense not to take it into account in this first study on micro injection molding, the simplest way being to consider amorphous polymers only.

7.1.1.2.2 Second assumption: focus on filling stage

In the first approach on micro injection molding, it was decided to only consider the filling stage. It would have been frustrating to model the packing phase without any hint of the material state in terms of velocities, pressure and constraints in the cavity at the end of filling. For the same reasons, the cooling phase modelling, as a first step, would not have been suitable either.

7.1.1.2.3 Third assumption: focus on micro part filling

The filling phase includes both the filling of the runner system and the filling of the micro cavity. Moreover, it is probably during this specific step that the major peculiarity of micro injection molding lies. However, micro cavity filling includes microscale issues that already constitute a numerical challenge and the first step towards the whole process modelling. It was

decided to concentrate on the filling of the micro cavity only, in order to avoid different length and time scales, as the case would have been if we had to simulate the whole part filling (runners and micro part). Besides, this postpones the problem of linking the different length scales in terms of mesh connections.

7.1.2 Dimensional analysis

Before going any further, assumptions on the flow have to be made. The injection flow rate at the gate location of the micro cavity was estimated according to machine capabilities, neglecting leakage at the injection unit and material compressibility. The velocity at the gate location was estimated by considering an injection screw velocity of 200 mm/s and a screw diameter of 32 mm:

$$V_{inj} = \frac{Q_{inj}}{A_{gate}} = 230 \text{ cm/s} \tag{33}$$

7.1.2.1 Micro cavity filling time

An approximation for the micro cavity filling time t_{fill} is given by:

$$t_{fill} = \frac{l}{V_{inj}} = \frac{6{,}5}{2300} = 2.8 \text{ ms} \tag{34}$$

7.1.2.2 Dimensionless numbers

Size effects associated with miniaturization can be either of the first order or of the second order. First order size effects can be predicted using the traditional theory of continuum mechanics, while the second order ones cannot. An example of a first order size effect in injection molding is the increasing contribution of the gapwise heat conduction in the thermal problem, when the part thickness decreases. The occurrence of second order size effects in injection molding could be attributed to the increased molecular level influences at small sizes. Due to the large characteristic size of a polymer

molecule (gyration radius about 10 nm to 100 nm), molecular effects such as steric forces, chain entanglement, and immobile molecules at the wall could play a significant role on the behaviour of polymeric flows in microscale and invalidate the continuum approximation. Although discussion concerning the influence of second order effects could be challenging, the subject of this thesis is first order size effects, which can be studied using standard continuum-based modelling.

7.1.2.2.1 Inertial forces

The Reynolds number Re is used to characterize the flow. It denotes the ratio of inertia and viscous forces:

$$\mathrm{Re} = \frac{\rho V_{inj} l}{\eta_o} \approx \frac{10^3 \cdot 2.3 \cdot 6 \cdot 10^{-3}}{10^3} \approx 10^{-2} < 1 \tag{35}$$

where ϱ and η_o are the melt density and the zero shear rate viscosity of a traditional polystyrene material. In conclusion, the action of inertia can be considered as being negligible compared to the action of viscous forces.

7.1.2.2.2 Gravity forces

The Froude number is the ratio of the inertial force to the gravitational force. It is estimated here at:

$$Fr = \frac{U^2}{g_o l} \cong \frac{2.3^2}{10 \cdot 6 \cdot 10^{-3}} \cong 10^2 \tag{36}$$

As a consequence, the ratio of viscous forces to gravitational force is given by Re/Fr, which appears in the dimensionless momentum equation. This ratio is evaluated to $\approx 10^{-6}$, which is small and therefore gravitational forces will be neglected.

7.1.2.2.3 Capillary forces

The capillary number, which is the ratio of viscous forces to surface tension forces, is used to estimate the importance of the surface tension force

at the free melt surface:

$$Ca = \eta \frac{V_{inj}}{\sigma} \tag{37}$$

The surface tension (σ) does not vary much with temperature. Typical values for polymer melts range from 13.6 to 33 mN/m [83]. It is, in any case, lower than the surface tension of water, which is 72 mN/m. The minimum capillary number is as follows:

$$Ca = \frac{10^3 \cdot 2.3}{33 \cdot 10^{-3}} \cong 7 \cdot 10^4 \tag{38}$$

which confirms what was expected, namely that the capillary effects are negligible (due to the polymer high viscosity).

7.2 CONVENTIONAL NUMERICAL SIMULATIONS

The commercial software program Moldflow® MPI 4.1 was used to evaluate whether the present numerical codes are suitable to characterize melt flow patterns in a micro cavity. The prediction from three dimensional models and standard 2½D flow were compared to molding results using the weld lines as a comparison term for filling validation. The main material functions implemented were Cross-WLF (William Landel Ferry) for viscosity and two-domain Tait for pvT. Details on the mathematical-physical models of the simulation, including the finite element formulation, have been given in [84]. A great number of options for specification of process conditions are offered in the simulation program and materials are selected from a large database of specific grades. These options make it possible to model real processes with a fairly high level of detail.

7.2.1 Mesh model and boundary conditions

The micro cavity was modelled in the simulation program. The geometrical model, including feed system, is shown in figure 7.2. A sensitivity analysis of software simulation to the mesh dimension was conducted [85]. It was decided, as a result, to completely mesh the .STL model imported from Pro Engineering® software and to decrease the mesh size in the cavity zones

where the weld lines were detected experimentally.

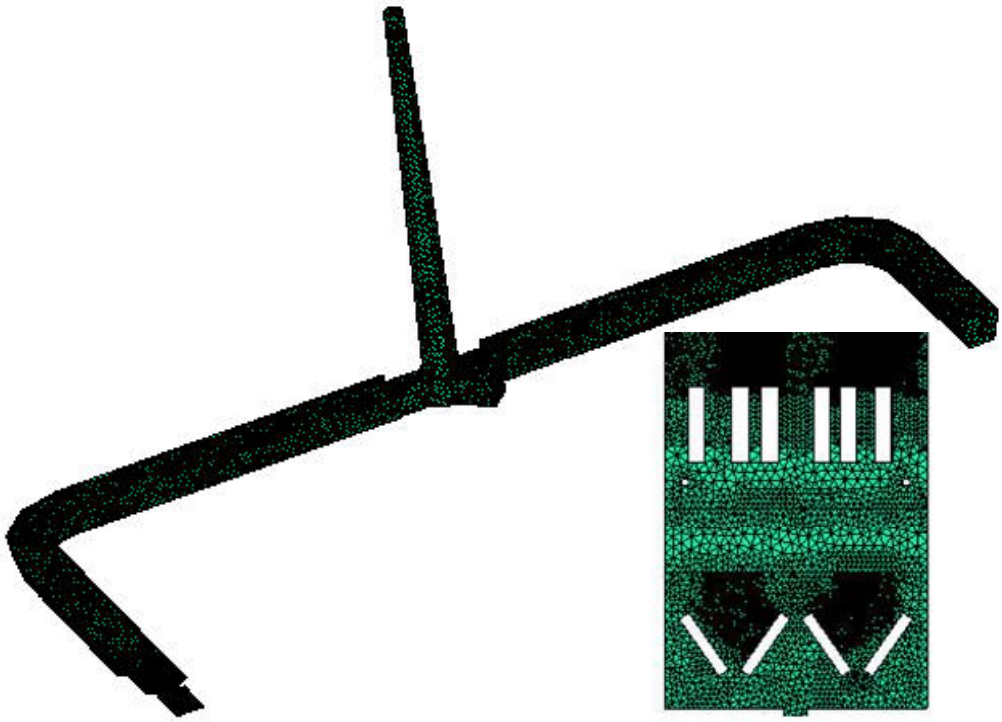

Figure 7.2 - Complete mesh model and micro cavity detail

Once the model was concluded, the boundary conditions were accurately defined. The melt temperature is a potential problematic parameter in terms of modelling [71]. In practice, the melt temperature was only indirectly controlled through the barrel temperature zones. A series of experiments were conducted where the melt temperature was measured manually at the injection location. The manual measurements were performed with a digital thermometer, Viking 3000, with a specified measurement uncertainty of ±0.2%. The difference between the barrel temperature and the measured melt temperature was relatively small (did not exceed 5°C). One possible strategy could be to simply reduce the melt temperature by 5°C in the simulation model, but the lower observed temperature could be due to the measurement method, where the melt was allowed some cooling. It was, therefore, decided to model the melt temperature as equal to the barrel temperature. On the other hand, the mold temperature was defined as being the mean value of the mold surface acquired by the temperature transducers

and controlled by a hydraulic heating system. Water, at the selected temperature, was forced to circulate through the channels of the cavity plate; the water temperature was controlled by retroaction, comparing the signal obtained from thermocouples with the temperature that was set in the heating system. While the previous parameters were easy to control, the injection speed setup was difficult to examine because of the screw inertia and the polymer compressibility, itself. The two profiles that were set in the machine have been set forth in figure 7.3.

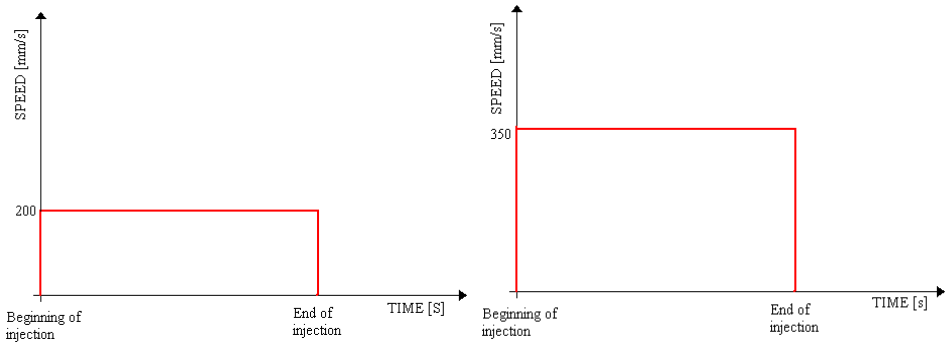

Figure 7.3 - Speed profiles set in the molding machine: injection speed of 200 mm/s (left); injection speed of 350 mm/s (right).

While a rectangular speed profile can be considered as being realistic in the conventional molding process, in micro molding the transitory time can be comparable to the injection time. The transitory time is considered as being the time elapsed between the moment when the ram starts to move and the moment when it reaches its stabilized speed (figure 7.4)

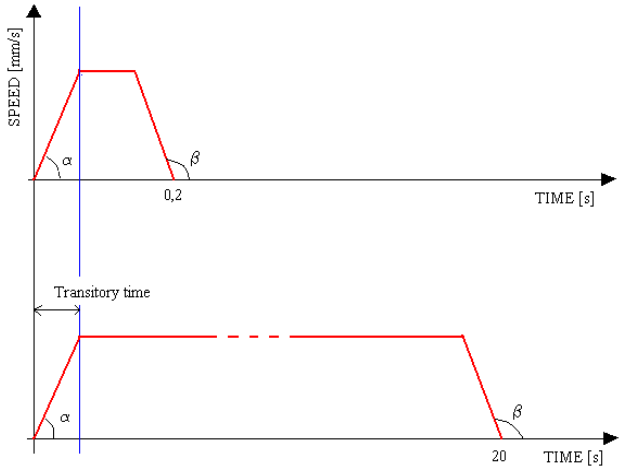

Figure 7.4 - Influence of the transitory in conventional and micro molding process.

This means that while in the conventional molding process it is possible to consider a rectangular speed profile, in the micro dimensional range an extensive analysis of the speed profile has to be executed, whenever it is wanted to provide an accurate speed profile as input to the software simulation. It was, therefore, decided to implement the real ram speed profile obtained from the screen output of the machine (figure 7.5).

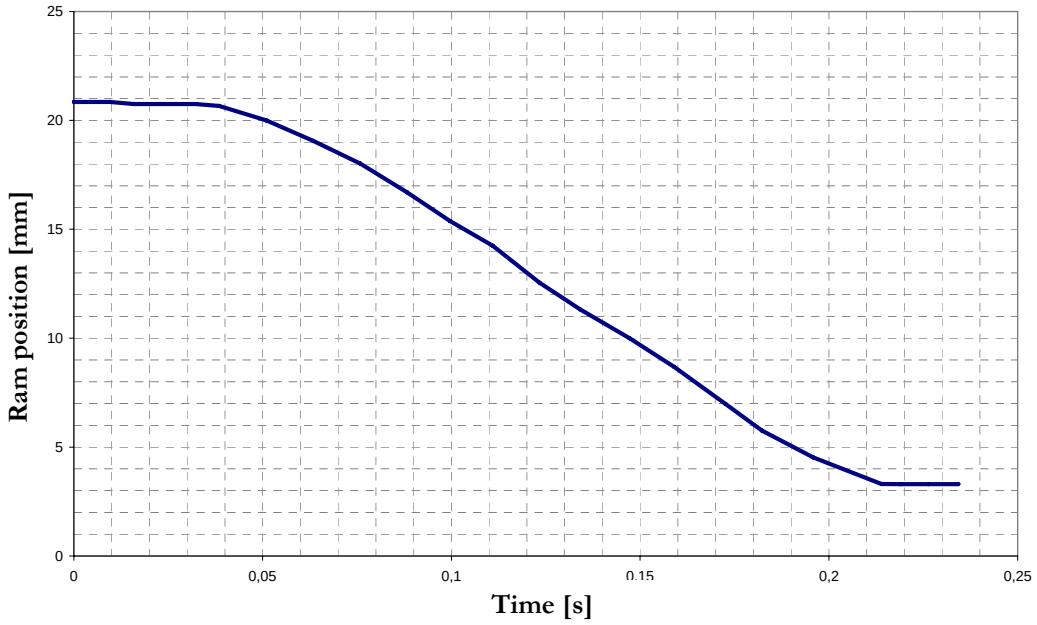

Figure 7.5 - Experimental ram speed profile

In order to have closer control over the boundary conditions setup and to improve the numerical simulation results, the same PS used in the experiments was characterized by means of both a rotational and a capillary rheometer. Steady shear measurements were performed on a dual bore Ceast® capillary rheometer at three different temperatures (230°C, 250°C and 270°C), in a shear rate range of 1000 to 10000 s^{-1}. On the other hand, at low shear rates, experiments were performed on a TA Instruments ARES machine at the same temperatures in a frequency range ω = 0.1 to 1000 $rads^{-1}$. The samples were maintained under a nitrogen atmosphere to avoid polymer degradation by oxidation. Measurements were performed in a frequency sweep mode with a 5% deformation range. Three measurement points per decade were taken with increasing frequencies. The data of dynamic and steady flow viscosities were simultaneously plotted (according to the Cox-Merz rule [86]) and fitted to the Cross-WLF model. The viscosity model coefficients implemented in numerical

simulations have been set forth in table 7.1.

Cross-WLF parameters	
n	0.25433
τ [Pa]	31210.18
D_1 [Pas]	9.478E+26
D_2 [K]	428.15
D_3 [K/Pa]	0
A_1	56.342
A_2 [K]	2.192

Table 7.1 - Cross-WLF model coefficients for PS 143 E

Secondly, the material was characterized on a differential scanning calorimeter (TA Instruments Q200). The thermal characterization was conducted at the maximum controlled rate of 30°C/min. Due to loss volatiles, the transition temperature was accurately determined only during a second heating rate and it was estimated in 88°C. Then the specific heat, in function of the temperature, was calculated according to ASTM 1269 E (table 7.2). On the other hand, the thermal conductivity in function of the temperature was implemented according to the Moldflow® database.

Temperature [°C]	Specific heat [J/Kg°C]
20	1222
85	1556
97	1702
106	1862
220	2246

Table 7.2 - Specific heat in function of the temperature

7.2.2 Sensitivity analysis of filling simulations to process parameters change

The same factorial plan design, carried out during the experiments, was performed in order to determine the influence of different process settings on numerical micro filling. Both 2½D (based on the Hele-Shaw assumption) and

3D numerical simulations were performed considering the weld line position as output. Unlike the two dimensional analysis, three dimensional simulation is not provided for automatic detection and evaluation of the weld lines location. Simulated weld lines were determined, reconstructing their path, by subsequent simulation steps collection. The first step was to detect the initial meeting point of two flow fronts and then to expand it from the initial meeting point to obtain the entire weld line. Since the accuracy of the prediction depends on the mesh size, it was decided to decrease the mesh size in the cavity zones where the weld lines had been detected experimentally. The minimal size was determined as a compromise between computing time and the accuracy of weld lines detection. An uncertainty assessment of the measured weld line position was carried out in order to verify the reliability of the investigation. Measuring uncertainty sources, which have been taken into account were:

- instrument resolution
- repeatability of the measurements.

The positions of the points were detected with an average expanded uncertainty of ±11 μm on the X and Y directions [85]. The flow front advancement and the weld line detection in 3D analysis have been illustrated in figure 7.6. The solid line is the predicted weld line location.

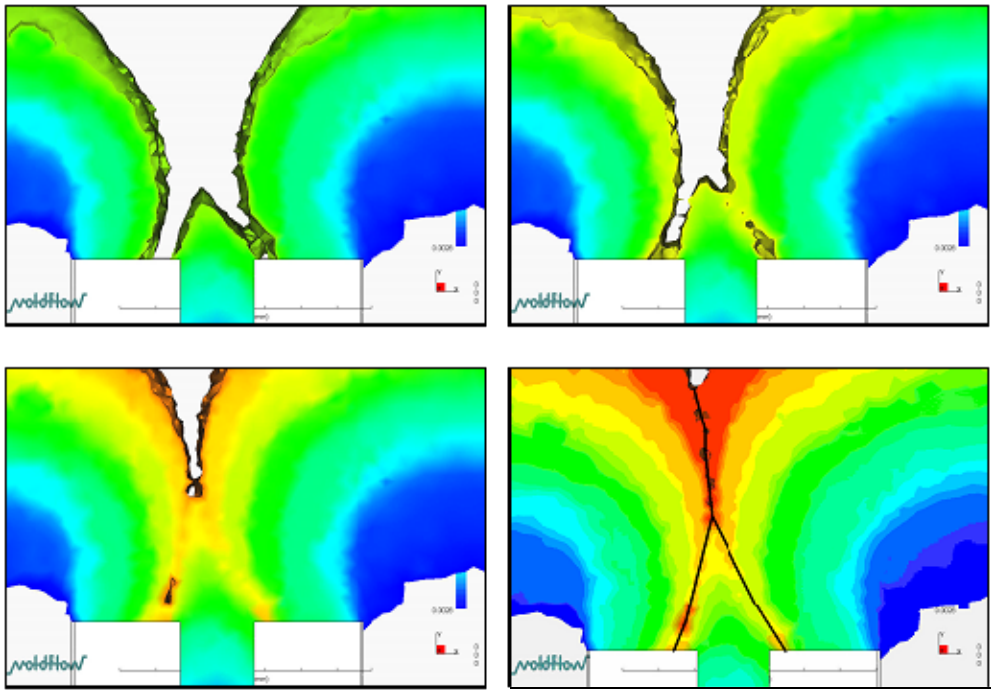

Figure 7.6 - Flow front advancement and detection of the weld line number 2

Then it was decided to analyze the software sensitivity to the process parameters change. By way of comparison, the same outputs and process conditions were considered, which, in the previous dimensional analysis, resulted as being significant (chapter 6). Therefore, only the X position of the weld line number 2, the horizontal line and the meeting point of the weld line number 3 were considered. Both 2½D and 3D numerical simulations were performed but no significant change in the weld line position was observed. For example, the influence of the injection velocity on the third weld line position has been set forth in figure 7.7. It is clear how the software (in contrast with the experimental results) is not sensitive to the injection speed variation.

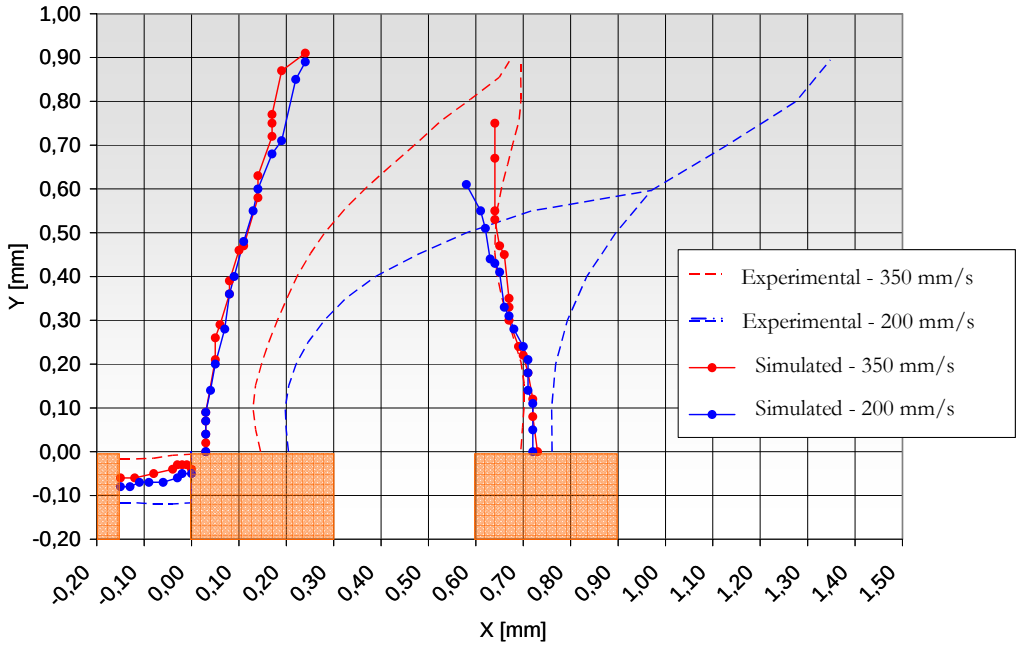

Figure 7.7 - Influence of different ram speed profiles on the weld line position

7.2.3 Validation of conventional filling simulations

As an initial approach, fast running 2½D simulations were performed in order to compare numerical results to the experimental ones. The standard Hele-Shaw approximation [87] involves creating a two dimensional finite

element mesh, which corresponds to the midplane of the modelled part. All surface effects and the heat flux are only calculated for the top and bottom of this midsurface. This simplification will clearly lead to problems when working on the micron scale, where all surface effects must be considered. Therefore, initial simulations with Moldflow® were performed to check their suitability for the micro injection molding process. As a second approach, a three dimensional finite element analysis was performed. Non-Newtonian, non-isothermal flow solutions were obtained by solving the momentum, mass and energy equations. No-slip boundary conditions were imposed on the cavity walls filled with the polymer, while on the unfilled part, a free boundary condition allowed for the formation of the typical fountain flow. The heat transfer between the cavity and the mold was modelled by imposing the convection heat flux (default value of 25000 W/m²K for global heat transfer coefficient was considered). Viscosity model coefficients were implemented according to the classical Cross-WLF model. Numerical constitutive equations did not account for inertia, elastic and surface effects. At each time step, the code computes velocity, pressure and temperatures fields within the cavity, by the solution of the conservation equations and polymer constitutive models, as well as the evolution of the flow front position (figure 7.8).

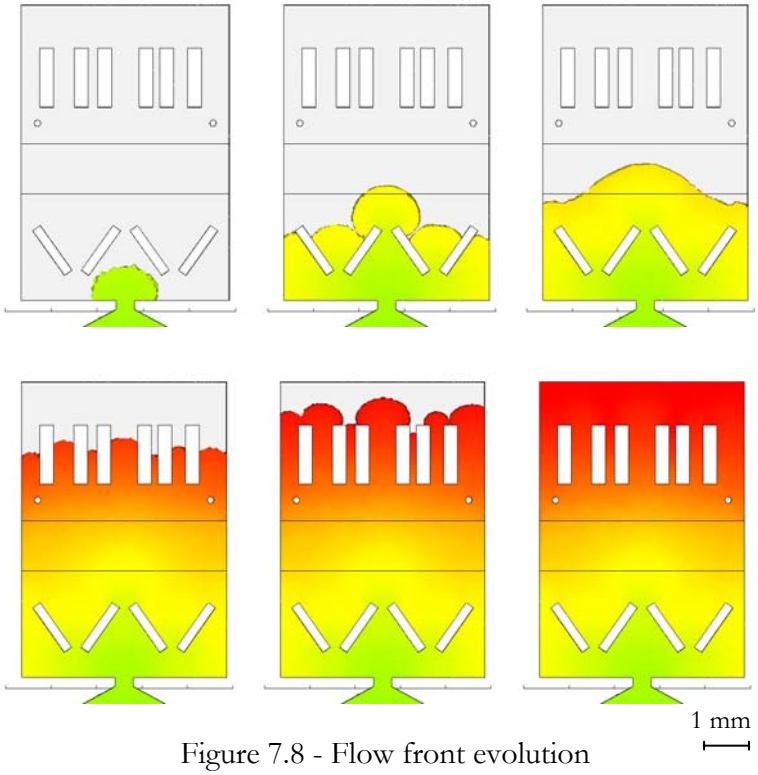

Figure 7.8 - Flow front evolution

The filling stage was simulated by imposing accurately defined boundary conditions. Since the software simulations resulted as being insensitive to the process parameters variation (paragraph 7.2.2), it was decided to only consider the simulation results of a single trial of the experimental plan (trial number 13). A real ram speed profile of 350 mm/s, a mold temperature of 70°C, a melt temperature of 270°C and a packing pressure of 100 bar were implemented. Each simulated weld line position was compared to the experimental one and correlations between the physical effects and the flow front development were established.

The characteristic shapes and extremely small dimensions of the micro cavity as well as the unique flow front shapes quickly revealed that a 2½D solution is no longer sufficient to describe all the effects. In the following, the comparison between 2½D, 3D and experimental positions of weld lines have been considered. In the first part of the cavity filling, where the thickness in the gapwise direction is negligible, if compared to the length and width of the part, and the thermal exchange through lateral walls can be disregarded, the 2½D and 3D simulations predicted the same results (weld line 1 in figure 7.9). Both of them overpredicted the flow front displacement after the contraction flow, if compared to the experimental results. On the other hand, the different position of the weld line 4 (figure 7.10) revealed that the midplane simulation is not appropriate in dealing with a juncture of planes with different thickness. This effect is known as the "step effect". The difference between the midplane and 3D simulations could be related to the flow splitting at the junctures, where three velocity components coexist. The velocity component of the gapwise direction is neglected by the Hele-Shaw approximation. Futhermore,

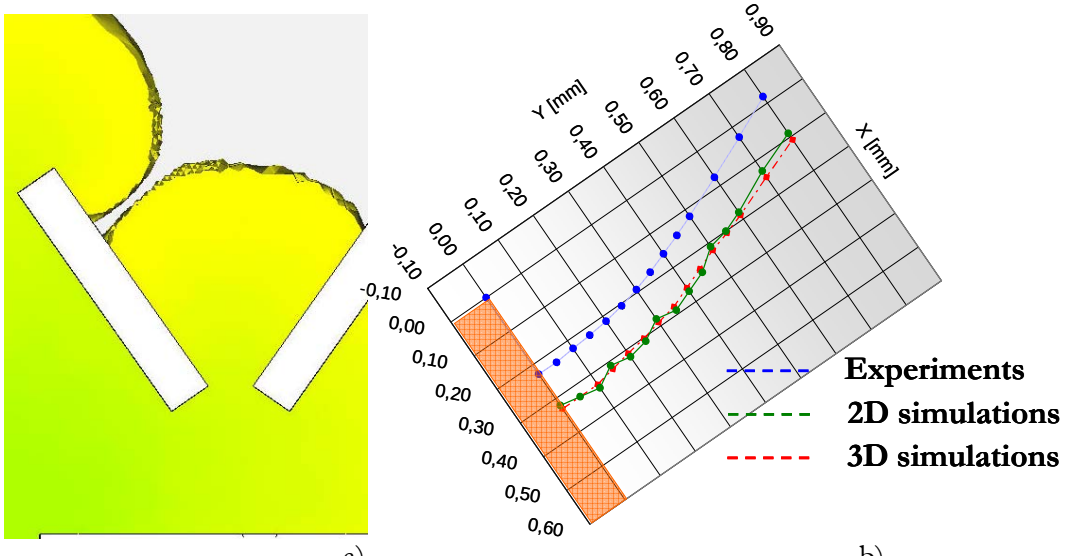

a) b)

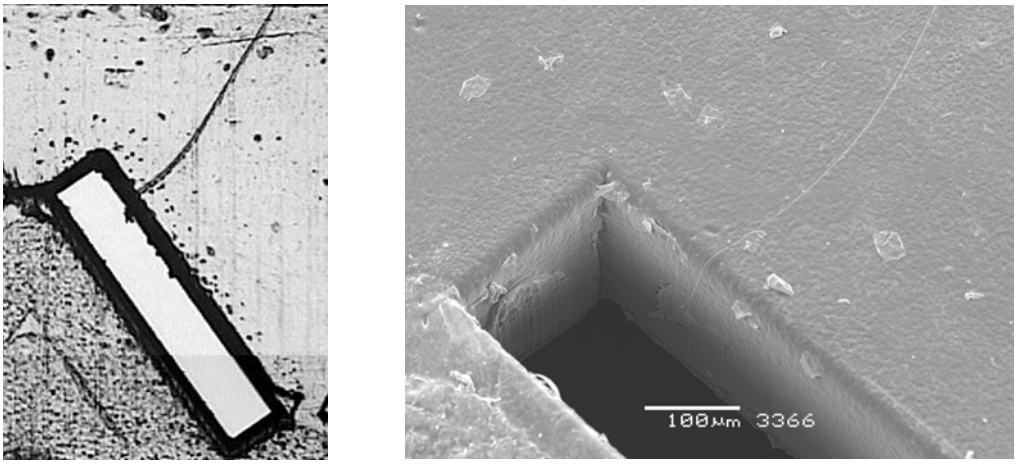

Figure 7.9 - Simulated formation of the investigated weld line (a); comparison between numerical and experimental results (b); DeMeet (c) and SEM (d) images

the 2½D solution did not give accurate results in correspondence of the micro channels (weld line number 2 and 3). When flowing through a shell element, the flow is assumed to be through two parallel planes with no edges. There is neither heat loss nor resistance to flow along two of the four sides. Like most micro plastic parts, the cavity is comprised of walls where the width is in the same order of the thickness. As a result, the program overpredicted the ease

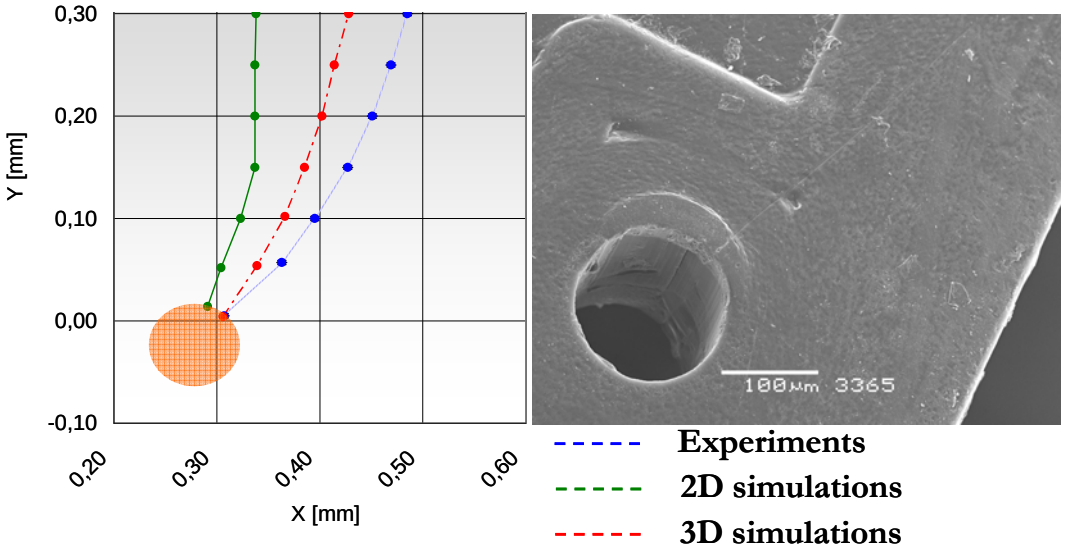

Figure 7.10 - Comparison between numerical and experimental results of weld line 4

with which the plastic would flow through these channels (figure 7.11). The smaller the ratio of width to thickness of the flow channel, the more the error increases. Further potential errors could be due to ignorance of the viscoelastic behaviour of the polymer, itself. In conventional simulations, the polymer is considered as a purely viscous material and elastic effects are disregarded.

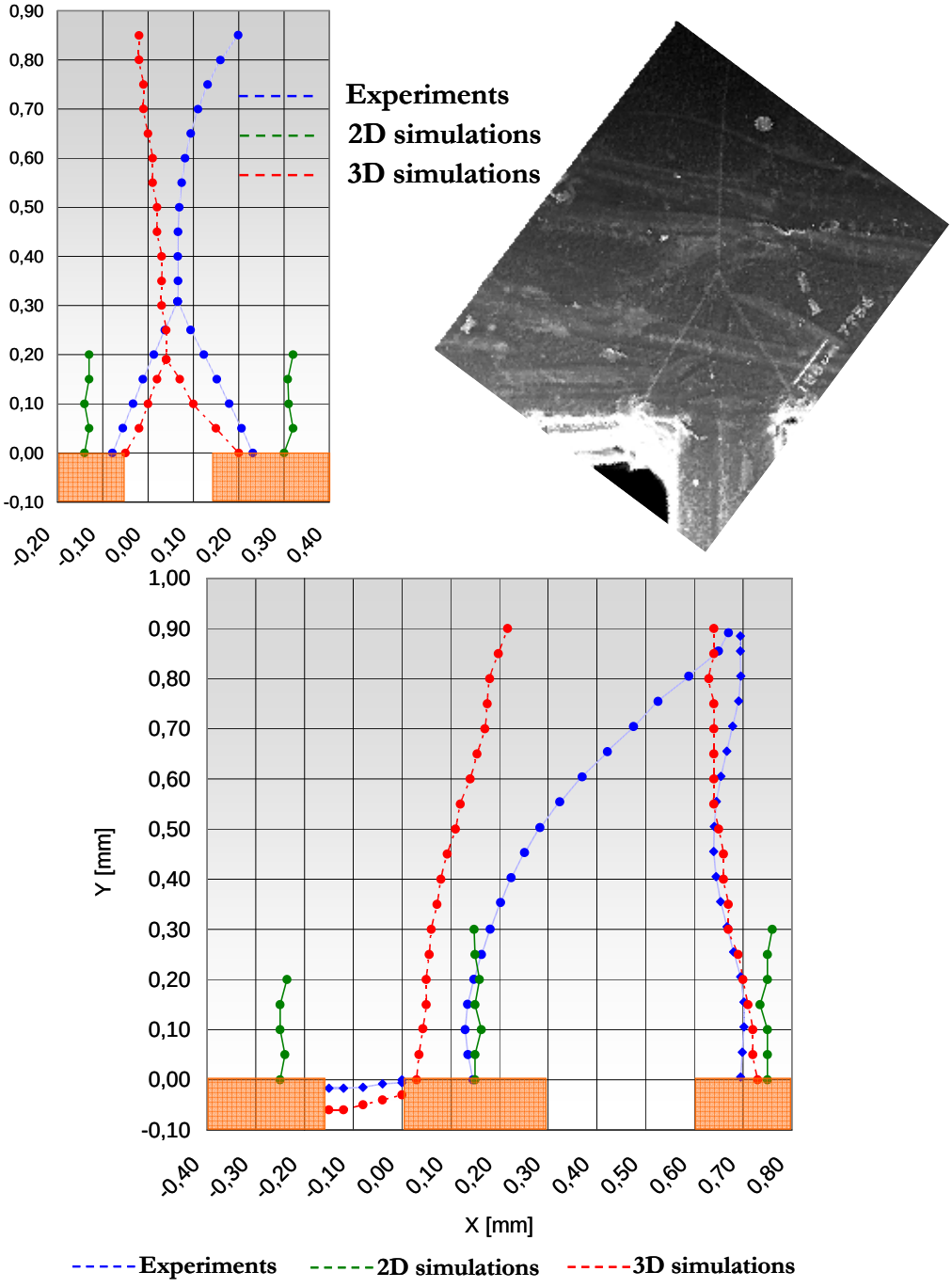

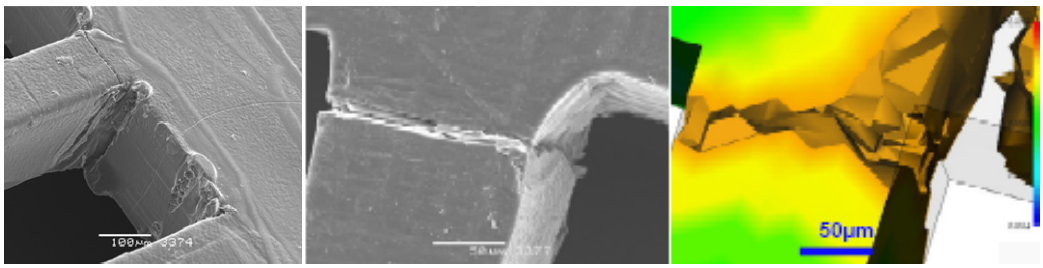

Figure 7.11 - Comparison between numerical and experimental results and the SEM image of the weld line 2 (above) and weld line 3 (below).

7.2.4 Sensitivity analysis of filling simulations to factors with different behaviour on macro/microscale

Until now, numerical simulations have been performed considering default boundary conditions and models, which usually gave accurate results in the conventional molding process. On the other hand, both 2D and 3D analyses resulted as being inappropriate when dealing with contraction-expansion flow, junctures of planes and flow in micro channels with different thicknesses. Furthermore, conventional simulations resulted as being insensitive to the process parameters variation. Moreover, the flow behaviour of polymer melts in micro mold-cavities has not been fully understood. It is believed that, due to the large surface-to-volume ratio, surface effects will dominate the flow behaviour at the microscale. Kemann et al. [88] showed that standard injection molding simulation packages are not able to describe all of the effects in micro-molding. Firstly, the rheological data used in current packages are obtained from macroscopic experiments. These macroscopic data would not be suitable for modelling microscale flows. Secondly, the polymer has a strong tendency to slip, especially in micro channels [92]. When a classic no-slip boundary condition is used in current packages, the consequences of wall slip cannot be predicted. Thirdly, the microscale dimensions of features and rapid filling rates, typically found occurring within micro molding cavities, ensure that the shear rates, experienced by the polymer during the micro molding process, are orders of magnitude higher than those experienced in conventional injection molding. However, the extensional behaviour in contraction flow or the pressure influence on the viscosity cannot

be disregarded. Furthermore, the mold/melt heat transfer coefficient was found to be a critical factor in determining the filling lengths [89]. A significant decrease in the Nusselt number was observed concerning the laminar flow in microscale channels. This means that a constant heat transfer coefficient may not be applicable to the heat transfer simulation involving flow through microscale channels. The development of flow models and effects, valid in microscale, is still in its infancy. Based on currently available data, it was decided to perform simulations implementing those factors that seem to have the most influence on the microscale flow. 3D simulations were, therefore, performed considering the influence of pressure on the viscosity, elongational behaviour, micro rheological behaviour and different heat transfer coefficients [90]. On the other hand, traditional viscous material coefficients were implemented according to the Cross-WLF model. At the moment, in dedicated numerical simulations, the elastic behaviour of the polymer is still disregarded. The outcome of the following study is aimed in evaluating whether the implementation of microscopic scale factors may improve the accuracy of the filling simulations. A one-factor at a time analysis was performed and it was decided to concentrate on the filling of the micro cavity only in order to avoid different length and time scales, as would have been the case if we had simulated the whole part filling (runners and micro part). Besides, this postpones the problem of linking the different length scales in terms of mesh connections [85]. Only results related to the position of the weld line number 2 have been presented, because the meeting point is a characteristic term of comparison and because its Y coordinate resulted as being insensitive to process parameters variation, both in simulations and experiments.

7.2.4.1 Effect of the heat transfer coefficient at melt/mold interface

The thermal exchange between the polymer and the mold is of critical importance in the micro injection molding process, due to the large surface to bulk ratio of microstructures. The default software setup assumes good contact between the plastic and mold wall for the entire contact time. The main problem is that perfect physical contact between the solidifying polymer and the mold does not exist. It has to be noted that in micro injection molding, the detachment of the polymer from the mold might occur earlier in the filling stage, because solidifying in microstructures may have already begun during the filling stage. The default value of 25000 W/m^2K, implemented in

Moldflow®, seems to be questionable to be used in simulations. During the micro filling stage, its typical values might be from 2000 to 5000 W/m²K [89]. To analyze the heat transfer coefficient (HTC) influence on the simulation analysis, a sensitivity study of the simulation to this parameter was executed. The governing equations of transient three dimensional, simultaneous momentum and heat transfer during the filling of micro-sized and macro-sized molds were solved using the commercial software Moldflow®. The micro cavity mold contains challenging features including high aspect ratio, sudden width and depth changes and flow through micro channels. The study examined the use of both Dirichlet (temperature) and Newman convection-type (heat flux) boundary conditions on the mold surface to obtain realistic filling profiles (figure 7.12). Each micro channel was modelled as a core insert and divided into 5 segments. The local heat transfer coefficient was estimated for each segment, according to equation 24. The same ram speed profile was imposed in both simulations [85], the one with a default coefficient of 25000 W/m²K and the other one with a local coefficient estimation. If a heat transfer coefficient of 25000 W/m²K was implemented in the main flow, commonly used as a default value in commercial macroscale injection molding, the results would show that the filling length in the micro channel is underpredicted (Y in table 7.3). This is because the polymer, in correspondence with the channel wall, freezes too quickly. On the other hand, using a variable and lower local heat transfer the polymer melt can flow much deeper into the 200 μ micro channel. It is possible to see in table 7.3 that movement occurs in the simulated weld lines, changing from a default condition to a local heat transfer definition. It is clear how the meeting point moved towards the experimental one.

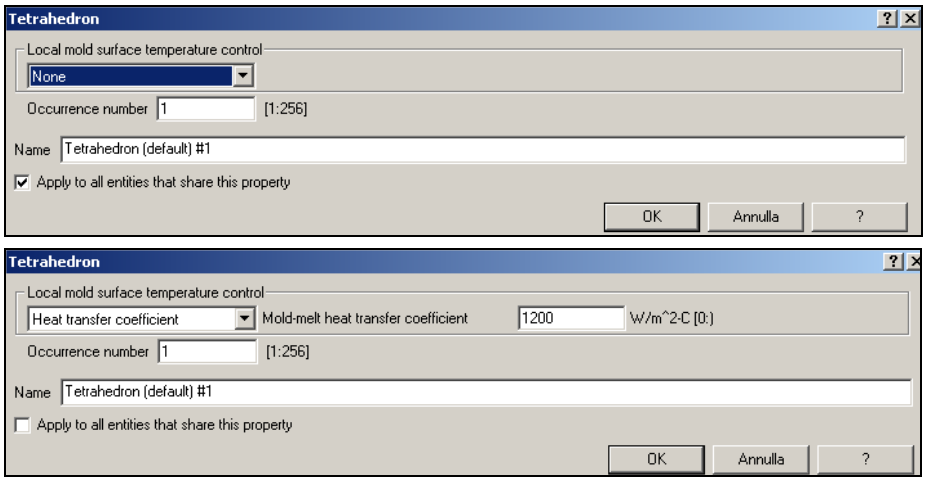

Figure 7.12 - Dirichelet (above) and Newman (below) condition

Although numerical simulation with a variable heat transfer coefficient could reasonably predict the filling of the micro channel, some discrepancy still exists between simulation and experiments. This is probably due to the fact that several issues were not considered in the modelling. For example, a thin gap between the polymer bulk and the mold wall could develop because of high cooling shrinkage. It could cause the melt temperature to drop much more slowly and enable the melt flow further. Furthermore, the wall slip could occur in micro channels. The increased elasticity makes slip more likely to occur in smaller scale.

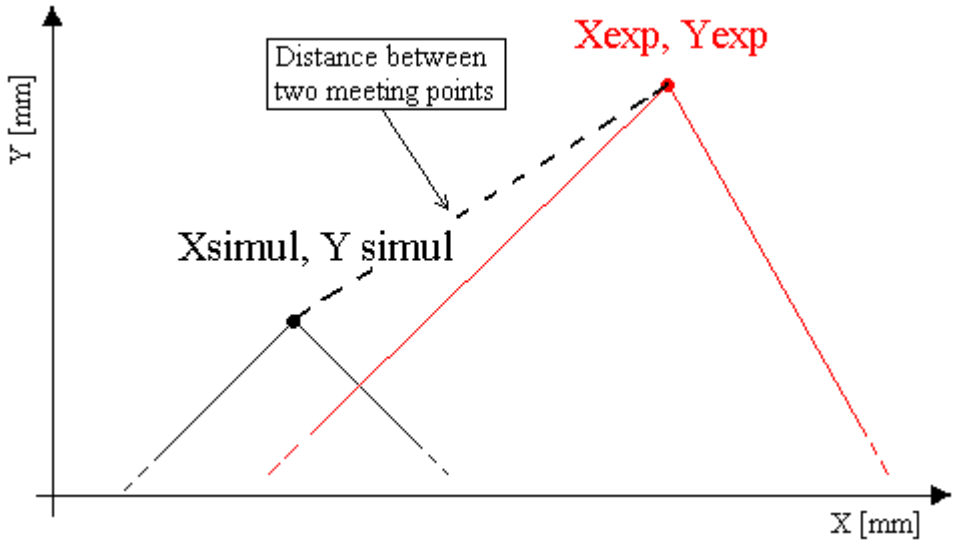

Coordinates	Experimental position [µm]	3D conventional simulation [µm]	Local heat transfer coef [µm]
Y	308	182.3	228.95
X	68.57	37.14	47.62

Table 7.3 – The experimental and simulated position of the meeting point

7.2.4.2 Slip or no slip condition

A good understanding of the interaction between the material behaviour and processing conditions is important in order to comply with stricter tolerances and demanding service conditions. This is particularly important in the case of micro forming processes involving the filling of a

mold, where the coupled phenomena of fluid flow and heat transfer determine, to a large extent, the final properties of the molded part. One of the boundary conditions that raises questions concerns the wall/polymer interface. In Moldflow® conventional simulations a sticking contact between the wall and the polymer is assumed [84]. Various studies [91, 92] have shown that polymer melts, unlike Newtonian fluids, may violate the classic no-slip boundary condition of fluid mechanics. Slip may occur over solid surfaces when the wall shear stress exceeds a critical value (0.1 MPa). In this high stress regime, the slip velocity increases with the shear stress raised to a large power. This slip mechanics has been attributed to the disentanglement of the bulk chains and the chains attached to the wall. Although classic slip determination techniques, such as the Mooney method, assume that slip occurs independently of the channel size if L/D is the same and the pressure drop is constant, it is conjectured that wall slip would occur more easily in micro channels based on the following observations. Firstly, the increased tendency in wall slip could be explained considering the viscoelastic behaviour of the polymer. Polymeric chains can be considered as being linked to each other by springs. As the channel becomes smaller, the number of springs across the gap decreases and therefore the material appears to be more rigid due to the constraints at the wall. The increased elastic effect makes the polymer more susceptible to wall slip. Secondly, the increased pressure required to fill micro cavities exerts more stress on the wall, thus promoting wall slip.

Determination of the melt rheological behaviour within microstructured geometry is very important for the accurate simulation modelling of micro molding. On the other hand, investigation of micro melt rheology is difficult due to the lack of commercial equipment. In Chien's work [92], a melt viscosity measurement system for polymer melt flowing through microfeatures was established using a micro channel mold operated at a mold temperature as high as the melt temperature. From measured pressures and volumetric flow rate, both capillary flow and slit flow models were used to calculate the viscosity, utilizing Rabinowitsch and Walters corrections. The mold contained a micro channel of square section that allowed sizes varying from 300 μm to 200 μm and 150 μm. It was found that the measured viscosity values in this test were significantly lower (about 30% to 80% lower) than those obtained from the traditional capillary rheometer. The reduction of the melt viscosity within the micro channel becomes more significant when the size of the micro channel decreases (figure 7.13). The wall slip may be the major reason causing this viscosity reduction and it was found that the percentage of slip velocity relative to mean velocity increases on decreasing the size of the micro channel.

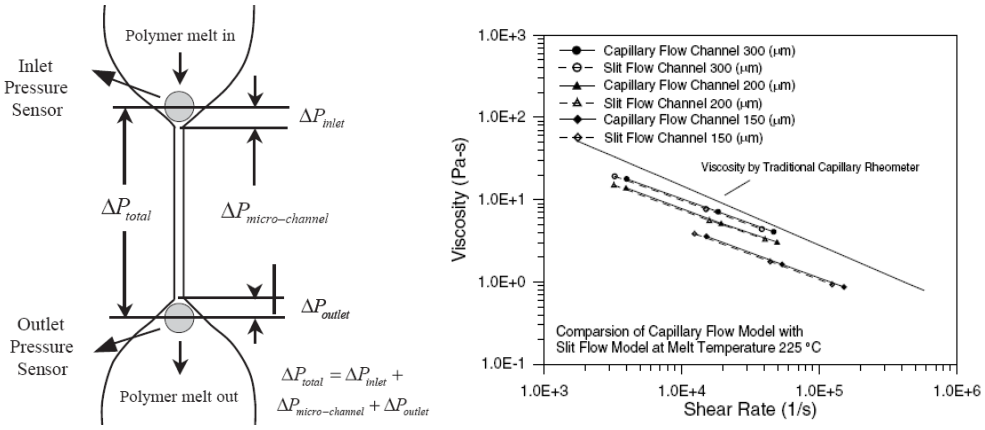

Figure 7.13 - Micro rheometer design and viscosity reduction in function of the channel depth at a reference temperature of 225°C [92]

In this section, it was decided to analyze the influence of an employed microscale rheology on the filling simulation of the micro cavity. The interest of the work was especially to verify whether the use of the microscale rheological data could improve the accuracy of the simulation results. The size of the cavity features, object of this thesis, ranges from 150 µm (thinner channel section) to 250 µm (maximum cavity thickness). It was decided to consider an average dimension of 200 µm (the representative dimension of the cavity microfeatures) and to fit the viscosity data according to the Cross-WLF model (figure 7.14). Simulations were performed to analyze the influence of a microscale viscosity, lower than the one measured by a traditional capillary rheometer in the same range of shear rates, without any desire for an absolute comparison between the simulated and experimental weld lines position.

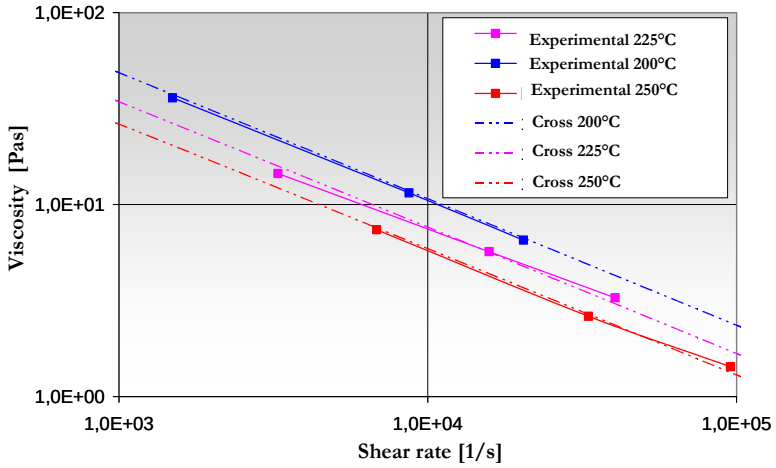

Cross-WLF parameters	
n	0.34
τ [Pa]	4759.8
D_1 [Pas]	3.89E+09
D_2 [K]	373.15
D_3 [K/Pa]	0
A_1	20.7
A_2 [K]	51.6

Figure 7.14 - Cross-WLF coefficients for PS 143 E in a microstructure 200 μm thick

The meeting point coordinates of the weld line number 2 was compared between the two simulations, the first one implementing default parameters and the other one implementing micro rheological data. When shifting from macro to micro viscosity model coefficients, the meeting point moves closer to the experimental one (table 7.4). Its movement, dominant if compared with the uncertainty budget, is due to the viscosity reduction in the 200 μm channel wide and to the lower pseudoplastic behaviour of the polymer. A lower difference of flow rates at the exit of the micro channels with different dimensions is expected and, consequently, a deeper filling depth in correspondence with the 200 μm channel wide.

Coordinates	Experimental position [μm]	3D conventional simulation [μm]	Micro-rheology simulation [μm]
X	68.57	37.14	62.79
Y	308	182.3	232.2

Table 7.4 - Experimental and simulated position of the meeting point

7.2.4.3 Pressure dependence of the viscosity

In the current situation of determining accuracy obtained from an ordinary filling analysis program, a typical under-estimation in the pressure loss was observed for the micro cavity, where hydraulic pressure becomes extremely high and a severe contraction flow takes place. The simulation underpredicts the maximum injection pressure of the cavity by approximately 5%. The cause of discrepancy between the simulation and the observation

seems to be the lack of knowledge of important parameters such as the pressure dependence of the viscosity (coefficient D_3 in the Cross viscosity equation) [93], the extensional flow and elastic effects. A further material characterization was performed on the Ceast® capillary rheometer, present at the Te.Si. research laboratory (University of Padova). It was necessary to derive a strategy that allowed an efficient quantification and separation of the pressure effect on the viscosity. A throttle was, therefore, arranged in series with the die at the piston driven capillary rheometer. The hydrostatic pressure in the die could be step-wisely increased at a constant mass flow rate. The principle has been illustrated in figure 7.15. The quantities of interest were the die inlet pressure P_i (acquired directly by the Ceast® in line computer) and the die exit pressure P_e (acquired by an additional Kistler® melt pressure transducer), their difference giving the pressure loss ΔP at the die:

$$\Delta P = P_i - P_e = \Delta P_D + P_c \tag{39}$$

A photograph of the arrangement is shown in figure 7.15. An electric heater was then applied in order to avoid the heat sink effect.

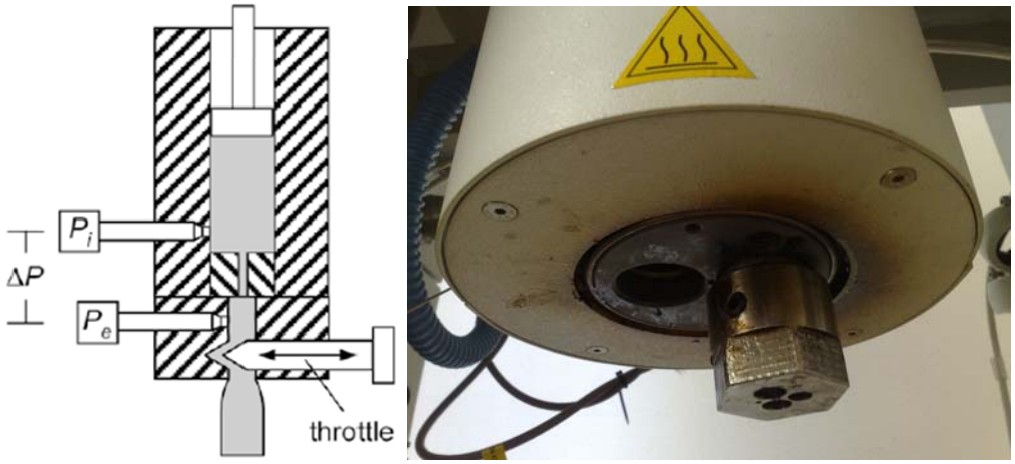

Figure 7.15 - Principle and photograph of the equipment present at Te.Si. laboratory

Data obtained from experiments in a pressure range of 40 MPa (the maximum pressure difference reached in the equipment due to throttle efficiency and the maximum load cell) were fitted according to the Cross model and the D_3 coefficient was estimated (2.1×10^{-7} K/Pa). Sensitivity analysis was performed in order to determine the influence of pressure dependence of the viscosity on the micro filling analysis. Simulations were performed with and without the introduction of the pressure-dependent viscosity coefficient. According to the

results set forth in table 7.5, it was impossible to conclude that the filling simulation code was sensitive to the pressure dependence of the viscosity in terms of the weld line position. The relative movement of the meeting point of the weld line number 2 was included in the uncertainty budget (±11 μm).

Coordinates	Experimental position [μm]	3D conventional simulation [μm]	P dependence of the viscosity [μm]
Y	308	182.3	172.1
X	68.57	37.14	40.98

Table 7.5 - Experimental and simulated position of the meeting point

7.2.4.4 Effect of the elongational viscosity

Flows in different polymer processing techniques range from highly shear dominated in processes such as conventional injection molding and transfer molding to highly elongation dominated in extrusion, blow molding and micro injection molding. In the processes with elongation-dominated flows, elongational viscosity, which is defined as the ratio of elongational stress to the elongational strain rate, has a considerable effect on velocity and pressure distribution. In confined regions of the mold, such as the runner, gates and parts of the mold cavity with abrupt changes in thickness, polymer goes through a significant elongational deformation, where the long chain polymer molecules exhibit stiff resistance. The pressure gradient in these regions with elongation-dominated flow, predicted by a generalized Newtonian formulation, can be significantly smaller than the pressure gradient encountered in the molding process. A conventional shear viscosity model is implemented as default in Moldlfow® simulations. The stress developed during simple shear flow is related to deformation by shear viscosity, which in turn is a function of temperature, pressure and shear rate. In mixed shear and extension deformations, a unified viscosity can be implemented in Moldflow® as a function of both extension rate and shear viscosity (Cogswell's model):

$$\eta_e(T,P,\dot{\gamma},\dot{\varepsilon}) = f(\dot{\varepsilon})\eta_s(T,P,\dot{\gamma}) \tag{40}$$

$$f(\dot{\varepsilon}) = 1 + \frac{A\cdot\dot{\varepsilon}}{B+\dot{\varepsilon}} \tag{41}$$

where η_e represents the unified viscosity, η_s the shear viscosity, $\dot{\varepsilon}$ the elongational rate, A and B data-fitted coefficients. In particular, A reflects the importance of extension stresses and B the extension rate of the transition to high extension stresses. The A, B coefficients were determined on the Ceast® capillary rheometer using experimental pressure measurements in a convergent flow (table 7.6).

Cogswell coefficients	A	B
	0.309	297.26

Table 7.6 - Extension viscosity coefficients determined for PS 143 E at the reference temperature of 270°C using a capillary of L=20/5 mm and D=1 mm

Numerical simulations were performed implementing, at first, a conventional shear flow viscosity and then the Cogswell's viscosity model. A different viscosity distribution, at the end of the filling phase, can be observed in the following figure:

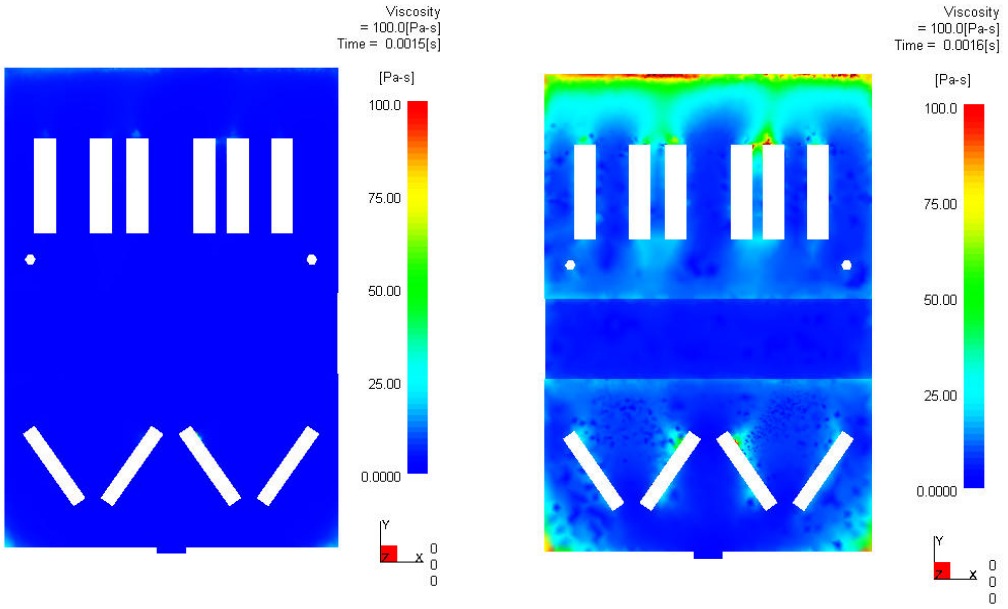

Figure 7.16 - Viscosity at the end of the filling phase with the default Cross-WLF viscosity model (left) and considering the unified viscosity model (right)

The two different approaches were compared in terms of the meeting point position (table 7.7) If the unified viscosity model was implemented, a relative

reduction of the meeting point Y position would be observed, due to the increased viscosity in the micro channel.

Coordinates	Experimental position [μm]	3D conventional simulation [μm]	Unified viscosity model [μm]
Y	308	182.3	170.2
X	68.57	37.14	50.2

Table 7.7 - Experimental and simulated position of the meeting point

7.2.4.5 Analysis of results and discussion

The development of flow and heat transfer models valid in microscale is still in its infancy. Based on currently available data, it was decided to perform simulations implementing those factors that seem to have more influence on the microscale flow. Three dimensional simulations were, therefore, performed considering the influence of pressure on the viscosity, the elongational viscosity, the micro rheological behaviour and different heat transfer coefficients [90]. On the other hand, default viscous material and heat transfer coefficients were considered. The parameters which resulted as having more influence on the micro cavity filling were the micro rheological data and the local heat transfer coefficient. On the other hand, the influence of pressure on the viscosity and the elongational viscosity could be disregarded. When the rheological data and the heat transfer coefficient were shifted from macro to microscale, improvements on the simulations results were acquired. The meeting point of the weld line 2 moved closer to the experimental one. An uncertainty assessment of the measured weld line position was carried out in order to verify the reliability of the investigation. The measuring uncertainty sources which were taken into account were:

- instrument resolution
- repeatability of the measurements.

The meeting point movement was dominant if compared with the uncertainty budget (figure 7.17). A complete validation of the software will be possible when more reliable models for local viscosity and heat transfer will be available.

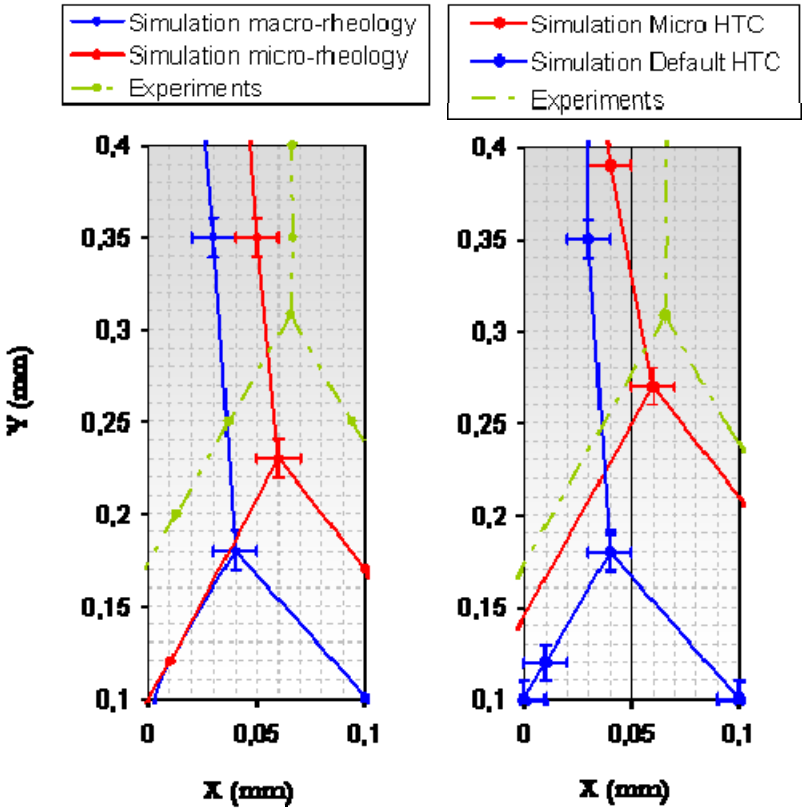

Figure 7.17 - Effect of micro rheology (left) and combined effect of micro rheology and local heat transfer coefficient (right) on the meeting point position

CHAPTER 8

NUMERICAL SIMULATION OF THE FILLING STAGE BASED ON A VISCOELASTIC CONSTITUTIVE MATERIAL MODEL

8.1 ON THE PERFORMAMCE OF VISCOELASTIC CONSTITUTIVE MODELS FOR POLYMER MELTS

In the previous chapter, finite element Moldflow® analyses were performed in order to simulate the micro injection molding process. The main rheological models considered were Cross-WLF and Cogswell for viscosity and two-domain Tait for pvT. Non-Newtonian, non-isothermal flow solutions were obtained by solving the momentum, mass and energy equations. No-slip boundary conditions were imposed on the cavity walls filled with the polymer,

while, on the unfilled part, a free boundary condition allowed for the formation of the typical fountain flow. Previous simulation results showed how a standard injection molding code was unable to describe all of the effects in micro molding. In particular, rheological models, implemented in conventional injection molding packages, do not take into account normal stresses in viscometric flows, high resistance to elongational deformation, the tendency of polymer to slip in micro channels and memory effects associated with the elasticity of the fluid. The assumption of a generalized Newtonian fluid is generally used for traditional injection molding because the importance of the elasticity compared to viscous effects seems negligible. Because of high deformation rates during the injection phase of high speed injection molding, it is expected that elastic effects will occur. The challenge is to translate the complex rheological behaviour of polymeric fluids into suitable equations, and to use these models to predict flow in the micro cavity. The outcome of this section will be to evaluate whether the implementation of a viscoelastic material model may improve the accuracy of micro filling simulations. This work also reports on the suitability of a multi-purpose software, such as Ansys Polyflow®, to be used for injection molding simulations.

8.1.1 Multiscale modelling of viscoelastic flow

Viscoelasticity is the property of a material exhibiting the combined behaviour of viscous fluid and elastic solid. In general, higher deformation speed causes the material to respond more elastically (strain hardening) and the deformation at lower speed causes a more viscous response. Polymer melt is characterized by its viscoelastic nature, which is intimately linked to its physical structure and chemical composition. Polymers are made up of many small structural units which form a macromolecule. The viscoelastic behaviour of molten polymers stems from the random-coil configuration of these macromolecules in the molten state, which allows the movement and slippage of molecular chains under the influence of both thermal agitation and applied load. However, the entanglement of the polymer molecular chains also makes the system behave like an elastic solid upon the application and removal of an external load. When a polymer material is constrained at constant deformation, the stress required to hold it diminishes gradually, while under constant stress, it stores some of the energy instead of dissipating it completely as heat and it may recover part of its deformation, when the stress is removed (elastic recoil) [94]. The recovery is not instantaneous because of the entanglement still

present in the system. The viscoelastic nature of molten polymers finds its expression in:

- a shear-rate dependent viscosity;
- non zero normal stress differences in shear flows;
- elasticity recoil or memory effects associated with the elasticity of the material (e.g. stress relaxation and recoil);
- high resistance to elongational deformation.

During the last decade, substantial progress has been made in the numerical simulation of viscoelastic flows. Extensions to non-isothermal and three dimensional viscoelastic simulations are in progress [95]. Many constitutive equations have been proposed over the last few decades, but none of them has proven to be superior to others [96]. Related to this, is the limited availability of experimental data to test and fit existing constitutive models. Linear viscoelastic and simple shear viscometric flow data are readily available, and a growing amount of extensional measurements (in particular, uniaxial extensional data) have been published. However, extensional data need to be interpreted with great care, as these experiments often give rise to spatially inhomogeneous flow fields, are time-dependent in a Lagrangian sense, and a steady state condition is rarely (if ever) achieved. Moreover, even if both viscometric shear and elongational functions are available, it is questionable whether the material behaviour is captured well in flows with a combination of shear and elongation. Combined numerical/experimental studies of complex flows can be used to evaluate different constitutive equations concerning their adequacy to describe the viscoelastic behaviour of polymer solutions and melts. A key factor in this approach is that field information is used rather than macroscopic, integrated quantities, as the latter may not reflect local material behaviour. The present availability of non-invasive optical techniques for measuring velocities (laser Doppler anemometry (LDA) and particle tracking velocimetry (PTV)) and stresses (flow-induced birefringence (FIB)) in a flow field, makes local, quantitative comparison with computations possible.

From the large number of non-linear viscoelastic constitutive equations availabe, relatively few have been evaluated in complex flows. Of the integral type models, the K-BKZ (Kaye-Bernstein, Kearsley and Zapas) model with the PSM (Papanastasiou, Scriven and Macosko) damping function has received most attention [97]. Its popularity can be attributed to the possibility of controlling the shear and elongational behaviour with different parameters. Among the differential type models, the PTT (Phan-Thien Tanner [98]) and Giesekus model [99] have been applied most frequently. The Giesekus model has only one adjustable parameter to control non-linearity, whereas the PTT model has two adjustable parameters, if the mixed upper-lower convected

derivative is used. To some extent, the PTT model has the ability to describe shear and elongational properties independently. However, the use of the lower convected derivative causes spurious oscillations in the predicted shear and normal stresses during start-up shear flow. Only a few studies have evaluated more than one constitutive equation. Armstrong et al. [100] evaluated six different models for a contraction flow of a polyisobutylene solution, and, for this solution, found the predicted stresses of the PTT model to be the closest to measured stresses along the centreline of a contraction. Using a similar solution for the flow past a confined cylinder, Baaijens [101] showed good to excellent agreement between computed and measured velocities and stresses for both the PTT and Giesekus models. De Bie et al. [102] have shown that for PIB, LDPE and HDPE melts in a converging channel, the predicted stress fields of the PTT and Giesekus models better agree with the experimental results than predictions based on the Leonov model. In all cases, the four mode versions proved to be superior to single mode predictions, which was also found by Rajagopalan et al. [103] for a Giesekus model. For different types of flow, Baaijens et al. [104, 105] found their computational results to be only moderately sensitive to the constitutive equations used (PTT and Giesekus). A drawback of the geometries that have been used so far (primarily contraction flows and flows past a confined cylinder) is that the achievable strain is limited. An exception is the stagnation point in the wake of the cylinder, but the associated domain with high strains is too small to be accessed experimentally. Consequently, only moderate excursions into the non-linear regime of the constitutive models are made. Based on the above results, it has been concluded that in shear-dominated flows (weak flows), experimentally observed stress fields can be predicted with great accuracy. Yet, whenever shear properties are predicted accurately, an increasing mismatch between predicted and measured normal stresses is observed with increasing flow rate (or, the equivalently, increasing Weissenberg number) in regions with a dominant elongational component (strong flows). It has been generally found impossible to describe both weak and strong flows for a large range of Weissenberg numbers with the same set of parameters for existing constitutive models, including the PTT and the Giesekus models. Therefore, enhanced independent control of the shear and elongational properties is required.

8.1.2 Analysis of differential viscoelastic models

In differential viscoelastic models the extra-tensor $\overline{\overline{\tau}}$ (equation 4) can be divided into a purely viscous part (Newtonian) and a viscoelastic part:

$$\overline{\overline{\tau}} = \overline{\overline{\tau}}_n + \overline{\overline{\tau}}_v \tag{42}$$

where the subscripts n and v stand for Newtonian and viscoelastic contributions, respectively. The Newtonian part, which can be seen as the stress response associated with fast relaxation modes, can be written as:

$$\overline{\overline{\tau}}_n = 2\eta_n \overline{\overline{D}}(\bar{u}) \tag{43}$$

where $\overline{\overline{D}}$ is the rate of strain tensor and η_n is the Newtonian contribution to the viscosity.
The differential models, used in numerical simulation for polymer melts, can take the following general form:

$$\lambda \overset{\nabla}{\underline{\underline{\tau}}}_v + F(\underline{\underline{\tau}}_v)\underline{\underline{\tau}}_v = 2\eta_v \underline{\underline{D}}(\underline{u}) \tag{44}$$

where λ is the relaxation time and η_v is the viscoelastic viscosity. The symbol F denotes a tensor function and the triangle symbol stands for the upper convective time derivative defined by:

$$\overset{\nabla}{\underline{\underline{\tau}}} = \frac{D\underline{\underline{\tau}}}{Dt} - \underline{\underline{\nabla u}}^T \cdot \underline{\underline{\tau}} - \underline{\underline{\tau}} \cdot \underline{\underline{\nabla u}} \tag{45}$$

Depending on the form taken by the function F, different models can be obtained.

8.1.3 The Giesekus model

Among differential viscoelastic models, the Giesekus one was chosen on the basis of simple criteria such as:

- the model is sufficiently elaborate to predict normal stress effects as well as time dependent elastic effects;
- the model is not too complex to implement;
- the model requires only four material parameters (for characterization and implementation problems);

- the model is considered as giving excellent predictions in shear [106] and complex flows [107].

In particular, the first criterion forbids models such as the UCM or Lodge models, which are far too simple, while the second criterion makes us turn to differential models to the detriment of simple integral models. Moreover, the Pom-Pom model has not been chosen as it implies solving a system of equations (orientation tensor, auxiliary tensor, backbone tube stretch and extra-tensor) which induces higher memory requirements and calculation times than if only one equation is to be solved for the extra-stress tensor. The third criterion brings the Giesekus model, as it contains only four material parameters as compared to the PTT model. The Giesekus model exhibits a rather simple form with no exponent and an extra stress tensor, which is the unknown. In spite of the fact that it is a non-linear model, it is possible to find analytical solutions for some of the simplest flows, such as steady simple extensional and simple shear flow, relaxation and start-up flow in simple extension. This model leads in simple shear to shear thinning and realistic non-vanishing normal stress differences, in uni- and bi- axial extension to extension thickening with finite asymptotic values, to non-exponential stress relaxation and to stress overshoot after the inception of simple shear flow.

The Giesekus model is based on anisotropic drag or the consideration that a dumbbell will not relax in the same way whether it is alone or surrounded by other oriented molecules. The model can be written as:

$$\lambda \overset{\nabla}{\underline{\underline{\tau}}}_v + \left(\underline{\underline{I}} + \frac{\alpha\lambda}{\eta_v} \underline{\underline{\tau}}_v \right) \cdot \underline{\underline{\tau}}_v = 2\eta_v \underline{\underline{D}}(\underline{u}) \tag{46}$$

where, according to equation 44, the tensor function F has been defined as

$$F(\underline{\underline{\tau}}) = \underline{\underline{I}} + \frac{\alpha\lambda}{\eta_v} \underline{\underline{\tau}}_v \tag{47}$$

and α is a dimensionless mobility parameter. This α parameter lies in the range [0, 1]. When α=0, the drag is isotropic and the Oldroyd-B model is recovered, while for α=1, the drag is at its utmost anisotropic value. If α were to lie outside this range, the stress could grow in magnitude rather than relax after the deformation ceases. Besides the non linear parameter α, this model contains other three input parameters: the polymer relaxation time λ, the Newtonian and the viscoelastic contributions to the viscosity (η_n and η_v respectively) .

8.2 VISCOELASTIC MATERIAL CHARACTERIZATION

As already discussed in the previous paragraph, choosing a viscoelastic constitutive equation to model polymer behaviour in complex flows is not at all straightforward. Consequently, it is not impossible that the choice of the Giesekus model might turn out to be unsatisfactory and, hence, might have to be reviewed. The usefulness of material characterization is, therefore, double: it allows to complete the model by providing the required material parameters and it permits to understand considered material behaviour.

Moreover, the intensity of the forces at stake are so much higher in the case of micro injection molding that a traditional rheological study could not be a proper means to qualify polymer behaviour. Nonetheless, it is the only mean available right now as the on-line rheology still contains a certain number of hazardous parameters (for instance, the sensor resistance to high temperatures and pressures).Consequently, as far as the material characterization is concerned, viscometric measurements were performed on both a rotational and capillary rheometers, bearing in mind that the deformation rates are far from being representative of those encountered during the micro injection molding process. Dynamic experiments were conducted in order to determine the linear viscoelastic properties in the form of the storage and loss moduli G' and G", from which the dynamic spectrum (λ, η) was fitted, while the non-linear mobility parameter α was determined from steady shear experiments.

8.2.1 Determination of the dynamic moduli G' and G"

Below a critical strain value, the linear dependency of stress relaxation on strain is observed for polymer melts. As a consequence, small strain material functions such as stress relaxation modulus, creep compliance, storage and loss moduli can be determined through small strain experiments, where the material is in its linear region. In this section, small amplitude oscillatory shear experiments have been used to determine the linear viscoelastic properties of PS 143 E. This kind of experiments is best adapted to determine the storage and loss moduli compared to other linear viscoelastic experiments [108]. As a first approach, a dynamic strain sweep test was performed on a TA Instruments ARES rheometer to determine the linear viscoelastic region (figure 8.1). A decay in the storage modulus was observed

concerning a deformation range superior to 100%.

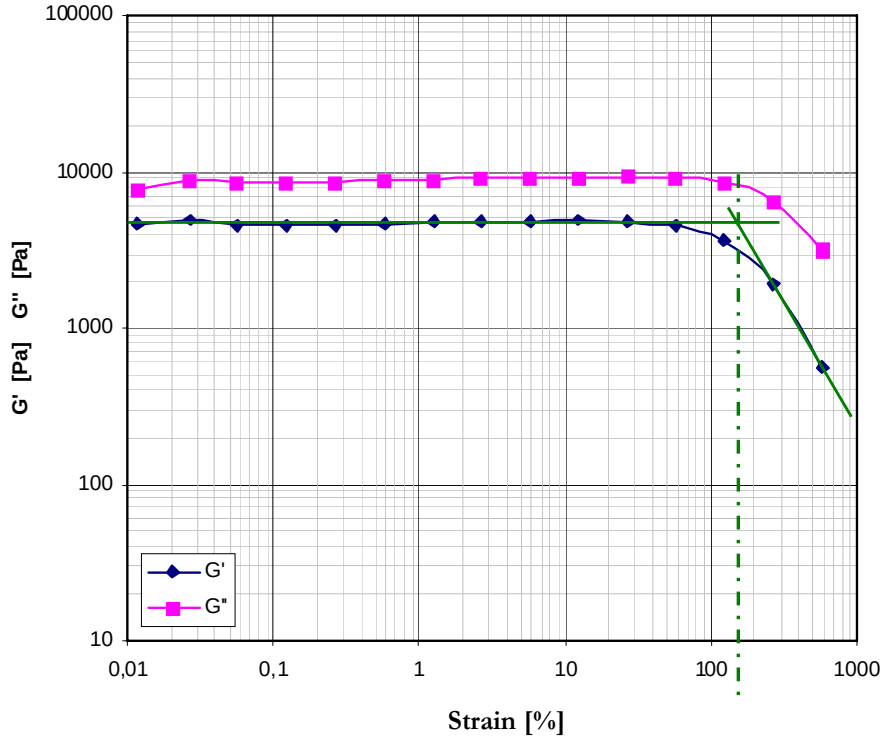

Figure 8.1 - Dynamic strain sweep test to determine the linear viscoelastic region

8.2.1.1 The dynamic measurements principle

In the general case of dynamic experiments, the polymer resistance to shear strain is measured. More specifically, in a relaxation experiment, the strain is imposed on the cone plate by rotation and the torque required to achieve the prescribed rotation is measured. In the particular case of small amplitude oscillatory shear experiments, the unsteady response of a polymer sample contained between the cone and plate is measured. Whereas the lower plate is fixed, the upper geometry undergoes small amplitude sinusoidal oscillations of frequency ω, while remaining in its own plate. Accordingly, there is a phase difference between the imposed shear strain ($\gamma=\gamma_0 \sin\omega t$) and the shear stress ($\tau=\tau_0 \sin(\omega t+\varrho)$).

8.2.1.2 Determination of the relaxation spectrum

The principle used to determine the linear viscoelastic properties G' and G" has been briefly described here. The constitutive equation of an upper convected Maxwell model can be written as:

$$\underline{\underline{\tau}} + \lambda \overset{\nabla}{\underline{\underline{\tau}}} = 2\eta \underline{\underline{\dot{\gamma}}} \tag{48}$$

where λ and η stand for the relaxation time and the viscosity, respectively, while $\overset{\nabla}{\underline{\underline{\tau}}}$ denotes the upper-convected derivative of the extra-stress tensor. For small amplitude motions, the solution of this equation is:

$$\underline{\underline{\tau}}(t) = \int_{-\infty}^{t} \left(\frac{\eta}{\lambda} \exp^{\frac{-(t-t')}{\lambda}} \right) 2\underline{\underline{\dot{\gamma}}}(t')dt' \tag{49}$$

It is possible to obtain a more elaborate model through the parallel superposition of several Maxwell elements. In this case, the extra-stress tensor is the sum of the different extra-stress tensors of each Maxwell element:

$$\underline{\underline{\tau}}(t) = \sum_{k=1}^{N} \underline{\underline{\tau}}_k(t) \tag{50}$$

where N is the number of considered parallel Maxwell elements. Equation 50 supposes that the different modes are decoupled or, in other words, that the presence of chain groups with a certain relaxation time has no influence on the other groups of chains (with a different relaxation time). As a consequence, the relaxation times should be sufficiently different so that their influence is supposedly negligible.

To take into account the phase difference between shear rate and shear stress, a complex viscosity η^* is introduced. It is defined as η'-iη", where η' is in phase with the shear rate and η" is in phase with the shear strain. Hence, η' may be viewed as representing the viscous contribution to the extra-stress (associated with power dissipation), while η" can be seen as the elastic contribution to the extra-stress (associated with energy storage). By solving the previous equations, the following expressions have been obtained for the linear Maxwell model:

$$G'(\omega) = \eta'\omega = \sum_k \frac{\eta_k}{1 + (\lambda_k \omega)^2} \omega \tag{51}$$

$$G''(\omega) = \eta''\omega = \sum_k \frac{\eta_k \lambda_k}{1 + (\lambda_k \omega)^2} \omega^2 \tag{52}$$

where G' is called the storage modulus and G" the loss modulus. The storage modulus is a measure of the relative elasticity of the resin, or the energy storage that takes place during deformation, whereas the loss modulus describes the viscous character of the resin, or the extent to which deformation work is dissipated into heat. As the experiments provide data for G' and G" as a function of ω, fitting the above series to G' (ω) and G" (ω) provides an approximation of the spectrum of viscosities and relaxation times (η_k, λ_k).

8.2.1.3 Experimental procedure

The experiments were performed on a TA Instruments ARES machine at three different temperatures (190°, 210°, 230° C) in a frequency range ω=0.1 to 1000 rads^{-1} using a cone plate geometry. The samples were prepared by compression molding and maintained under a nitrogen atmosphere to avoid polymer degradation by oxidation. To avoid any discrepancy from lot to lot, the tested pellets were taken from the same bag as the ones moulded during the trials. Measurements were performed in a frequency sweep mode with a 10% deformation range, acceptable value selected in the linear viscoelastic region (figure 8.1). Three measurement points per decade were taken with increasing frequencies. The complex viscosity, as well as the dynamic moduli G' and G" have been illustrated in figure 8.2.

8.2.1.4 Master curves

Amorphous polymers, which follow the linear viscoelastic laws, at uniform temperature exhibit a particular property with a change of temperature. The so-called time-temperature superposition principle [94] can be used to expand the frequency range of the dynamic spectrum far beyond the experimentally accessible range. According to this principle, letting temperature vary at a fixed frequency is equivalent to letting frequency vary at a fixed temperature. This principle rests on the assumption that the molecular processes, that govern each relaxation mode of a given polymer, are equally accelerated (or retarded) by a given increase (or decrease) in temperature.

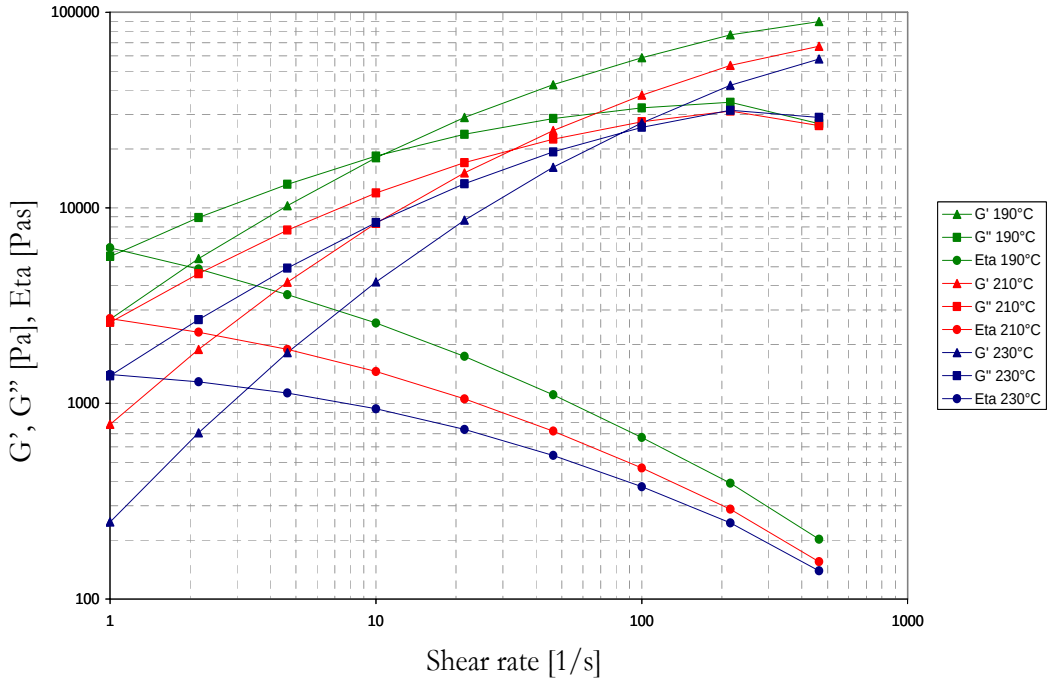

Figure 8.2 – The dynamic moduli G', G'' and complex viscosity

As a consequence, the experimental results, obtained for the dynamic properties at different temperatures, can be superposed onto a master curve at a single temperature spanning more frequency decades than the experimental ones. Let $G_T(t)$ be the relaxation modulus as a function of time at uniform temperature T, then the time-temperature superposition relation can be stated as:

$$G_T(t) = G_{Tref}[t \cdot a_T] \tag{53}$$

where T_{ref} is the reference temperature, and a_T is the shift factor at temperature T, with respect to the reference temperature T_{ref}. If one defines a "material time" as $\xi = t \cdot a_T$ in the isothermal temperature case and $\xi = \int_0^t \frac{1}{a_T(t)} dt'$ for the non-isothermal case, equation 53 can be written as:

$$G_T(t) = G_{Tref}(\xi) \ . \tag{54}$$

Williams, Landel and Ferry [109] showed that a single empirical function can describe the temperature dependence of all mechanical and electrical relaxation processes in an amorphous polymer above its glass-transition

temperature. They suggested that the shift factor takes the following form:

$$\log a_T = \frac{-c_1(T - T_{ref})}{c_2 + T - T_{ref}} \tag{55}$$

As the temperature goes down across the glass transition temperature, the WLF approximation is not valid because the relaxation time of free volume takes a long time for the polymer to reach its equilibrium volume. However, the WLF shift factor was used below the glass transition temperature by introducing the free volume theory that regards the non-equilibrium state as the equilibrium state based on the concept of effective temperature. In order to obtain the master curve, a second one shift was required. The curve at temperature T was first vertically shifted to the reference temperature T_{ref} and the resulting curve was then horizontally shifted (b_T), in such a way that the reference temperature curve and the shifted one superposed. The resulting variables of the vertical shift were called reduced variables. The expressions for the reduced variables are the following ones:

$$G_r^{'}(\omega, T_{ref}) = G'(\omega, T)\frac{T_{ref}\,\rho(T_{ref})}{T\rho(T)} \tag{56}$$

$$G_r^{''}(\omega, T_{ref}) = G''(\omega, T)\frac{T_{ref}\,\rho(T_{ref})}{T\rho(T)} \tag{57}$$

$$\left|\eta^*(\omega, T_{ref})\right|_r = \left|\eta^*(\omega, T)\right|\frac{T_{ref}\,\rho(T_{ref})}{a_T \cdot T\rho(T)} \tag{58}$$

The vertical shift factor $b_T=(T_{ref}\rho_{ref})/(T\rho)$ represents the volume variation with the temperature and the influence of the temperature on the system free enthalpy.

The master curves of the viscoelastic properties for PS 143 E, at the process temperature of 230°C, have been set forth in figure 8.3. A low level melt temperature of the experimental plan (table 5.3) was considered as being the reference temperature to avoid material degradation during the experiments. Furthermore, the experiments conducted at the rotational rheometer showed an unwanted yield stress at low frequencies and temperatures higher than 230°C, which makes it difficult to superpose the experimental curves. In the following section, the comparison between 3D viscous conventional simulations and 3D viscoelastic simulations will be performed at a reference temperature of 230°C.

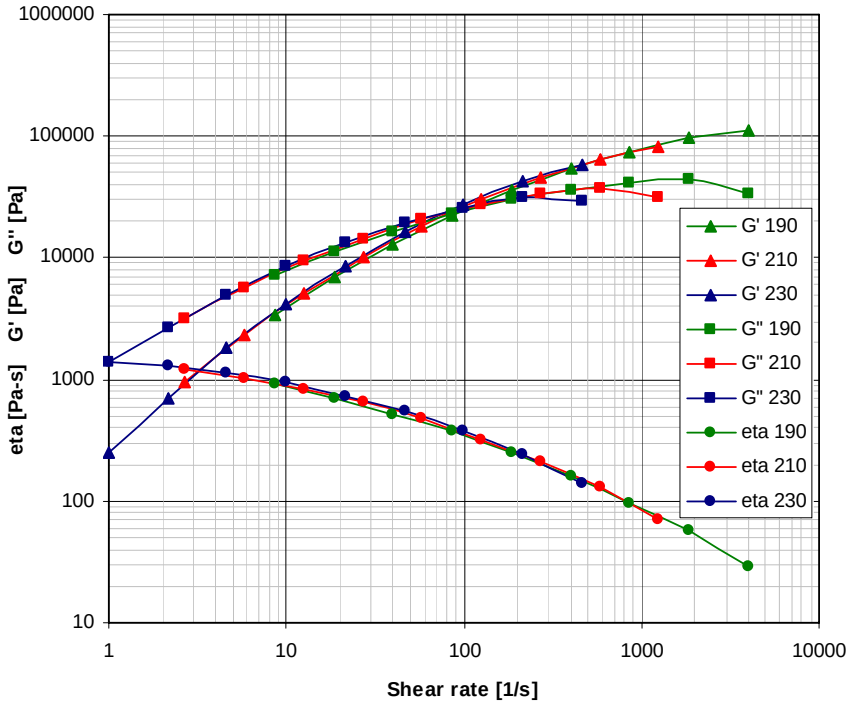

Figure 8.3 – The master curves of the dynamic properties for PS 143 E at 230°C

The values obtained experimentally for a_T and b_T have been set forth in table 8.1. Furthermore, the shift factor a_T, obtained from the best fit of experimental data, has been introduced as a WLF function at the high temperature region for the shear modulus (table 8.2).

Temp. (°C)	a_T	b_T
190	8.63	1.25
210	2.7	1.21
230	1	1

Table 8.1 - Horizontal (a_T) and vertical (b_T) shift factors obtained from experiments for a reference temperature of 230°C

WLF	
C_1	6.2571
C_2	310.86
r^2	0.9996

Table 8.2 - The horizontal shift factor dependence of temperature expressed as a WLF function.

8.2.1.5 Determination of the relaxation time spectrum

Dynamic experiments allow for the definition of the relaxation spectrum, i.e. the set of relaxation times, viscosity couples for a given model by fitting with experimental data the expressions predicted by the model in the case of small-amplitude oscillatory shear flow. For a multimode version of the Giesekus model, the linear viscoelastic properties G' and G" can be described by the following expressions:

$$G'(\omega) = \eta'\omega = \sum_i \frac{\left(1 + \frac{\eta_i^n \lambda_i^2 \omega^2}{\eta_i^T}\right)\eta_i^T}{1 + (\lambda_i \omega)^2}\omega \tag{59}$$

$$G''(\omega) = \eta''\omega = \sum_i \frac{\left(1 - \frac{\eta_i^n}{\eta_i^T}\right)\eta_i^T \lambda_i}{1 + (\lambda_i \omega)^2}\omega^2 \tag{60}$$

where the notation η^n and η^T represent the Newtonian viscosity and the total viscosity (i.e. the Newtonian and viscoelastic contribution $\eta_n+\eta_v$) respectively. Hence, in the case of the Giesekus model the relaxation spectrum consists of three material parameters for each mode i: λ_i, η_i^T and η_i^n. Numerically, relaxation times and viscosities were modelled by minimizing the difference between the measured and predicted moduli at the frequencies used in the experiments. The expression to be minimized is the following one:

$$R = \sum_{j=1}^{N}\left[\left(\frac{G'(\omega_j)}{G'_{\exp,j}} - 1\right)^2 + \left(\frac{G''(\omega_j)}{G''_{\exp,j}} - 1\right)^2\right] \tag{61}$$

where j indicates the data points and N the total number of frequencies for which the moduli were evaluated. The standard deviation SD between experimental data and the last fit was defined as:

$$SD = \sqrt{\frac{1}{N}R} \tag{62}$$

The minimum standard deviation between experimental and fitted values was obtained for a three-mode Giesekus model. Figure 8.4 shows the predicted curves for the moduli and the complex viscosity norm with the Giesekus model, compared to the master curves at the reference temperature of 230°C.

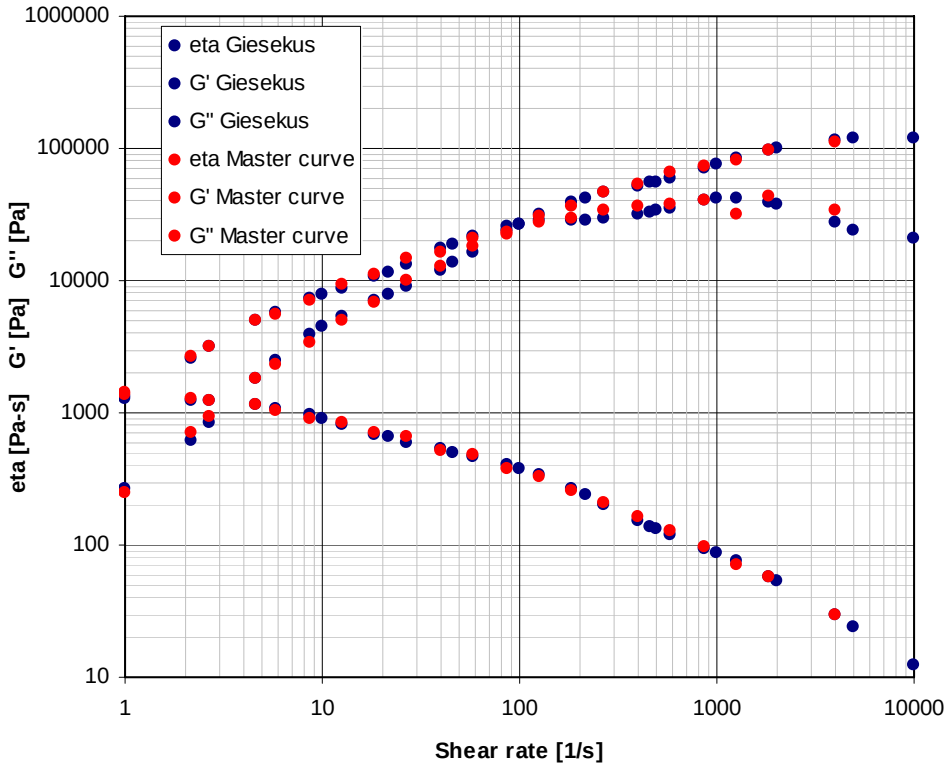

Figure 8.4 - Comparison of viscosity, loss and storage moduli predicted by a 3-mode Giesekus model (blue markers) with experimental data (red markers) for PS 143 E at the reference temperature T=230°C.

The minimization of R in equation 62 leads to the viscoelastic parameters set forth in table 8.3. From these results, it clearly appears that the Newtonian contribution to the total viscosity is very small, which means that the latter is mainly composed of a viscoelastic contribution.

Parameters	**i=1**	**i=2**	**i=3**
λ(s)	0.117	0.00943	0.00077
η^n (Pa.s)	1.11	1.32E-09	1.47E-09
η^T(Pa.s)	798.95	388.76	57.21

Table 8.3 - Discrete relaxation time spectra for PS 143 E melt at the reference temperature T=230°C.

Due to the fact that experimental data are not available for high frequencies, while the relaxation times obtained are very small (and, therefore, play a role at high frequencies), it is impossible to establish the optimum numbers of modes necessary to best fit the data, because there is no data to fit at high frequencies, precisely where the model differences related to the number of modes lie.

8.2.1.6 Determination of the non-linear parameter α

In the Giesekus model, the nonlinear effects are introduced by taking into account an average anisotropy of the molecular conformation during flow. The strength of influence to the conformation and the retroaction to the flow is determined by an anisotropic mobility parameter α. At α=0, the isotropic Maxwell model is recovered. When α is set to unity, the model predicts similar behaviour in elongational flows as the corotational Maxwell model. A non-zero value for α leads to a bounded steady extensional viscosity and a shear-rate dependence of the shear viscosity. At intermediate values of α, the Giesekus model fits steady and transient shear flows better than any other differential constitutive equation. A best fit for the α parameter (figure 8.5) was obtained by minimizing the deviation from the steady shear experiments conducted on the Ceast® capillary rheometer at 230°C with the following function:

$$\sum_i \left(\frac{\eta(\dot{\gamma}_j)}{\eta_{\exp,j}} - 1 \right)^2 \tag{63}$$

where $\eta(\dot{\gamma})$ is given by the Giesekus model in steady shear flow:

$$\eta(\dot{\gamma}) = \frac{\eta_v (a - n_2)}{1 + (1 - 2\alpha) n_2} + \eta_n \tag{64}$$

with

$$n_2 = \frac{1 - \Lambda}{1 + (1 - 2\alpha)\Lambda} \tag{65}$$

$$\Lambda = \sqrt{\frac{\sqrt{1 + 16\alpha(1-\alpha)\lambda^2 \dot{\gamma}^2} - 1}{8\alpha(1-\alpha)\lambda^2 \dot{\gamma}^2}} \tag{66}$$

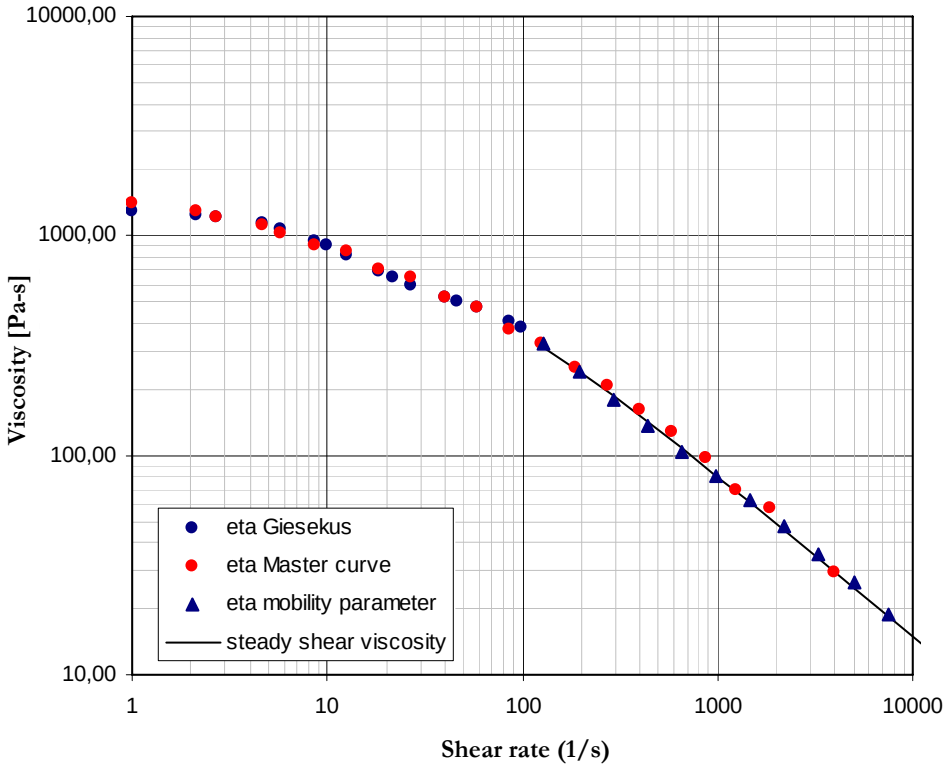

Figure 8.5 - Fitting of the non-linear parameter α. Comparison between steady shear viscosity (as a function of shear rate) and linear viscosity (as a function of frequency).

8.3 THREE DIMENSIONAL VISCOELASTIC SIMULATION

In this section, a dimensionless analysis is performed, firstly, to study the size effect on the flow, succeeded by a comparison analysis with conventional simulations results. A three dimensional viscoelastic simulation was performed on Ansys Polyflow® environment to evaluate its suitability on the micro injection molding process. Polyflow® is a finite-element program, primarily designed for the analysis of industrial flow processes dominated by non-linear viscous phenomena and viscoelastic effects. The theoretical foundation is provided by the general principles of continuum mechanics, together with phenomenological and kinetic theoretical models for describing

the rheological behaviour of the fluid.

8.3.1 Modelling of viscoelastic forces

Besides the previous adimensional numbers (paragraph 7.1.2.2.), a new one (Deborah number) has been introduced to characterize fluid elasticity. It is the ratio of the characteristic relaxation time (λ) to the observation time, which is taken as the micro-cavity filling time:

$$De = \frac{\lambda}{t_{fill}} \tag{67}$$

The weighted relaxation time was calculated according to equation 68, which is to say, as the contribution of chains relaxing before time λ_i:

$$\lambda = \frac{(\sum_{i=1}^{3} \eta_i^T \lambda_i)}{\sum_{i=1}^{3} \eta_i^T} \tag{68}$$

The estimated Deborah number is 27. This value seems to confirm the hypothesis that filling behaviour is influenced by viscoelastic effects [106]. This important value, obtained from previous flow field analysis and material characterization, is not comparable to values appreciable in traditional injection molding. This establishes that the elastic behaviour of the polymer melt can not be disregarded.

8.3.2 Mesh model and boundary conditions

This section examines the coupled problem of a non-isothermal viscoelastic flow of a fluid and heat conduction in an axisymmetrical steel mold. The problem involved flow, heat transfer by conduction and convection and heat generation by viscous dissipation. Energy, momentum and mass equations were solved in the fluid domain. The energy equation for heat transport problems was solved in the solid domain. The model was created and meshed in the Gambit® environment. Three solid and one fluid sub-domains were defined (figure 8.6):

- a fluid domain (SD1)

- a plunger (SD2)
- the upper part of the mold (SD3)
- the lower part of the mold (SD4).

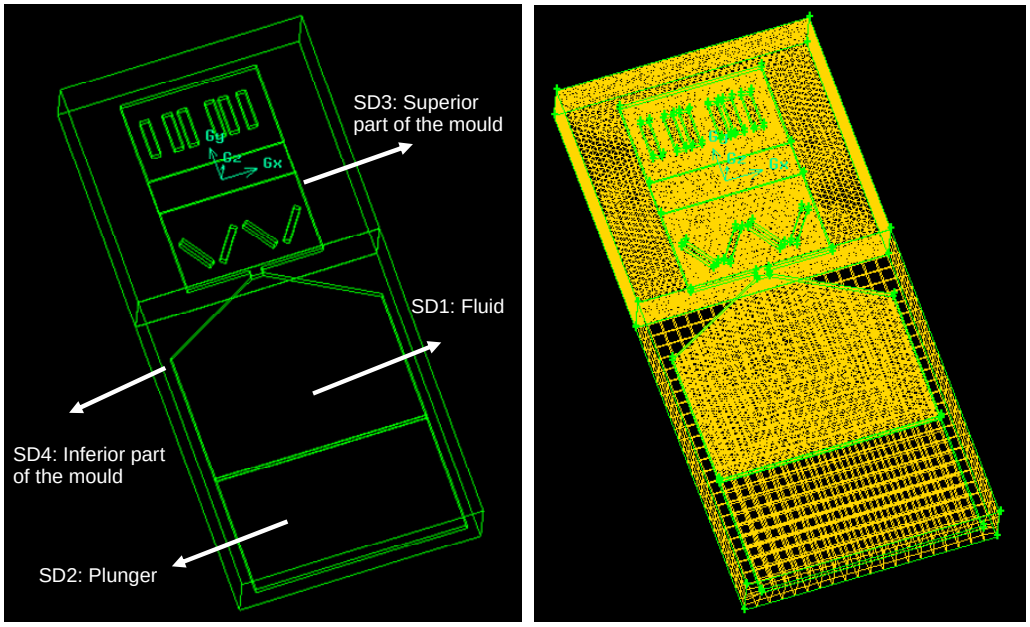

Figure 8.6 - Sub-domains definition and finite element mesh of the model

Three dimensional finite elements were defined for the fluid gob, mold and plunger. In particular, the fluid domain and the upper part of the mold were meshed by triangles, while the inferior part of the mold and the plunger were meshed by quadrilaterals. The 3D mesh model has been represented in its initial configuration, before pressing the fluid. At a prescribed time, the plunger moves downwards according to the ram speed profile and presses the fluid domain in the mold cavity.

A major difficulty to be overcome in the simulation arises from the fact that the filling domain evolves considerably over time. The position of the front is an unknown, which means that the limit of the domain under investigation (i.e. filled with polymer melt) is an unknown. This is called a free surface problem and has given rise to a large number of methods, which can be classified into two categories. The first approach consists in using control volumes defined on a fixed mesh, covering the entire domain to be filled, with the use of an additional variable representing the volume fraction of the injected polymer within the control volumes (and without front discretization). The second approach is based on accurately tracking the flow front and

adapting the mesh, at each time step, in order to cover only the filled domain. This latter front tacking-remeshing approach was selected to solve the micro injection molding problem, since it was thought that an accurate representation of the front yet at an affordable computational cost was required in this small scale problem. Indeed, the second class of methods requires refined finite element meshes in the front vicinity. Besides this, the exact position of front meetings was intrisacally interesting as related to the weld line position. The fluid domain was, therefore, considered as a free surface and a Lagrangian remeshing technique was applied. In the Polyflow® environment, remeshing techniques are based only on the positions and displacements of the boundary nodes, and not on kinematic considerations, unless a Lagrangian or streamwise method is used for remeshing. Tangential remeshing preserves the original node distribution along a surface for three dimensional moving domains. In transient iterative parameters a maximum value of 10^{-6} s was set as the time step in order to contain deformation of the elements before remeshing [111].

Numerical simulations were performed in the Polydata® environment, implementing the same boundary conditions considered for viscous conventional numerical simulations (paragraph 7.2.4). On the other hand, a viscoelastic constitutive material model was considered. The three parameters in table 8.3 and the non-mobility parameter α were implemented according to the Giesekus model. For viscoelastic flows, the total extra-stress tensor was decomposed into a viscoelastic component $\overline{T}_1$ and a purely-viscous component $\overline{T}_2$:

$$\overline{T} = \overline{T}_1 + \overline{T}_2 \tag{69}$$

where $\overline{T}_1$ was computed according to the Giesekus model. On the other hand, $\overline{T}_2$ is an optional component, which was calculated as:

$$\overline{T}_2 = 2\eta_2 \overline{D} \tag{70}$$

where $\overline{D}$ is the rate-of-deformation tensor and η_2 is the viscosity factor for the Newtonian (i.e., purely-viscous) component of the extra-stress tensor. When a multi-mode viscoelastic model is used, the total extra-stress tensor is decomposed into a sum of individual viscoelastic components and any purely-viscous component. To prevent an ambiguous definition of the purely-viscous component, the corresponding viscosity factor was defined together with the first mode. Consequently, the remaining modes did not contain any purely-viscous component.

8.3.3 Experimental validation of viscous and viscoelastic simulations

Conventional numerical simulations, based on a viscous constitutive material model, showed how a standard injection molding package was unable to describe all the effects in micro molding. In particular, the rheological models, implemented in conventional injection molding codes, do not take into account normal stresses in viscometric flows, high resistance to elongational deformation, the tendency of polymer to slip in micro channels and memory effects associated with the elasticity of the fluid. The assumption of a generalized Newtonian fluid is used for traditional injection molding because the importance of the elasticity compared to viscous effects appears to be negligible. Because of the high deformation rates during the injection phase of a high speed injection molding, it is expected that viscoelastic effects will occur (equation 67). It was, therefore, decided to perform numerical simulations based on a viscoelastic constitutive material model and to compare filling results in terms of the weld lines position. A melt temperature of 230°C (selected according to the limits of the dynamic material characterization (paragraph 8.2.1.4)), a mold temperature of 70°C and a ram speed profile of 350 mm/s were implemented in both simulations. Two different outputs were considered: the weld line number 1 and the line 1 of the weld line number 3. These two weld lines were selected because they originate in zones of the micro cavity where the elastic behaviour of the fluid should not be disregarded. In correspondence with the first part of the micro cavity, a contraction flow is opposed to an expansion flow. Two different streamlines were acquired at 1.2 ms both in Moldflow® (yellow) and in Polyflow® (red) simulations (figure 8.7). In the expansion flow, the streamline in the viscoelastic simulation reveals more elastic behaviour if compared to the viscous simulation one. On the other hand, the streamline at the contraction exit is delayed due to normal stresses and resistance to elongational deformation during the contraction flow. As a consequence, the viscoelastic numerical weld line moves towards the experimental one (figure 8.7). As a second case, the horizontal line in the 150 μm wide micro channel was considered. Figure 8.8 shows how the viscous numerical simulation overpredictes the ease at which the plastic would flow through this channel; on the other hand, the viscoelastic one underpredictes (with a lower absolute error) the weld line position. The difference may be justified considering geometrical constraints and the viscoelastic nature of the polymer itself. Normal stresses and resistance to elongational deformation reduce the filling

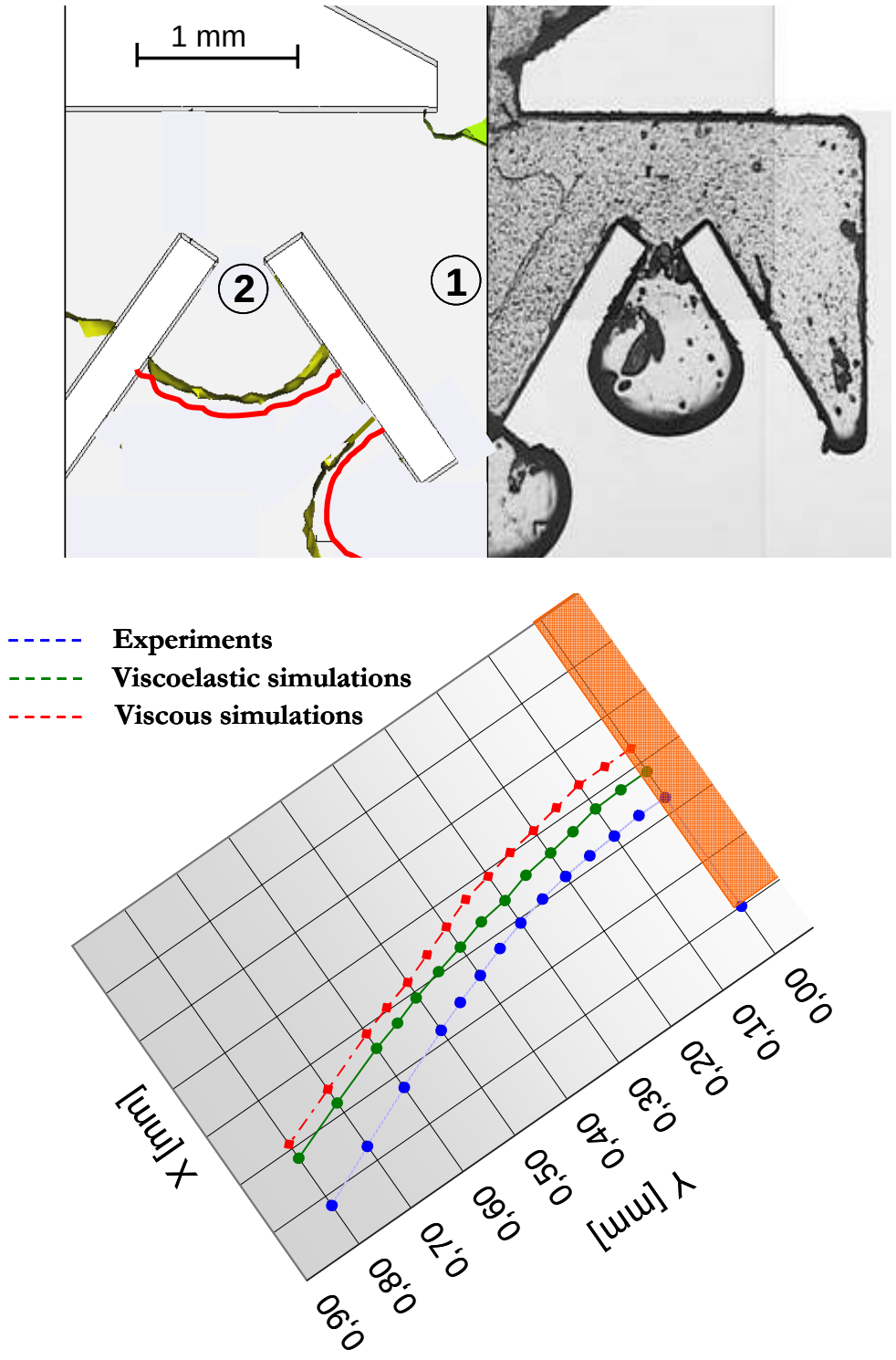

Figure 8.7 - Streamlines at 1.2 ms and subsequent weld line formation.

length in the micro channel. This effect is not as clear as in the other channels with higher dimensions, because as the channel dimensions decrease the material appears to be more rigid due to the constraints at the wall. Differences between numerical and experimental results may be related to inadequate boundary conditions. No-slip conditions were imposed on the cavity walls filled by the polymer whereas wall slip is expected to occur due to the increased shear stress. A complete validation of the software will be possible when more reliable models about local viscosity and heat transfer will be available.

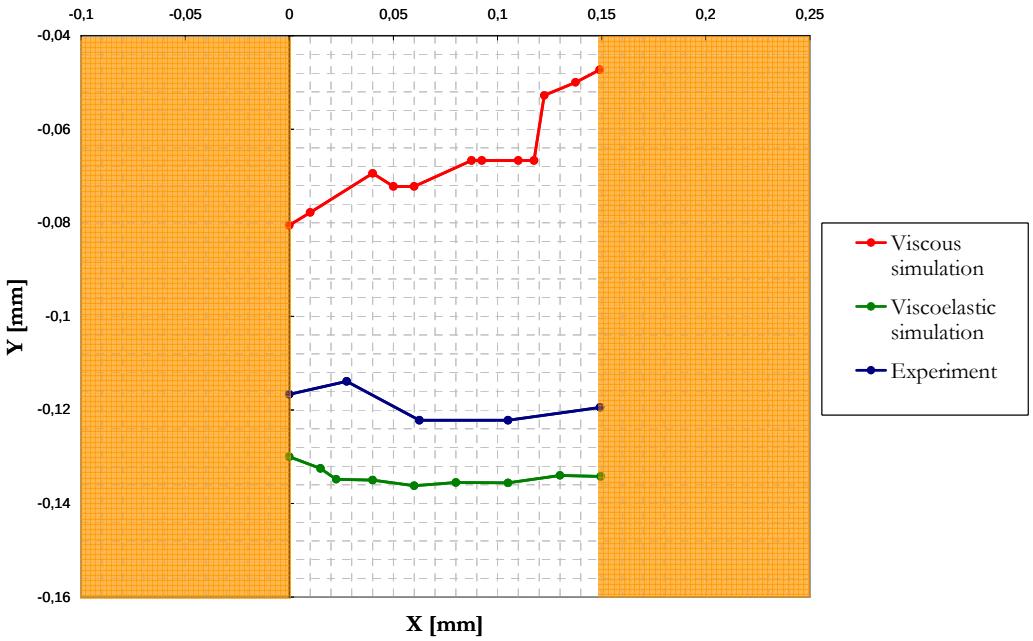

Figure 8.8 - Line 1 of the weld line number 3

CHAPTER 9

AN EXPERIMENTAL CASE STUDY:

A TENSILE BAR

9.1 From process to filling validation

A new experimental case has been considered to evaluate the accuracy of molding simulations based on both a viscous and viscoelastic constitutive material model. The mold cavity considered in this study is a traditional tensile bar, composed of a rectangular region 15 mm long, 3 mm wide and 0.3 mm thick, including three thin ribs with a semi-circular section (150 μm radius) and lengths from 1.5 mm up to 2 mm (figure 9.1). The experiments were performed using the same high fluidity polystyrene 143 E considered in the

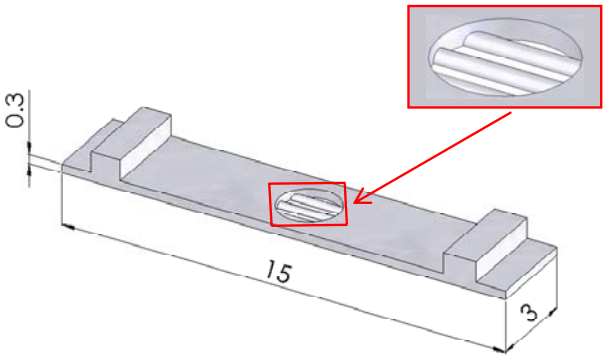

Figure 9.1 - Micro cavity design (part volume 130 mm^3)

previous analysis. Injection molding experiments were conducted on a Battenfeld Microsystem 50 molding machine at the University of Freiburg (Department of Microsystems Engineering) [112]. Its injection system is made up of a screw plasticising barrel, a plunger injection system and a melt dosage control barrel. By using the screw plasticising extruder, a small diameter plunger/needle can be used for melt injection to achieve precise measurable strokes to control melt accuracy. The plasticizing screw of the molding machine has a diameter of 14 mm, and a 5 mm diameter dose barrel is employed for storage of polymer melt. Based on the injection unit size and actual part size, the positional resolution required for consistent volumetric transfer was lower than 0.01 mm. During the molding process, plastic pellets were plasticized by the fixed extruder screw and fed into the metering chamber. In the metering chamber an optical sensor monitored the amount of melt in the chamber against the pre-set volume. After the set volume had been achieved, the plunger in the dosage barrel delivered the shot volume to the injection barrel. The polymer was then injected into the mold cavity setting a rectangular speed profile of 100 mm/s. The melt temperature in the feeding zone was maintained at 230°C. The mold temperature was controlled by a heater and maintained at a temperature of 70°C . To obtain stricter control of the boundary conditions and a good comparison between simulations and experiments, temperature transducers were positioned near the cavity surface. Furthermore, in-cavity injection pressure samplings were executed using a piezoelectric pressure sensor applied at the injection location of the two-cavity micro mold represented in figure 9.2. The experimental pressure evolution was used to obtain objective information about flow rate, the evolution of filling progress and validation of filling simulations.

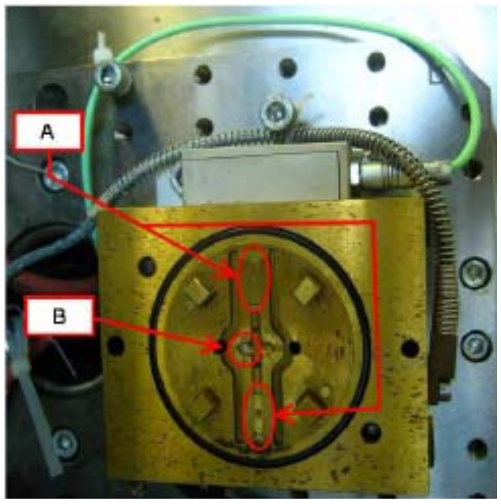

Figure 9.2 - Two cavity micro mold (A) equipped with in-cavity pressure sensor at the injection location (B)

Moldflow® and Ansys Polyflow® injection molding simulations were performed to predict the flow pattern and injection pressure of the micro tensile bar. The simulations results were then compared to the actual molded part flow pattern and required injection pressures. The purpose of this study was to develop a method to accurately validate the predicted fill patterns and injection pressures and build a level of confidence in the mold flow simulation procedure. As an initial approach, a three-dimensional finite element Moldflow® analysis was performed to simulate the micro injection molding process. The main rheological models considered were Cross-WLF and Cogswell for viscosity and two-domain Tait for pvT. Non-Newtonian, non-isothermal flow solutions were obtained by solving the momentum, mass and energy equations. No-slip boundary conditions were imposed on the cavity walls filled by polymer, while on the unfilled part, a free boundary condition allowed for the formation of the typical fountain flow. The melt temperature is a potential problematic parameter in terms of modelling. In practice, the melt temperature was only indirectly controlled through the barrel temperature zones. It was, therefore, decided to model the melt temperature as equal to the barrel temperature. The mold temperature, on the other hand, was defined as the mean value of the mold surface acquired by the temperature transducers. The simulations were performed implementing the ram speed profile as set in the machine. The 3D model mesh is shown in figure 9.3. As a second approach, a three dimensional viscoelastic simulation was performed in Ansys Polyflow® environment. The model was created and meshed in Gambit®

environment (figure 9.3) and simulations were performed in Polydata®, implementing the same previous boundary conditions. Stress (one stress field for each mode, or relaxation time), velocity and pressure were computed simultaneously. Furthermore, the problem involved flow, heat transfer by conduction and convection and heat generation by viscous dissipation. Energy, momentum and mass equations were solved in the fluid domain implementing viscoelastic properties of the material.

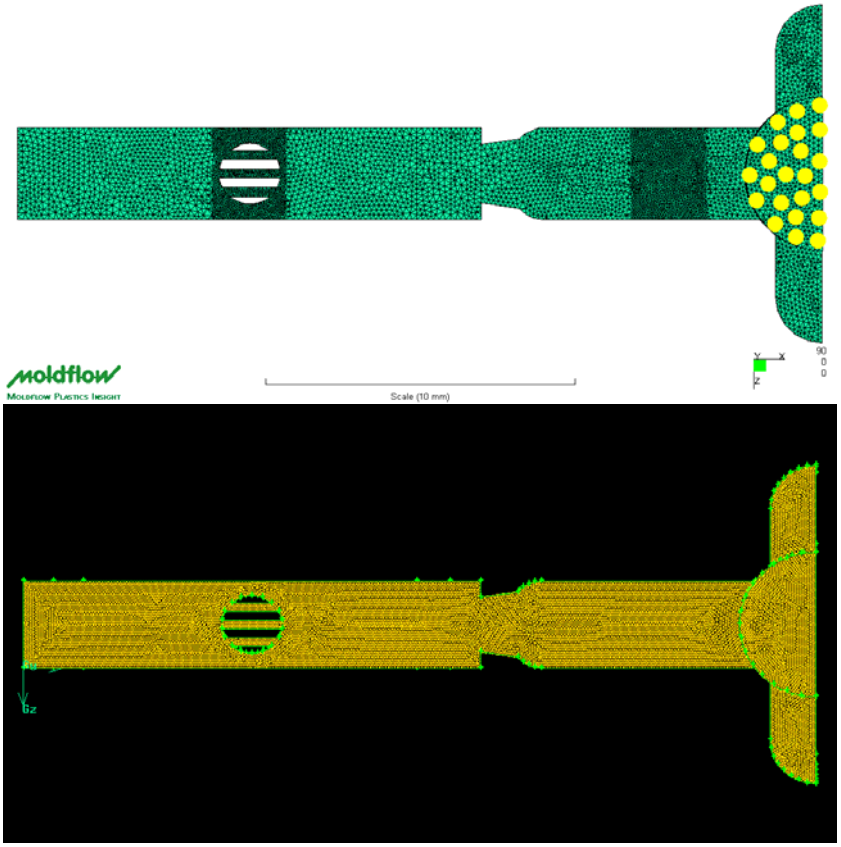

Figure 9.3 - 3D model mesh considered in Moldflow® and Polyflow® simulations

The simulation results were then compared to the experimental ones, considering the flow front position and the pressure evolution during micro cavity filling. The proposed approach introduced in this thesis consists in determining the flow pattern by using the weld lines as flow markers. The experimental position of a weld line, visible on the central micro channel surface, was compared to the numerical one. It was noticed that when the simulations were performed in Polyflow® environment, improvements on the

simulation results were achieved. Normal stresses and resistance to elongational deformation reduce the filling length in the micro channel, according to the experimental results (figure 9.4) [113].

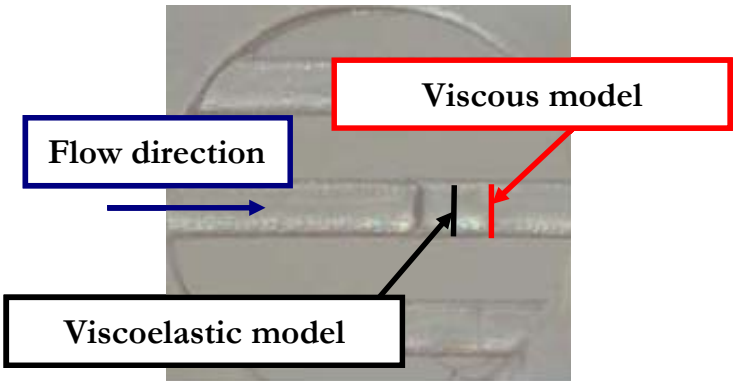

Figure 9.4 - Experimental and simulated weld line position

Finally, the pressure evolution determined by the simulations was compared and correlated with the experimental one. Previous work in this area, within conventional injection molding, has shown that the integration of select regions of the injection pressure curve during mold filling can provide a useful parameter for the evaluation of the repeatability of a process [4]. This method would not be seen as being directly applicable to the micro molding process because of the short injection times, but integration of the entire injection pressure curve, up to the point when the mold opens, may provide useful information about the process [4]. The predicted injection pressure from the Moldflow® and Polyflow® simulations was lower than the actual injection pressure of the tensile bar by 7 MPa and 2 MPa, respectively. The pressure distributions at the end of filling are shown in figure 9.5.

The pressure history is imposed on the material during the molding cycle and is closely associated with several process parameters (injection pressure, shot size, clamping force and injection rate), but its evolution over time depends on material behaviour during filling and cavity geometry. A correlation between pressure evolution and geometrical variation was observed for the two different material models in correspondence with the cavity gate, where a coupled phenomena of contraction flow and heat transfer is present. To this end, shot size and transfer position were incrementally adjusted to obtain one shot at the gate entrance and one at the gate exit. Experimental short shots have been analyzed with a calibrated high-magnification optical microscope. The distance between the centre of the part at the injection

location and the tip of the short shots along the middle plane of the part was measured. At corresponding partial injection times, the pressure drop was estimated, evaluating the pressure profile acquired at the injection location for a complete component (figure 9.6). The same pressure drop was calculated from numerical simulations and compared to the experimental one. The quality of measurements was assured by calculating the measuring uncertainty for both experimental and simulated short shots. The uncertainty of actual measurements on the μIM molded parts (U_{exp}=0.18mm) included microscope uncertainty, pixel calibration uncertainty, measurement repeatability as well as μIM process repeatability (3 short shots for each injected volume were randomly chosen from the production batch and measured). The uncertainty of measurements on the simulated short shots (U_{sim}=0.25mm) included average mesh size and digital imaging resolution [112]. Numerical and experimental results regarding pressure drops at the gate position have been compared in table 9.1. It is clear how the viscoelastic compressible computation on the three dimensional part revealed more reliable results, if compared with the experimental ones (figure 9.6). The relative increase of the pressure drop acquired in Polyflow® simulation, if compared to the viscous one, could be due to normal stresses and resistance to elongational deformation at the gate contraction flow. Based on the rheological data obtained from the material characterization, further differences in the pressure drops, between simulations and experiments, could be due to the process variability, machine time acquisition uncertainty, normal material variability and incongruent starting conditions.

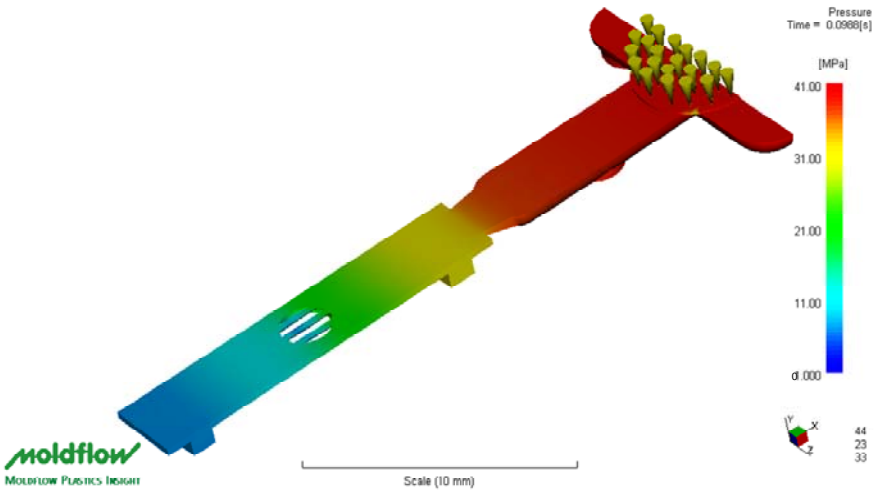

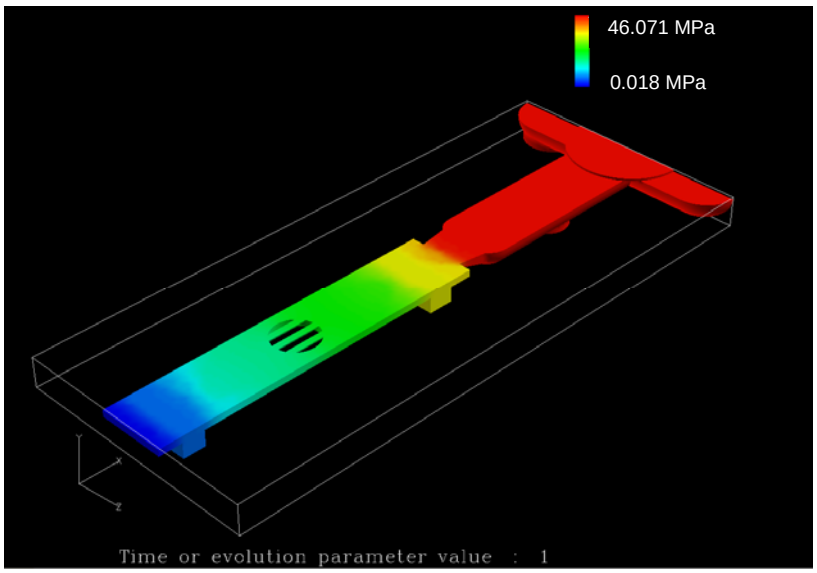

Figure 9.5 - Pressure distribution at the end of the filling stage

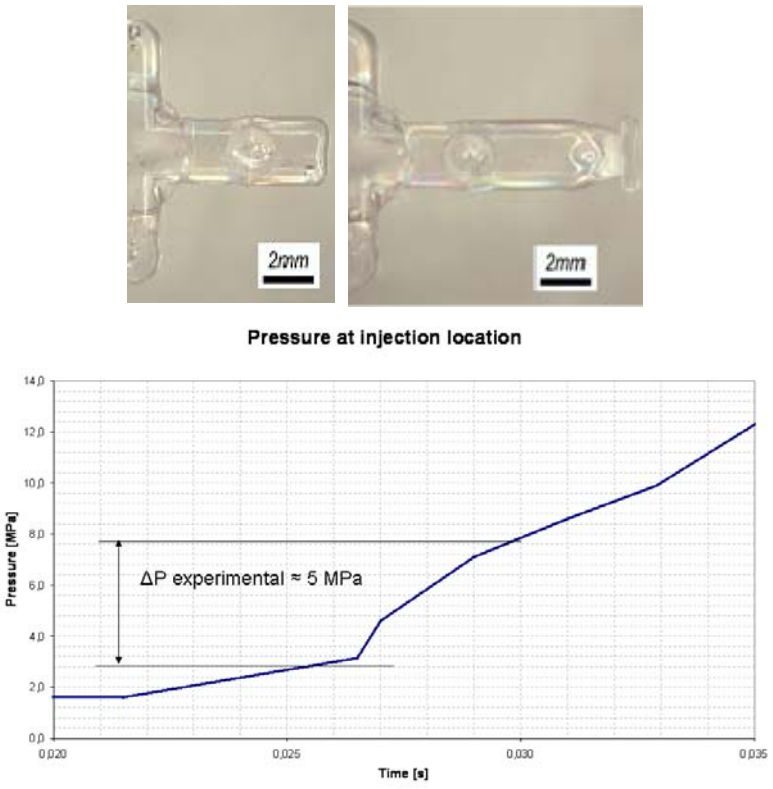

Figure 9.6 - Experimental short shots and estimated pressure drop at gate location

	Pressure drop estimated at injection location
	ΔP [MPa]
Viscous	3.7
Viscoelastic	4.5

Table 9.1 - Simulated pressure drops comparison

.
.

CHAPTER 10

FINDINGS

The rapid growth in the use of advanced materials in a large number of highly demanding automotive, electronic and consumer applications has promoted the development of new and more complex material forming processes. A good understanding of the interaction between material and processing conditions is important to comply with stricter tolerances and demanding service conditions. This is particularly important in the case of forming processes involving the filling of a mold, where the coupled phenomena of fluid flow and heat transfer determine, to a great extent, the final properties of the molded part. Because of their cost effectiveness and rapid response, numerical simulations have become an increasingly important tool for the design and evaluation of processing parameters. Numerical investigations are able to estimate aspects of the physical model which would

otherwise be difficult to quantify. They allow quick responses on what will be the effects of process parameters changes on the final part. Although Computer Aided Engineering (CAE) has been used with increasing success in the design and manufacture of polymer products and processes, the injection molding process involving microstructures (μIM) presents many challenges. The flow behaviour of polymer melts in micro mold cavities is not fully understood. It is believed that, due to the large surface-to-volume ratio, surface effects will dominate flow behaviour at the microscale. Material data and constitutive equations are together with software processors and validation procedures, the three elements that equally contribute to the effective use of the process simulation technology. In order to evaluate whether these numerical commercial codes were suitable to characterize melt flow patterns, a new approach has been introduced in this work. It consists in determining the flow pattern by using the weld lines as flow markers. A dedicated micro cavity was designed in order to create an effective response variable to compare the results of numerical simulations with the experimental ones. To investigate the influence of process parameters on the weld lines formation in the micro cavity, a statistical design experiment was carried out. Four different process parameters were varied in order to determine their influence on the micro injection molding process: the melt temperature, the mold temperature, the injection velocity and the packing pressure. The factors having the most important effect on the weld line placement and shape have been found to be the injection speed and the mold temperature. Conventional midplane and three dimensional simulations were then tested and found to be inappropriate for multi-scale structures and insensitive to the process parameters change. Furthermore, based on currently available data for polystyrene, the simulation results indicated the importance in employing microscale viscosity of the material and local heat transfer coefficient. It was expected that further differences between experiments and numerical investigations would be due to the assumption of a generalized Newtonian fluid, generally used for traditional injection molding, where the importance of the material elasticity compared to viscous effects appears to be negligible. Because of high deformation rates during the injection phase, it was expected that viscoelastic effects might occur. Viscoelasticity is the property of the material exhibiting the combined behaviour of viscous fluid and elastic solid. In general, higher deformation speed causes the material to respond more elastically (strain hardening) and deformation at a lower speed causes a more viscous response. The challenge was to translate the complex rheological behaviour of polymeric fluids into suitable equations, and to use these models to predict flow in the micro cavity. Careful material characterization was

conducted on both a capillary and rotational rheometer and data obtained were fitted according to a non linear viscoelastic model (Giesekus model). Three dimensional viscoelastic numerical simulations were then performed to evaluate whether the implementation of a viscoelastic material model could improve the accuracy of micro filling simulations. The problem involved flow, heat transfer by conduction and convection and heat generation by viscous dissipation. Energy, momentum and mass equations were solved in the fluid domain. The energy equation for heat transport problems was solved in the solid domain. Improvements in the viscoelastic simulation results were observed in predicting the flow front position in microstructures and the pressure evolution during the filling phase. Further differences between experiments and numerical simulations could be related to the absence of a robust local heat transfer model. Furthermore, the intensity of the forces at stake during the process were so much higher that a conventional rheological study could not be the proper means to qualify the polymer behaviour. Nonetheless, it is the only means available right now as the on-line rheology still contains a certain number of hazardous parameters (for instance, the sensor resistance to high temperatures and pressures).Consequently, as far as the material characterization is concerned, viscometric measurements have been performed bearing in mind that the deformation rates are far from being representative of those encountered during the micro injection molding process. Further development of material characterization technologies and constitutive equations modelling are required throughout the supply chain to improve simulations accuracy for the production of polymer products with complex micro- and nanoscale features.

REFERENCES

[1] Bourne, M., guest columnist, http://www.smalltimes.com, July 16, 2004.

[2] Weber, L., Ehrfeld, W., Freimuth, H., Lacher, M., Lehr, H., Pech, B., SPIE (1996) 2879, pp. 156-167.

[3] Kazmer, D., Precision process control of injection molding, Precision injection molding, (2006), p. 265

[4] Whiteside, B.R., Martyn, M.T., Coates, P.D., An introduction to micromolding, (2006), p.239.

[5] Madou, M.J., Fundamentals of microfabrication: the science of miniaturization, 2nd edition (2002) CRC Press, Boca Raton, FL.

[6] Snyder, M.R., Modern plastics, January (1999), p.85.

[7] Stone, H.A., Kim, S., AIChE J. (2001) 47 (6), p. 1250.

[8] Kang, K., Lee, L.J., Koelling, K.W., Experiments in fluids (2005) 38, p. 222.

[9] Despa, M.S., Kelly, K.W., Collier, J.R., Microsystem Technologies (1999) 6, p.60.

[10] Kim, B., NSF design, service and manufacturing grantees and research conference proceedings, (2003) p. 1972.

[11] Yao, D. and Kim, B., Journal of injection molding technology (2002) 6(1) p.11.

[12] Xu, G., L., Lee, L.J. Koelling, K.W., Polym. Eng. Sci. (2005) 45, p. 866.

[13] Yu, L., Koh C.G., Lee, L.J. and Koelling, K.W., Polym. Eng. Sci. (2002) 42, p. 871.

[14] Warrington, R.O., Proceedings of novel microfabrication options for BioMEMS conference, July (1999), chapter 7, p. 67.

[15] Momma, C.S., Nolte, N., Chichkov, B., Alvensleben, V. and Tunermann, F.A., Appl. Surf. Sci. (1997) 15, p. 109.

[16] Roberts, M.A., Rossier, J.S., Bercier, P., Girault, H., Anal. Chem., (1997) 69 (11), p. 2035.

[17] Ginger, D.S., Zhang, H., Mirkin, C.A., Angewandte Chemie, International Edition (2003) 43 (1), p. 30.

[18] Ehrfeld, W., Lehr, H., Radiat. Phys. Chem. (1995) 45 (3), p. 349.

[19] Malek, C.K., Saile, V., Microelectronics journal (2004) 35 (2), pp. 131-143.

[20] Heyl, P., Olschewsky, T., Wijnaendts, R.W., Microelecttronic Engineering (2001) 57-58, pp. 775-780.

[21] Giboz, J., Copponnex, T., Mèlè, P., Microinjection molding of thermoplastic polymers: a review, J. Micromech. Microeng. 17 (2007) p. 96-109.

[22] Eicher, J., Peters, R.P., Rogner, A., VDI-Verlag report No. VDI-Bericht (1992) 960, Dusseldorf.

[23] Hanemann, T., Piotter, V., Ruprecht, R., Hausselt, J.H., ACS Symposium Series (1998) 706, p. 67.

[24] Ruprecht, R., Bacher, W., Haubert, J., Piotter, V., Proc. SPIE, (1997) 3223, p. 91.

[25] Chen, M., Yao, D., Kim, B., Polym. Plast. Technol. Eng. (2001) 40, p. 491.

[26] Yao, D., Kim, B., Polym. Eng. Sci., (2002) 42 (12), p. 2471.

[27] Ganz, M., Polymer Process Engineering, ed. P.D. Coates, IOM Communications Ltd., London (1999) p. 8-17.

[28] Whiteside, B., Martyn, M.T., Coates, P.D., ANTEC 2003-Proceedings of the 61st annual technical conference, vol. XLIX, Nashville, TN, pp. 592-596.

[29] Speight, R.G., Coates, P.D., Hull, J.B., Peters, C., Proceedings ImechE

(1997) 211 (E), pp. 115-128.

[30] Speight, R.G., Coates, P.D., Hull, J.B., Peters, C., Proceedings ImechE (1997) 211 (E), pp. 115-128.

[31] Ono, Y., et al., ANTEC 2004 – Proceedings of the 62nd annual technical conference exhibition, Vol. L., Chicago, Society of Plastics Engineers, pp. 556-560.

[32] Schmidt, D., Shah, D., Giannelis, E.P., Current opinion in solid state and materials science (2002) 6, pp. 205-212.

[33] Xiao, M., et al., Polymer (2002) 43, pp. 2245-2248.

[34] Zhang, J., Wilkie, C.A., Polymer degradation and stability (2003) 80, pp. 163-169.

[35] Harris, P.J.F., International materials reviews, 49(1), pp. 31-43.

[36] Whiteside, B.R., Martyn, M.T., Coates, P.D., Introduction to micromolding, Precision injection molding, Hanser, pp. 250-251.

[37] van Wijngaarden, H., Dijksman, J.F., and Wesseling, P., J. Non-Newtonian Fluid Mech. (1982) 11, p.175.

[38] Hieber, C.A. and Shen, S.F., J. Non-Newton Fluid Mech. (1980) 7, p. 1.

[39] Boshouwers, A.H.M., Werf, J.J., Inject-3, A simulation code for filling stage of the injection molding process of thermoplastics, PhD Thesis (1988), University of Technology, Eindhoven.

[40] Barrie, I.T., Understanding how an injection mod fills, SPE journal, (1971) 27, pp. 64-69.

[41] Williams, G., and Lord, H.A., Mold filling studies for the injection molding of thermoplastic materials, Polym. Eng. Sci., (1975) 15, pp. 553-568.

[42] Lord, H.A., Williams, G., Mold-filling studies for the injection molding of thermoplastic materials, Polym. Eng. Sci., (1975) 15, pp 569-582.

[43] Hieber, C.A., Shen, S.F., A finite element/finite difference simulation of the injection molding filling process, J. non-newtonian fluid mech., (1980) 7, pp. 1-32.

[44] Gurtin, M.E., An introduction to continuum mechanics (1981) Academic press, San Diego.

[45] Bird, R.B., Armstrong, R.C., Hassager, O., Dynamics of polymeric

liquids, Vol. 1: fluid mechanics, 2nd Edition (1987) John Wiley and sons, New York.

[46] Richardson, S., Hele-Shaw flows with a free boundary produced by the injection of fluid into a narrow channel, J. Fluid Mech. (1972) 56, pp. 609-618.

[47] Hieber, C.A., Shen, S.F., A finite element/finite difference simulation of the injection molding filling process, J. non-newtonian fluid mech., (1980) 7, pp. 1-32.

[48] Kennedy, P.K., Flow analysis of injection molds (1995) Hanser, Munich.

[49] McCormick, R.M., Nelson, R.J.,, Alonso-Amigo, M.G., Benvegnu, D.,J., Hopper, H.H., Anal. Chem. (1997) 69, p. 2626.

[50] Kemmann, O., Weber, L., Jeggy, C., Magotte, O., Dupret, F., Proc. SPE ANTEC (2000), p. 576.

[51] Piotter, V., Muller, K., Plewa, K., Ruprecht, R., Hausselt, J., Microsystem Technologies (2002) 8, p. 387.

[52] Yu, C.J., Sunderland, J.E., Poli, C., Polym. Eng. Sci. (1990) 30, p. 1599.

[53] Ainoya, K., Amano, O., Proc. SPE ANTEC, (2001), p. 726.

[54] Narh, K.A., Sridhar, L., Proc. SPE ANTEC (1997), p. 2277.

[55] Wang, V.-W., Ph. D. Dissertation, Cornell University (1985).

[56] Ainoya, K., Amano, O., Proc. SPE ANTEC, (2001), p. 726.

[57] Peng, X.F., Perterson, G.P., Wang, B.X., Experimental heat transfer, (1994) 7, p. 265.

[58] Gao, P., Person, S.L., Favre-Marinet, M., Inter. J. Thermal Sciences (2002) 41, p. 1017.

[59] Shah, R.K., London, A.L., Advances in heat transfer, (1978), Academic Press, New York.

[60] Wimberger-Friedl, R., Balemans, W.J.M., Proc. SPE ANTEC (2003), p. 539.

[61] Eringen, A.C., Okada, K., Int. J. Eng. Sci. (1995) 33, p. 2297.

[62] Israelachvili, J.N., Colloid interface sci. (1986) 110, p. 263.

[63] Eringen, A.C., Okada, K., Int. J. Eng. Sci. (1995) 33, p. 2297.

[64] Yao, D., Kim, B.J., Micromech. Microeng., (2002) 12, p. 604.

[65] Rosenbaum, E.E., Hatzikiriakos, S.G., J. AIChE (1997) 43, p. 598.

[66] Yao, D., Kim, B.J., Micromech. Microeng., (2002) 12, p. 604.

[67] C. M. Ho and Y. C. Tay, Micro-electro-mechanicalsystems (MEMS) and fluid flows, Annu. Rev. Fluid Mech, 1998.

[68] Yang S.Y., Nian S.C. and Sun I.C. Flow visualization of filling process during micro-injection molding, International Polymer Processing (2002) Vol.17, Issue 4, pp.354-360.

[69] Ono, Y., et al., ANTEC 2004 – Proceedings of the 62nd annual technical conference exhibition, Vol. L., Chicago, Society of Plastics Engineers, pp. 556-560.

[70] Motta, P., Validation of numerical simulation in micro injection moulding, MSc student thesis, April 2006.

[71] Uffe, A.R.T., Surface micro topography replication in injection moulding, Ph.D. thesis, May 2004.

[72] Sarholz, Spritzgießen, Hanser, 1979.

[73] S. Stitz, Analyse der Forteilbilding beim Spritzgießen von Plastomeren als Grundlage für die Prozeßsteurung, IKV, 1973.

[74] J. P. Holmann, Heat transfer, McGraw-Hill, 1997, 8th int. edition.

[75] Tosello, G., Gava, A., Hansen, H.N., Lucchetta, G., Marinello, F., Characterization and analysis of weld lines on micro-injection moulded parts using atomic force microscopy (AFM), Wear (2008).

[76] Tosello G., Gava, A., Hansen H. N., Lucchetta G., Marinello F., Measuring uncertainty applied to design of experiment analysis: a micro injection moulding case study, Proceedings of the Joint ENBIS-DEINDE 2007 International Conference, Torino, Italy, April 2007.

[77] Guarise, M., Filling of micro injection moulded parts: an experimental investigation, MSc student thesis, January 2007.

[78] Morace, R.E., Traceability of measurements on optical coordinate measuring machines, Ph.D. Thesis, 2004.

[79] Tosello, G., Gava, A., Hansen, H.N., Lucchetta, G., Influence of process parameters on the weld lines of a micro injection moulded component, Proceedings of Antec Conference, USA, May 2007.

[80] Montgomery, D.C., Design and analysis of experiments – 5th edition,

John Wiley & Sons Inc., 2001.

[81] Yao, D., Kim, B., Scaling Issues in Miniaturization of Injection Moulded Parts, Journal of Manufacturing Science and Engineering, (2004) Vol. 126, 733.

[82] Jeggy, C., Micro-injection molding, Ph.D. thesis, Mai 2004.

[83] Elias, H., An introduction to plastics, 2., complete new revised ed. Wiley-VCH, Weinheim, 2003.

[84] Kennedy, P., Flow analysis on injection molds (1995) Hanser Publishers, Munich.

[85] Dal Molin, M., Validation and optimization of FEM simulation of micro injection molded parts, MSc student thesis, January 2007.

[86] Cox, W., Merz, E., Correlation of dynamic and steady flow viscosities, Journal of Polymer Science 28 (1958), 619 – 622.

[87] Hieber, C. A., Shen, S. F., A finite-element/finite-different simulation of the injection-molding filling process J. Non-Newtonian Fluid Mech. 7 1–32, 1982.

[88] O. Kemmann, Weber, L., Jeggy, C., Magotte, O., Dupret, F., Simulation of the micro injection moulding process, Proc. SPE ANTEC, 2000.

[89] Yu, L., Experimental and numerical analysis of injection moulding with microfeatures, Ph.D. Thesis, Ohio University, p.192, 2004.

[90] Gava, A., Tosello, G., Hansen, H.N., Salvador, M., Lucchetta, G., A new approach for the filling validation in micro injection moulding, Proceedings of Numiform conference, May 2007.

[91] Hatzikiriakos, S., Dealy, J., Wall slip of molten high density polyethylene, Journal of rheology 35, 4 (1991), 497-523.

[92] Chien, R.D., Jong, W.R, Chen, S.C., Study on rheological behaviour f polymer melt flowing through micro-channels, Journal of Micromechanics and Microengineering 15, pp. 1389-1396, (2005).

[93] Ainoya, K., Amano, O., Accuracy of filling analysis program, Proceedings of PPS conference, 2005.

[94] Ferry, J., Viscoelastic properties of polymers, 3rd ed. John Wiley & Sons, New York, 1980.

[95] Peters, G.W.M., Schoonen, J.F.M., Baaijens, F.P.T., Meijer H.E.H., On

the performance of enhanced constitutive models for polymer melts in a cross-slot flow, J. Non-Newtonian Fluid Mech. 82 (1999) 387-427.

[96] Larson, R.G., A critical comparison of constitutive equations for polymer melts, J. Non-Newtonian Fluid Mech. 23 (1987) 249-268.

[97] Papanastasiou, A.C., Scriven, L.E., Macosko, C.W., An integral constitutive equation for mixed flows: viscoelastic characterization, J. Rheol. 27(4) (1983) 387-410.

[98] Phan-Thien, N., Tanner, R.I., A new constitutive equation derived from network theory, J. Non-Newtonian Fluid Mech. 2(1977) 353-365.

[99] Giesekus, H., A simple constitutive equation for polymer fluids based on the concept of deformation-dependent tensorial mobility, J. Non-Newtonian Fluid Mech. 11 (1982) 69-109.

[100] Armstrong, R.C., Brown, R.A., Quinzani, L.M., McKinley, G.H., Byars, J.A., Measurement of velocity and stress fields in complex polymer flows, Proc. XI Int. Cong. Rheology, Theoretical and Applied Rheology, Brussels, Elsevier, Amsterdam, 1992, pp. 16-23.

[101] Baaijens, H.P.W., Peters, G.W.M., Baaijens, F.P.T., Meijer, H.E.H., Viscoelastic flow past a confined cylinder of a polyisobutylene solution, J. Rheol. 39(6) (1995) 1243-1277.

[102] De Bie, F., Visco-elastische stromingen in een convergerend kannal; Reo-optische experimenten en numerieke simulaties, Master's Thesis WFW 94.026, Eindhoven University of Technology, 1994.

[103] Rajagopalan, D., Byars, J.A., Armstrong, R.C., Brown, R.A., Comparison of numerical simulations and birefringence measurements in viscoelastic flow between eccentric rotating cylinders, J. Rheol. 36(7) (1992) 1349-1375.

[104] Baaijens, H.P.W., Evaluation of constitutive equations for polymer melts and solutions in complex flows, Ph.D. Thesis, Eindhoven University of Technology, The Netherlands, 1994.

[105] Kajiwara, T., Ninomiya, S., Kuwano, Y., Funatsu, K., Numerical simulations of converging flow of polymer melts through a tapered slit die, J. Non-Newtonian Fluid Mech. 48 (1993) 111-124.

[106] Macosko, C., Rheology principles, measurements and applications, 1994.

[107] Hulsen, M., Van Der Zanden, J., Numerical simulation of contraction

flow using a multi-mode Giesekus model, Journal of Non-Newtonian fluid mechanics 38 (1991), 183-221.

[108] Henning Winter, H., Analysis of dynamic mechanical data: inversion into a relaxation time spectrum and consistency check, Journal of Non-newtonian Fluid Mechanics 68 (1997), 225-239.

[109] Williams, M.L., Landel, R.F., Ferry, J.D., J. Am. Chem. Soc. (1955) 77, 3701.

[110] Cox, W., Merz, E., Correlation of dynamic and steady flow viscosities, Journal of Polymer Science 28 (1958), 619-622.

[111] Gava, A., Lucchetta, G., Three dimensional viscoelastic simulation of thin-wall injection moulding with microfeatures, Proceedings of Antec Conference, May 2008.

[112] Tosello, G., Gava, A., Hansen, H.N., Reinecke, H., Lucchetta, G., Schoth, A., Influence of different process settings conditions on the accuracy of micro injection moulding simulations: an experimental validation, In pres. Antec Conference, June 2009.

[113] Gava, A., Tosello, G., Lucchetta, G., Reinecke, H., Hansen, H.N., Schoth, A., Experimental validation of viscous and viscoelastic simulations of the micro injection molding process, In pres. Antec Conference, June 2009.